2010

In Vitro Evaluation of Mechanical Heart Valve Performance Using a Novel Test Chamber in an Automated Mock Circulatory Loop

Antonio Walker
Virginia Commonwealth University

IN VITRO EVALUATION OF MECHANICAL HEART VALVE PERFORMANCE USING A NOVEL TEST CHAMBER IN AN AUTOMATED MOCK CIRCULATORY LOOP

A thesis submitted in partial fulfillment of the requirements for the degree of Master of Science in Biomedical Engineering at Virginia Commonwealth University.

By

Antonio R. Walker

B.S. in Biomedical Engineering,
North Carolina State University, 2006

Director: Gerald E. Miller, Ph.D.
Department Chair of Biomedical Engineering

Virginia Commonwealth University
Richmond, Virginia

ACKNOWLEDGEMENTS

I would first like to thank my advisor Dr. Gerald Miller for his support and guidance during my time at Virginia Commonwealth University. The opportunities and experiences presented to me in the Artificial Heart Laboratory will remain with me throughout my professional career and for that I am extremely grateful. In addition, I would like to show my heart felt appreciation to Dr. Amy Throckmorton for her invested time and support in all of my educational and career endeavors. I also thank my remaining committee member, Dr. Ding-Yu Fei and the rest of the Biomedical Engineering faculty and staff for their efforts in providing a rewarding educational experience for me over the last few years.

I would be severely erroneous if I did not express tremendous gratitude for my fellow Artificial Heart Laboratory researchers, especially Charles Taylor. For without his insightful knowledge base and everyone's positive personality and contributions, my graduate accomplishments would not have been possible. Furthermore, I would like to thank the rest my fellow graduate colleagues in the Biomedical Engineering Department and beyond for their additions to my VCU experience.

Last but certainly not least, I'd like to thank my family and friends for their unwavering support and encouragement throughout my life. Without them I would not be who I am and for that I am eternally grateful. My grandmother has always been and will continue to be my source of inspiration because without her I would not have accomplished half of what I have. Thank you all.

TABLE OF CONTENTS

LIST OF TABLES

LIST OF FIGURES

ABSTRACT

IN VITRO EVALUATION OF MECHANICAL HEART VALVE PERFORMANCE USING A NOVEL TEST CHAMBER IN AN AUTOMATED MOCK CIRCULATORY LOOP

By Antonio R. Walker, B.S. in Biomedical Engineering

A thesis submitted in partial fulfillment of the requirements for the degree of Master of Science in Biomedical Engineering at Virginia Commonwealth University.

Virginia Commonwealth University, 2010

Director: Gerald E. Miller, Ph.D.
Department Chair of Biomedical Engineering

Valvular heart disease (VHD) continues to have significant effects on many people's lives, with numbers expected to grow tremendously over the next few years. Individuals suffering from severe valvular heart disease usually require a heart valve transplant in order to restore the native valve's vital unidirectional flow regulation. Therefore, artificial heart valve (AHV) research is of very high importance. Previous research studies have provided substantial input in the realm of AHV design relative to durability, thrombotic and hemolytic potential, and overall functionality. However, modifications continue to be warranted due to limitations in the accuracy and time efficiency of the in vitro physiological flow replication process. The objective of this investigation is to develop and analyze a method of AHV performance evaluation using a novel

test chamber within an automated mock circulatory loop. The constructed mock loop was designed to maintain consistency of current industrial and academic research systems while providing innovative loop component control that allows for run-time changes and performance screening to various physiological conditions. Pressure sensors, ultrasonic flow meter, process controls and mechanical feedback sensors are managed via Labview in order to provide sufficient real-time performance analysis during system operation. In addition, a unique mechanical heart valve (MHV) test chamber was constructed to incorporate the test AHV in the mock loop flow path. This research exposes a test tilting disk MHV to a series of 12 heart rate and stroke volume combinations so as to evaluate the system's effectiveness in pathological condition replication with respect to AHV design research. A Particle Image Velocimetry (PIV) system was utilized to illuminate particles in the flow field and obtain representative vector plots. Results of this study validate the combined experimental test chamber and automated mock circulatory loop as a viable MHV performance evaluation system by using real-time pressure and flow data to analyze system fluid dynamics at the MHV test site. Consequently, the use of this arrangement in MHV performance analysis greatly improves upon time restraints and accuracy concerns associated with currently used manually controlled setups.

1 INTRODUCTION

1.1 Motivation and Significance

Nearly 4.9 million Americans presently suffer from heart failure with over 500,000 new patients diagnosed each year [1]. Consequently, cardiovascular heart disease (CHD) is the leading cause of death in the United States, fatally affecting approximately one person every 34 seconds [2]. While these statistics alone are reason for alarm, concern is heightened by evidence of similar trends worldwide. Therefore, as the number of people suffering from CHD continues to grow, so does the significance of research focused on cardiological deficiencies. One particular group of ailments, known as valvular heart disease (VHD), provide the impetus for this research and support the broader theme of finding novel solutions to cardiovascular disorder prevention and treatment.

VHD affects more than 100 million people worldwide and accounts for 10% to 20% of all cardiac surgical procedures in the United States [3]. In addition, there are currently over 290,000 surgical heart valve procedures conducted globally each year [4] with, roughly, one-third of those being in North America [5]. This global total is expected to exceed 850,000 by the year 2050 [4], which denotes an annual percentage rate increase of 10-12%. As a direct result of the realities associated with these growth estimates, the prominence of heart valve exploration will progressively increase and, thus, provide an ever expanding contribution to society.

1.2 Function and Anatomy

Heart valves control the unidirectional blood flow through the heart and, consequently, can have major effects on the overall efficiency of the entire cardiovascular system. They are facilitated via the formation of pressure gradients during each heart cycle which cause them to open and close as appropriately intended.

There are four major valves in the human heart, excluding the coronary sinus and inferior vena cava valves. The tricuspid and bicuspid valves are the atrioventricular (AV) valves that lie between the respective atria and ventricles. The pulmonary and aortic valves are classified as semilunar (SL) valves and are located between the ventricles and exit arteries. Each side of the heart, right and left, contains two valves, one AV and one SL.

1.2.1 Right Side of the Heart

The right side of the heart transports CO_2 rich blood through the pulmonary cycle for oxygenation. The right atrium serves as the collection container for deoxygenated blood from the superior and inferior vena cava after it successfully undergoes systemic circulation through the body. Following blood return into the right atrium, blood moves into the right ventricle. During systole, the right ventricle pumps blood through the pulmonary arteries and down to the lungs for CO_2-O_2 gas exchange via diffusion. The right heart contains the tricuspid AV valve (controls flow from right atrium to right ventricle) and the

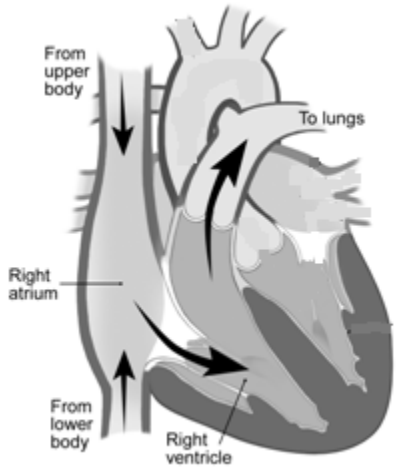

Figure1.1. [6] Right heart anatomy.

pulmonary SL valve (controls flow from the right ventricle into the pulmonary arteries). **Figure 1.1** depicts blood flow through the right heart.

The normal tricuspid valve possesses three leaflets connected to three papillary muscles by chordae tendineae located in the right ventricle. The papillary muscles and chordae tendineae, subvalvular apparatus, do not affect valve function and primarily help hold the tricuspid valve in place using tension to provide stability. The tension also stops prolapse of the leaflets into the atrium, maintaining a tight seal. The tricuspid valve opens when the pressure of the right atrium surpasses the pressure in the right ventricle. This occurs during atrial contraction, ventricular diastole. At the beginning of right ventricle contraction, ventricular systole, blood attempts to flow back into the atrium. It is this flow, in conjunction with intraventricular pressure, which pushes against the valvular flaps causing the triscupid valve to close.

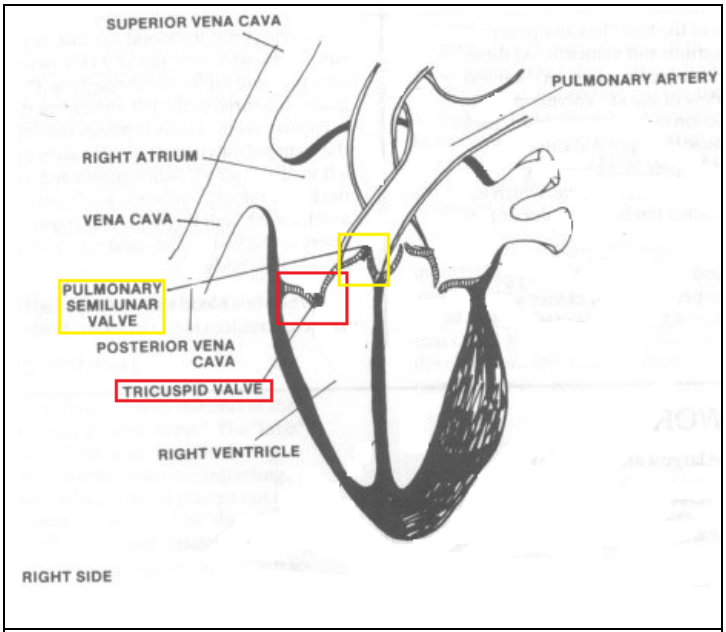

Figure 1.2. [7] Tricuspid (Red) and Pulmonary (Yellow) valve orientation.

The pulmonary valve has three cusps. It opens during ventricular systole when right ventricle pressure exceeds pulmonary artery pressure. Similarly, pulmonary valve closure occurs at the end of the systolic cycle when right ventricular pressure quickly drops, allowing pressure

in the pulmonary artery to once again become the larger of the two. **Figure 1.2** illustrates pulmonary and tricuspid valve orientation, relative to the right heart chambers.

1.2.2 Left Side of the Heart

The left side of the heart is the pumping mechanism for systemic circulation. It drives oxygenated pulmonic blood through the aorta and out to the tissues, muscles, and end organs where it undergoes O_2-CO_2 gas exchange. Blood exiting pulmonary circulation fills the left atrium, which then passes on to the left ventricle and, finally, out the aorta. The left heart encloses the bicuspid AV valve (controls flow from left atrium to left ventricle) and the aortic SL valve (controls flow from the left ventricle into the aorta). **Figure 1.3** navigates blood flow through the left heart.

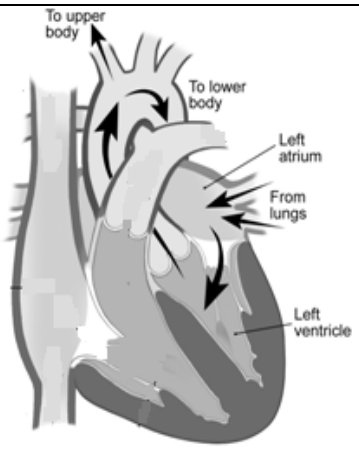

Figure1.3. [6] Left heart anatomy.

The bicuspid valve (commonly known as the mitral valve) has two leaflets and typically occupies an area of 4-6 cm^2. The valve orifice is surrounded by a ring of fibrous tissue called an annulus. Like the tricuspid valve of the right heart, the mitral valve leaflets are attached to papillary muscles by chordae tendineae in the left ventricle. The mitral valve opens due to increased pressure from the left atrium as it fills with blood, which causes pressure increases above that of the left ventricle and allows blood to flow through the valve. The initial surge of blood occurs during early left ventricular diastole and accounts for 70-80% of the total filling of the ventricle (called early rapid filling). The other 20% of complete left ventricular volume

comes from atrial contraction (atrial systole), which drives the remaining blood out of the left atrium. Valve closure ensues at the end of atrial contraction to prevent blood backflow.

The normal aortic valve contains three cusps, resembling the pulmonary valve. During ventricular systole, pressure rises in the left ventricle. When the pressure in the left ventricle rises above the pressure in the aorta, the aortic valve opens, allowing blood to exit the left ventricle into the aorta. Once ventricular systole ends, pressure in the left ventricle rapidly drops. The decrease in left ventricular pressure enables the force of the aortic pressure to close the aortic valve. **Figure 1.4** illustrates aortic and mitral valve orientation, relative to the left heart chambers.

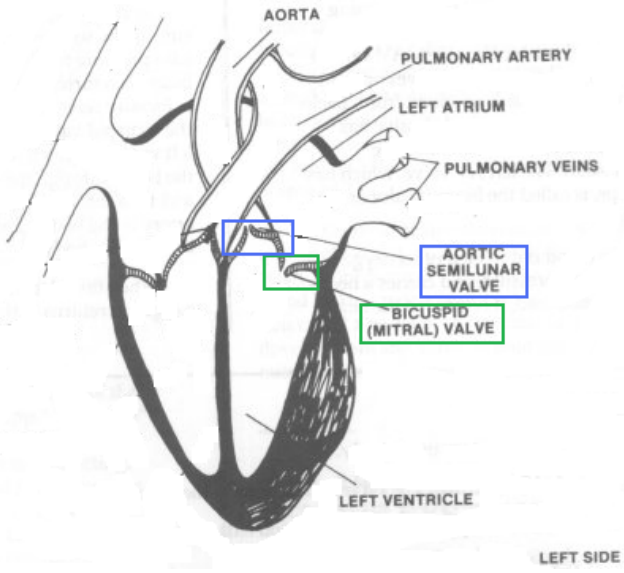

Figure 1.4. [7] Mitral (Green) and Aortic (Blue) valve orientation.

Identical to the right side, the lower ventricle on the left side of the heart is thicker and stronger than the upper atrium. However, the muscle wall surrounding the left ventricle is more bulky than the right ventricle, which makes the left ventricle more physically powerful. This difference allows the left side of the heart to provide a greater amount of force to successfully push the heavier, nutrient-rich blood through the longer systemic circulation. Using the general formula: WORK = FORCE X DISPLACEMENT, the greater force and longer distance of blood travel produced by the left side of the heart implicates a superior workload. Due to this massive difference in workload between the two sides, the left heart components are subjected to more strenuous circumstances than

those of the right. As a result, left heart valves have an increased potential for failure. Thus, the majority of the previously noted 290,000 global surgical heart valve procedures [4] attempt to correct mitral and aortic valve complications on the left side of the heart.

1.3 Pathologies and Diagnoses of Left Heart Valve Disease

In cases of heart valve disease, problems arise when normal regulatory functionality of the valve is disrupted, leading to disturbances in blood flow [2, 8]. The primary diagnoses of heart valve disease include the incidence of stenosis, regurgitation, or a combination of the two. Stenosis occurs when the valve fails to open completely and fails to transfer the standard amount of blood through the opening. Regurgitation is the leakage of blood back through the valve in the reverse direction due to improper prevention of backflow. Both diagnoses have the potential to instigate additional cardiovascular complications, including failure and/or blood seepage into the lung.

1.3.1 Mitral Valve Heart Disease

1.3.1.1 Mitral Stenosis

Mitral stenosis is characterized by the narrowing of the mitral valve orifice within the heart. When the mitral valve area shrinks below the normal 4-6 cm^2, specifically below 2 cm^2, blood flow into the left ventricle is blocked, creating an abnormal pressure gradient increase across the mitral valve. This gradient is multiplied as the heart rate or cardiac output rises, which also raises the necessary amount of time needed to completely fill the left ventricle with blood.

As the heart rate increases, ventricular diastole decreases along with the amount of time needed for the ventricle to fill (diastolic filling period). Therefore, once the heart rate reaches a certain threshold, the diastolic filling period is insufficient to fill the ventricle with blood and pressure builds up in the left atrium, leading to pulmonary congestion. Severe mitral stenosis occurs when the orifice is less than 1 cm^2 and is often characterized by a pressure gradient across the mitral valve of more than 10 mmHg [9]. Meaning a pressure gradient of 20 mmHg, coupled with a normal left ventricular diastolic pressure of about 5 mmHg, results in a left atrial pressure of about 25 mmHg. Atrial pressures of this caliber lead to a variety of other complications including pulmonary hypertension, pulmonary edema, and atrial fibrillation [3, 9]. Furthermore, the accelerated heart rate joined with the shortened diastolic time produces a decreased cardiac output, often resulting in sudden congestive heart failure.

1.3.1.2 Mitral Regurgitation

Mitral regurgitation is the abnormal leaking of blood from the left ventricle, through the mitral valve, and into the left atrium during left ventricular systole. It can be brought on by a malfunction of any of the mitral valve components, leaflets, annulus, chordae tendineae, or papillary muscles, and occurs in three phases, acute, chronic compensated, and chronic decompensated.

Acute mitral regurgitation causes an abrupt volume overload of both the left atrium and the left ventricle. The left ventricle develops volume overload because with every contraction it pumps blood into the aorta (forward stroke volume), while blood regurgitates back into the left atrium (the regurgitant volume). The total stroke volume of the left ventricle (forward stroke volume plus regurgitant volume) increases with more regurgitation, which raises the percentage

of blood pumped from the left ventricle during one heart beat (ejection fraction). This increased ejection fraction deteriorates the left ventricular contractile function over time and thus eventually leads to a dysfunctional left ventricle with a decreased ejection fraction [10]. In addition, the regurgitant volume causes a volume and pressure overload of the left atrium, which inhibits drainage of blood from the lungs via the pulmonary veins and causes pulmonary congestion [10].

Chronic compensated mitral regurgitation develops slowly. It is characterized by thickening of the left ventricle wall (hypertrophy) as an attempt to compensate for the larger than normal stroke volume. This hypertrophy, in conjunction with an increased diastolic volume, increases the stroke volume to higher than normal levels. As a result, the forward stroke volume approaches the normal levels in spite of the regurgitant volume. The volume overload of the left atrium causes enlargement of the left atrium chamber. The increased chamber size allows the left atrium filling pressure to decrease. This improves the drainage from the pulmonary veins and lowers the signs and symptoms of pulmonary congestion. So, these changes in the left ventricle and left atrium improve the state of the low forward cardiac output and the pulmonary congestion that occur in acute mitral regurgitation. Frequently, patients diagnosed with chronic compensated mitral regurgitation do not exhibit symptoms of regurgitation [10].

Individuals with advanced stage chronic compensated mitral regurgitation are diagnosed with chronic decompensated mitral regurgitation. It is characterized by overload of the left ventricular contractile elements, calcium within the cardiac myocytes, resulting in left ventricle dysfunction [3, 10]. The ventricular muscles, myocardium, lose the ability to adequately contract and cannot compensate for the volume overload associated with mitral regurgitation.

Subsequently, the left ventricle stroke volume decreases and forces an increase in the end-systolic volume that translates to increased filling pressures of the ventricle. This once again leads to increased pulmonary venous congestion, which often results in symptoms of congestive heart failure. Furthermore, the left ventricle widens and causes an enlargement of the mitral valve annulus, which may worsen the degree of mitral regurgitation [10].

1.3.2 Aortic Valve Heart Disease

1.3.2.1 Aortic Stenosis

Aortic stenosis transpires when the aortic valve narrows and prevents blood flow from the left ventricle to the aorta. It causes an increased pressure gradient between the left ventricle and the aorta. The more constricted the valve, the higher the pressure gradient. To compensate for the elevated pressure gradient, the left ventricle generates an increased pressure to drive blood into the aorta. This pressure overload results in left ventricle hypertrophy and, over time, produces a decline in systolic function. Aortic stenosis is the most prevalent form of cardiovascular disease in the Western world after hypertension and coronary heart disease [3].

1.3.2.2 Aortic Regurgitation

Patients suffering from aortic regurgitation experience blood leakage in the reverse direction of the aortic valve during ventricular diastole (from the aorta into the left ventricle). It is usually caused by abnormalities of either the aortic valve or the aortic root. When the pressure in the left ventricle falls below the pressure in the aorta, the aortic valve is not able to completely close, which means that forward stroke volume blood regurgitates back into the heart. The percentage of blood that flows back through the aortic valve due to stenosis is known as the

regurgitant fraction [3]. This causes a decrease in the diastolic blood pressure in the aorta, and, therefore, an increase in the pulse pressure (systolic pressure minus diastolic pressure). It ultimately leads to both a volume (elevated preload) and pressure (elevated afterload) overload of the heart. The pressure overload causes left ventricle hypertrophy and could eventually lead to more serious complications.

1.4 Treatment of Left Heart Valve Disease

1.4.1 Valve Repair

Stenosis and regurgitation can generally be corrected via surgical procedures that either enhance blood flow, stenosis, or rectify closure inefficiencies, regurgitation. Most valve repairs conducted on the left heart involve the mitral valve and the applied surgical procedure ultimately depends on the diagnosis. Mitral valve repair techniques generally include:

- **Commissurotomy** removes blood flow blockage caused by enlarged leaflets that may stick together. Surgery consists of severing the leaflets at their bonding point, which reopens the orifice and allows normal function to ensue.

- **Vavuloplasty** is a reinforcement procedure that restores the complete closing ability of the valve. Annulus dilation is combated by implanting a cloth-covered, ring-like mechanism around the native annulus to provide support and return it to its original size. This brings the leaflets back into contact with each other.

- **Reshaping** compensates for leaflet elongation by a method commonly referred to as quadrangular resection. Unneeded, loose leaflet segments are removed and the remaining leaflet is sutured so as to fix closing complications.

- **Decalcification** eliminates the calcium buildup from the leaflets and/or annulus, which increases the orifice area and restores function.

- **Chordae tendineae repair or replacement** re-establishes the structural support of the valve by surgically shortening or using synthetic material, Gore-Tex, to replace the native chordae tendineae. Chordae tendineae may lose tension due to stretching or failure of papillary muscle function, but material length and function restoration permits valve closure.

- **Patching** uses tissue sections to conceal valve apertures in the leaflet and/or annulus.

Of these methods, only commissurotomy and decalcification are utilized in treatment of stenosis. Furthermore, more recent research focuses on the adaptation of percutaneous repair techniques [2, 11]. Several of these methods can also be used in aortic valve repair; however, they are infrequently attempted because of the technical difficulty involved.

1.4.2 Valve Replacement

Despite the success of left heart valve repair, patients with severe physiological impediment face complete native valve replacement as the only viable solution. Consequently, these “one solution” scenarios escalate the significance of effective replacement valve

development [2]. Since the first successful heart valve replacement procedure in 1952 by Dr. Hufnagel, there have been over 4 million, 300,000 annually, prosthetic replacement implants worldwide of over 50 developed artificial heart valve designs [4, 5]. These designs have effectively advanced the realm of heart valve research and are categorized into two major divisions, biological and mechanical.

1.4.2.1 Bioprosthetic Valves

Bioprosthetic replacements include, but are not limited to, valves taken from human donors as well as specified animals. The most widely utilized bioprosthetic valves have porcine origins or are constructed from a sheet of bovine pericardium that is cut to form valve leaflets and sewn into the valve structure [5]. The first commercial porcine valve was the Hancock valve introduced in 1970. Since then additional bioprosthetic valves have been developed, using a variety of other biological material. They include bovine pericardial valves, Carpentier-Edwards Perimount, and equine tissue valves, original Cribier-Edwards. The Carpentier-Edwards Perimount valve is the only

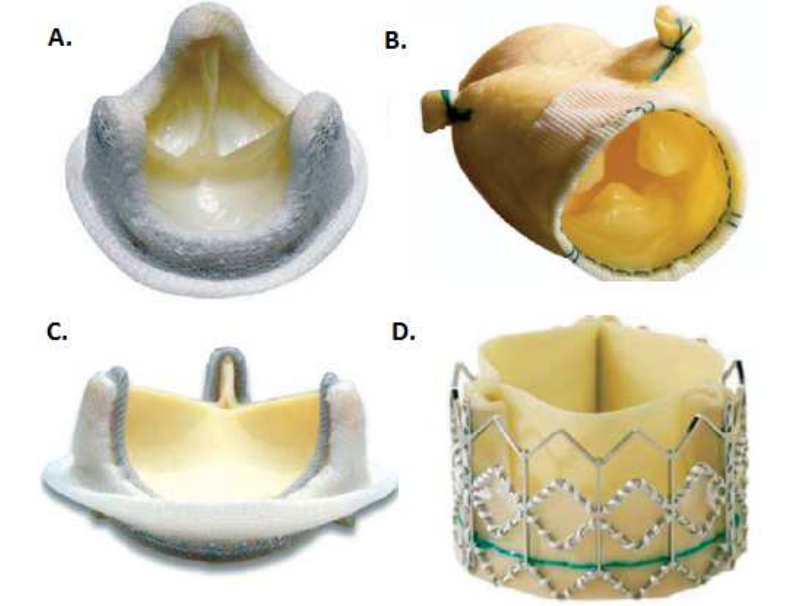

Figure 1.5. [5] Different models of bioprosthetic heart valves**.** (A)Medtronic HK II ultra porcine valve (with permission from Medtronic Inc). (B)Medtronic Freestyle porcine valve (with permission from Medtronic Inc). (C)Carpentier-Edwards Perimount bovine pericardial valve. (D)Edwards SAPIEN transcatheter pericardial aortic valve (courtesy of Edwards Lifesciences LLC, Irvine, CA, USA).

pericardial valve widely available in North America [5]. Most bioprosthetic valves are preserved in glutaraldehyde and mounted on a metal or plastic covered frame/stent with fabric that acts as the sewing ring. In cases where a larger than normal valve orifice is required, stentless bioprosthetic valves are used. These valves lack a stent/frame as part of their structure and thus, provide a larger effective orifice area and lower postoperative transvalvular gradients, compared to stented valves. In contrast to mechanical valves, bioprosthetic valves mimic native heart valve operation by providing unobstructed central flow. **Figure 1.5** shows some well-known bioprosthetic valves.

1.4.2.2 Mechanical Valves

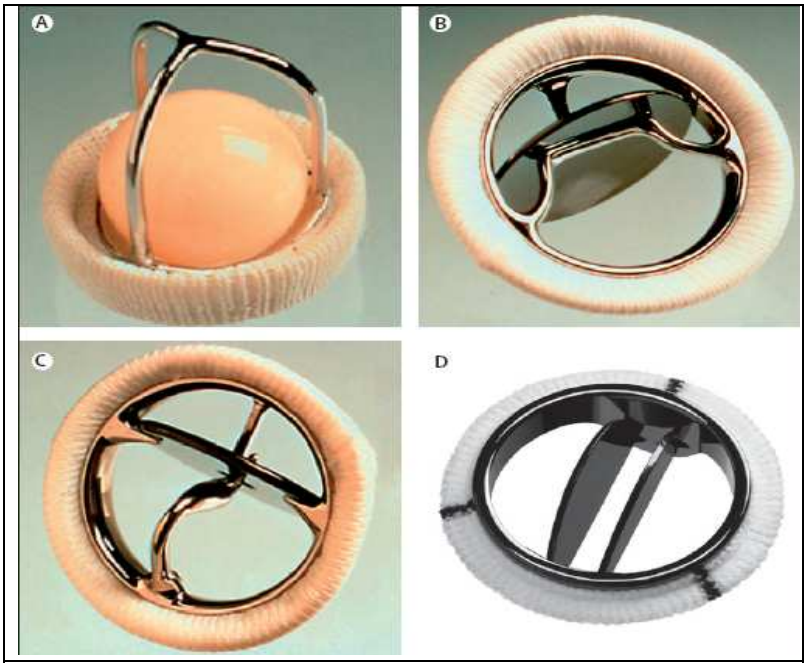

Figure 1.6. [5] Different models of prosthetic mechanical heart valves. (A)Starr-Edwards caged-ball valve (courtesy of Edwards Lifesciences LLC, Irvine, CA, USA). (B)Bjork-Shiley tilting-disk valve (courtesy of Sorin Group of Canada Inc, Canada). (C)Medtronic Hall tilting-disk valve (with permission from Medtronic Inc, Canada). (D)St Jude Medical Regent bileaflet valve (courtesy of St Jude Medical Canada).

Currently, there are three main classes of mechanical valves, caged-ball, single leaflet or tilting-disk, and bileaflet valves. They are all comprised of three main elements: a closure mechanism (occluder), housing, and sewing ring. The first prosthetic heart valve was the Starr-Edwards caged-ball valve introduced in 1960. The original version of the Starr-Edwards valve utilized a free-ball design

with a silicone rubber (silastic) ball that freely moved inside a three-strut alloy cage. Subsequent models had a metal ball and a four-strut cage. Following the Starr- Edwards caged-ball design, the single leaflet or tilting disk valve was pioneered in 1969 by Bjork-Shiley. It consists of a pyrolytic carbon disk that is stabilized by a large inflow and small outflow alloy strut and enclosed by a Teflon sewing ring. The Medtronic-Hall tilting-disk valve remains one of the most implanted valves of all time [5]. Even more utilized than the Medtronic-Hall tilting-disk valve is the St Jude Medical valve introduced in 1977 [5]. It was the first bileaflet valve and is made of two pyrolytic carbon coated leaflets, with graphite, that pivot on a ring and is encircled by a sewing ring. The St Jude Medical bileaflet valve is the single most implanted mechanical valve to date [5] and has been modeled to form several other commercially available bileaflet designs. Consequently, bileaflet valves are the most commonly used of the three main classes [5]. **Figure 1.6** shows some of the more prominent mechanical valves.

1.5 Disadvantages of Prosthetic Heart Valve Implantation

Bioprosthetic valve replacements have exceptional histocompatibility, but are susceptible to problems attributable to natural degenerative effects [12]. Subjects who receive biological valve replacements often experience a recurrence of issues dealing with regurgitation or calcification, which often require additional surgery to repair or replace. For this reason, most bioprosthetic valves last approximately 15 or so years after implantation, making durability the major concern.

In contrast to bioprosthetic valve replacements, mechanical valve replacements have little to no durability concerns. On the other hand, mechanical valves lack the excellent histologic characteristics of bioprosthetic valves [12]. As with the implantation of all foreign devices in the circulatory system, it is essential for mechanical heart valve replacements to keep normal blood flow disruption to a minimum. For this reason, patients with mechanical heart valves must constantly take blood thinner to reduce the potential of blood clot formation in and around the replacement valve. Research shows the chief factors that influence thrombus development are changes in vessel wall morphology, changes in blood flow through the vessel, and changes in blood composition [13, 14]. Since blood composition usually remains constant before, during, and after mechanical valve replacement surgery, the remaining two factors are the foundation of clot formation at the replacement site. Coincidentally, both morphology and blood flow variability depend heavily on the design of the replacement [15]. The morphology of the mechanical replacement valve does not change following fabrication; however, flow variability within the valve is a product of its morphology. Sudden changes in flow dynamics tend to have a negative impact on red blood cells by causing incidences of turbulent flow and flow separation. At these locations of flow disturbance, an amplification in the stress on red blood cells is noticed, which often lead to rupture (hemolysis) and platelet aggregation. Research support the use of certain design types over others based upon the design's tendency to prompt flow turbulence [16]. Therefore, the way to control thrombus activity in the mechanical replacement valve is to incorporate design specifications that theoretically induce laminar flow while minimizing flow disturbances such as turbulence and flow separation. Furthermore, study results indicate area specificity in blood clot formation of existing mechanical heart valve replacement designs, especially at the struts of caged-ball and tilting disk valves and the hinges of bileaflet valves

[17]. These research results designate exact interest areas for improvement purposes and progression towards the continual goal of ideal histocompatibility, which implies little to no blood clot formation. Evidence of prior research confirms that, of the three chief mechanical models, bileaflet valves experience the least amount of clot formation. However, hemolysis and thrombosis continue to be major issues of concern in all mechanical heart valve (MHV) replacement designs.

Both biological and mechanical prosthetic heart valves have made enormous progress over the years; however, improvements continue to be warranted because of shortcomings that include durability and the propensity to incite thrombosis and/or hemolysis [18]. The ideal, functional replacement valve will maximize biocompatibility while also minimizing longevity and histologic concerns.

1.6 In Vitro Evaluation of Prosthetic Heart Valves

In the case of MHV replacements, advancement towards an ideal design primarily centers on the evolution of proven existing, operable models. Researchers continuously search for ways to improve these models via the study of things such as prosthetic valve geometry and manufacturing material. Likewise, there is a constant need to assess flow when using newly renovated bioprosthetic heart valves. In order to investigate these various artificial heart valves prior to implantation, it is necessary to recreate the natural valve in in vivo conditions so as to better assess the biofluid dynamics. Therefore, the enduring pursuit of the ideal heart valve design is accompanied by the ever-changing development of an in vitro testing environment that

effectively simulates in vivo conditions. As previously stated, the majority of valve replacement procedures occur on the left side of the heart. For that reason, much of the valvular research concentrates there as well. These analyses serve as a method of evaluating the effects of the prosthetic valve biofluid dynamics on hemolytic and thrombotic activity before patient insertion.

1.7 Research Aims

Currently there exist several devices used to assess MHVs in a variety of mock circulatory loop setups. These tools readily provide information for in vitro MHV performance evaluation, including but not limited to thrombosis, hemolysis, and material failure. Translation of these concepts into a mechanism that allows for quicker and more efficient MHV interchangeability and hemodynamic condition manipulation will potentially improve upon the required time needed for assessment and comparative testing. The purpose of this research is to develop and validate an instrument and procedure for evaluating MHV replacements in the Artificial Heart Laboratory at Virginia Commonwealth University. The goals of this research include:

- Design and construction of a quick, interchangeable MHV holding chamber
- Implementation of the MHV holding chamber into a fully automated mock circulatory loop
- Visualization of fluid flow through the test MHV at varying physiologic conditions

2 LITERATURE REVIEW

Over the years, a major focal point of valvular investigation has been the effective performance testing of artificial heart valves (AHV) using proficient simulation of the native left heart environment. Several studies have been conducted to determine the causes and locations of valvular induced flow disturbances that may lead to hemolysis or thrombosis. These studies have been done on both FDA approved and unapproved designs as well as in comparative analyses that provide evidence of the advantages of one particular design over another. These research approaches have provided groundbreaking information used in AHV design.

2.1 History of AHV In Vitro Test Results

One major concept that was investigated early was the clinical affects of regurgitant backflow and low cardiac outputs on AHV performance. Meyer et al [19] and Kini et al [20] have completed numerous experimental procedures on regurgitation backflow. They used their findings to effectively predict regurgitant leakage flow regions and correlated these locations with high magnitudes of Reynolds shear stress, which has been found to be a major factor in hemolysis. Similarly, Sabbath and Stein [21] conducted comparative analyses of four AHVs in order to investigate backflow and its relation to other cardiac elements. They stated that valve closure and leakage contribute, independently, to total valvular backflow measurements and primarily focused on the association between the amounts of total backflow of examined

prosthetic aortic valves when exposed to specific mean aortic pressures. Furthermore, they presented evidence of the effects of cardiac output on backflow and provided response measurements to changes in heart rate and/or stroke volume. They deduced that the risk of clinical significance is heightened when exposed to lower cardiac outputs, which was further explored by researchers such as Z. Wu and company. Wu et al [22] evaluated AHVs during low cardiac output conditions and found that valve size and closure volume were directly related to one another, meaning that increasing or decreasing one induces a similar response in the other. Therefore, designing AHVs with this in mind allows normal valve functionality at lower cardiac outputs. These studies advanced the significance of in vitro AHV evaluation under low cardiac output conditions and support the importance of regurgitation backflow. As a result, they greatly contribute to AHV design progression.

Another notable investigative dynamic of valvular-induced fluid mechanics is the analyses of vortex and microbubble formation. Gross, Shermer, and Hwang [23] focused on flow fields distal to the prosthetic heart valve. They concluded that the distal flow was affected by valvular opening angle by relating the valve leaflets to a set combination of rectangular plates and utilizing prior airfoil studies to characterize them. Thus, factors such as drag force, lift coefficient, drag coefficient, and momentum coefficient were used to analyze the observed distal flow patterns and explain boundary layer flow separation at the end of the valve leaflet. The establishment of this relationship between the valve leaflets and earlier validated airfoil evaluations allowed Gross, Shermer, and Hwang to realize a trend stating that increased opening angle leads to increased flow separation and vortex shedding (i.e. turbulence). Moreover, Milo et al [24] expanded on Gross and company's research by linking observed vortex regions to clinical complications such as left atrial wall mechanical damage, thrombotic issues, and inflammatory

reaction effects. In addition, they verified the isolated existence of microbubbles at mechanical valve closure and connected the event to the valve shutting process. These bubbles enhanced the potential of the blood to clot and made these locations, local and abroad, more susceptible to thrombosis. Conclusively, the observed results of these research endeavors, along with their clinical implications, were very important to AHV performance testing and led to improvements in future design and operation.

Lastly, a principle clinical concern of heart valve analysis is the development of cavitation. Johansen et al [25] Manning et al [26] conducted an in depth analysis of vortices and regurgitant jets during the closure and rebound phases of MHV operation. They were able to associate these phenomena with potential cavitation growth and clinical implications based upon prior investigative studies done by others. One such prior investigative study was performed by Lamson et al [27]. Their research involved AHV cavitation pattern detection in real-time. Through this real-time detection process, they were able to characterize areas of replicating cavitation formation and develop a cavitation cycle that corresponds with that of the normal cardiac cycle. In addition, they plotted this cavitation cycle as a function of atrial pressure. The techniques developed in this study provided a means of exposing the causes and locations of cavitation formation during the usage of AHVs, which helps in the design and implementation of cardiac heart valves, drive systems, and/or device control schemes.

2.2 AHV Experimental Test Setups

As stated above, a major component of the previously described research was the simulation of the native left heart environment. Several AHV assessment mechanisms only seek to reproduce natural flow conditions and do not take into account other anatomical feature effects. The majority of studies that employ this type of arrangement are focused on the performance of a particular AHV at very specific conditions and locations. However, for researchers that want to better replicate human physiology, a typical experimental setup consist of a mock circulatory loop in conjunction with an image capture apparatus. The common theme of these systems is their attempt to imitate native conditions so as to expose the trial AHVs to circumstances similar to those encountered after implantation. However, they have evolved over the course of time due to variability in study focus.

2.2.1 AHV Test Chamber

An investigator's AHV test system is heavily based on the intended goals of their experimentation. For instance, Browne et al [28] neglected common components such as compliance and peripheral resistance. Consequently, the primary observation area of their experimental setup consisted of flow, supplied by a centrifugal pump, through a mounted AHV and into a clear, anatomically correct aortic root model where imaging was completed. **Figure 2.1** shows the Browne et al AHV test system. In this study, Browne et al were more focused on the imaging technique so the test arrangement was indicative of that focus.

Other examples of this type of arrangement were Meyer et al [19] and Kini et al's [20] "single shot" chamber system shown in **Figure 2.2**. These groups sought to supply an all-inclusive interpretation of mechanical heart valve flow fields with both global and localized data [19, 20]. These experimental objectives permitted a fairly simplistic test chamber setup that consisted of a two compartment box connected on one side by a mechanical heart valve mounted in a constructed valve holder. The ventricle was represented by the smaller compartment, which was sealed and linked to a pneumatic pressure regulator system, and the atrium was the larger chamber that was open to the atmosphere. The pressure was controlled in the ventricular chamber so as to simulate the physiological systolic cycle where pressure was held constant to symbolize systolic duration and then released.

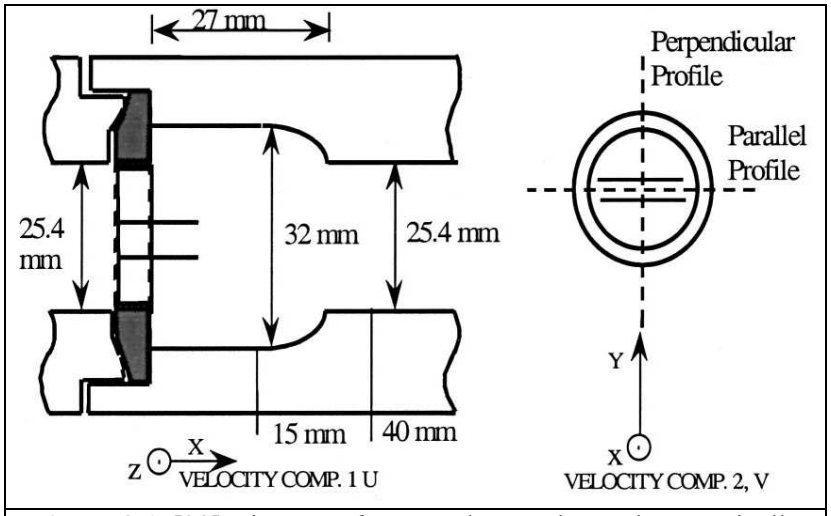

Figure 2.1. [28] Diagram of mounted test valve and anatomically designed aortic model in Browne et al's experimental setup.

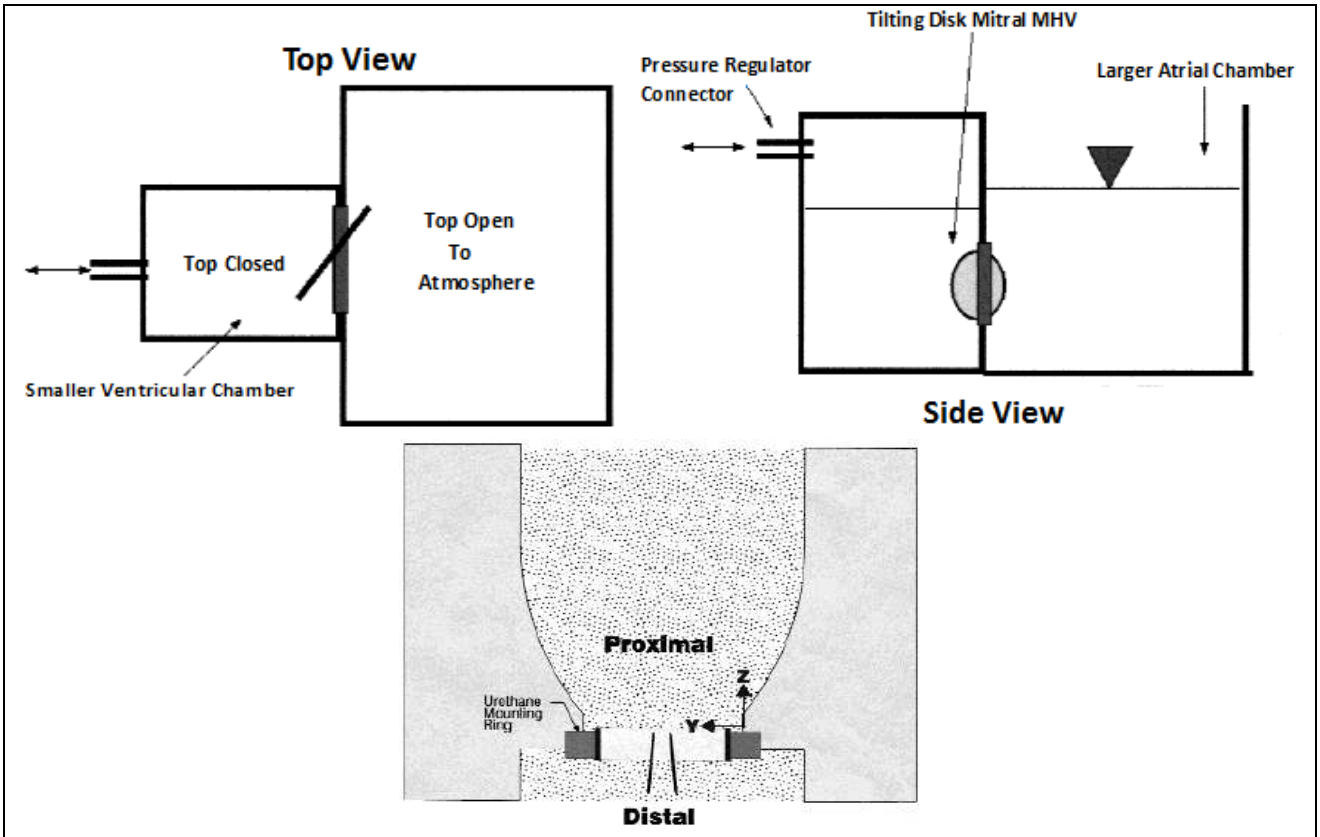

Figure 2.2. [19, 20] Diagrams of Kini et al MHV test setup, Top View (top left) and Side View (top right). Diagram of Meyer et al MHV in mounting arrangement (bottom).

Correspondingly, the test arrangement employed by Milo et al [24] for vortex evaluation was manufactured to imitate fluid flow during early systole, at the point where backflow is at its peak and immediately following heart valve closure. More specifically, they wanted to recreate the high velocity leakage through the narrow gap of the closed leaflets. To accomplish this, the experimenters used a single test chamber with a static valve mounted in the closed position and controlled fluid flow via a high-speed solenoid valve that connected to a regulated pressure basin. In addition, a microbubble generator was attached to the test chamber to produce hydrogen bubbles that served as tracers for vortex visualization. Milo et al's experimental AHV test chamber is depicted in **Figure 2.3**.

Validation from prior literature supports the use of these arrangements in these scenarios and, thus, defends the significance of the acquired data in AHV performance research. However, it is recognized that these setups do not adequately depict the pulsatile flow or the peripheral resistance of the native cardiac system. Both of which notably affect blood flow.

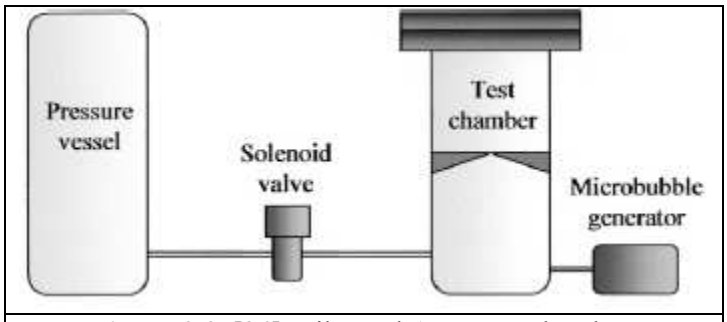

Figure 2.3. [24] Milo et al AHV test chamber.

2.2.2 Mock Loop Testing

Despite the success of the above mentioned studies, several researchers prefer the application of a more physiologically correct understanding. An early in vitro test arrangement, based on a larger version introduced by Davila, Trout, Sunner, and Glover in 1956, was utilized by Bjork, Intonti, and Meissl [29] to examine prosthetic mitral and aortic valves. In choosing this system, Bjork et al placed heavy emphasis on the ability to accurately simulate a variety of physiological conditions. The system contained a mechanical pulse duplicator and was equipped with the capability to adjust systolic-diastolic range and ventricular, atrial, and aortic pressure curve shape. The pulse duplicator, shown in **Figure 2.4**, had a closed loop arrangement with two independent, hydraulic components: 1. pumping system and 2. testing system. The pumping system consisted of a one-armed roller pump that regulated stroke volume and pulse rate via the manual control of RPM and tube occlusion. The testing system was the interconnected valve testing chambers, aortic analogue, peripheral resistance, and left atrium analogue. Manual mechanical adjustments of the testing system included changeable peripheral resistance and the height of the reservoir above the mitral valve chamber.

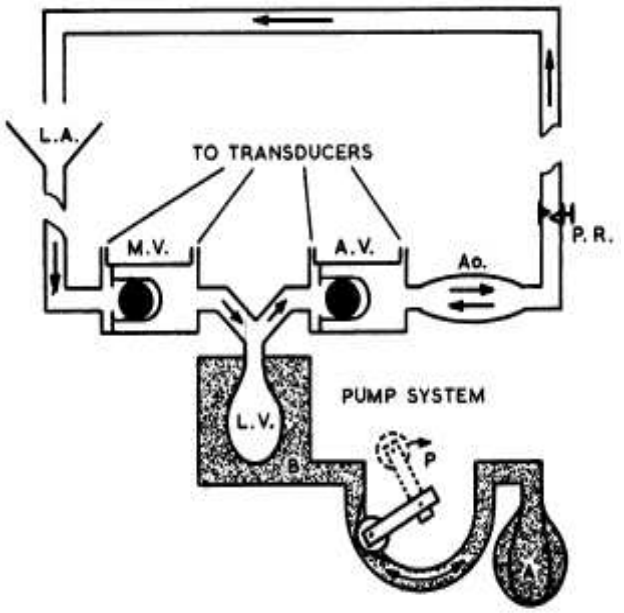

Figure 2.4. [29] Pulse duplicator. L.A.=left atrium; M.V.=mitral valve; L.V.=left ventricle; A.V.=aortic valve; A=elastic container; B=rigid container; P=pump; P.R.=peripheral resistance.

Bjork, Intonti, and Meissl utilized the positive outcome of this experiment to help establish the importance of simulating left ventricular, left atrial, and aortic physiological dynamics during in vitro evaluation of mitral and aortic cardiac valves. As a result, numerous ensuing AHV studies employed similar mock loop setups. These latter studies often had relatively minor modifications such as a human-shape molded, collapsible rubber sac for the left ventricle and a calf aortic root mold with the Sinus of Valsalva in place of the aortic analogue [21]. In spite of these modifications, the system consistently produced overall static performance results.

Eventually, as a better understanding of natural cardiovascular simulation was developed, several elements of the aforementioned mock circulatory loop were eliminated. Conversely, new components were added such as programmed waveform generators [30]. Johansen et al [25] used a mock loop with an Electric Ventricular Assist Device in conjunction with mechanisms to simulate atrial and venous compliance. While these compliance chambers were not found in the Bjork et al setup, Johansen et al also utilized identical key features such as systemic resistance and a venous reservoir. Pressure tranducers and flow probes were positioned at specific locations in the loop to better monitor and facilitate fluid flow. Lastly, the loop contained a bubble filter to

remove air bubbles from the blood analog fluid that may negatively affect observation results. A diagram of Johansen et al's test system is seen in **Figure 2.5**.

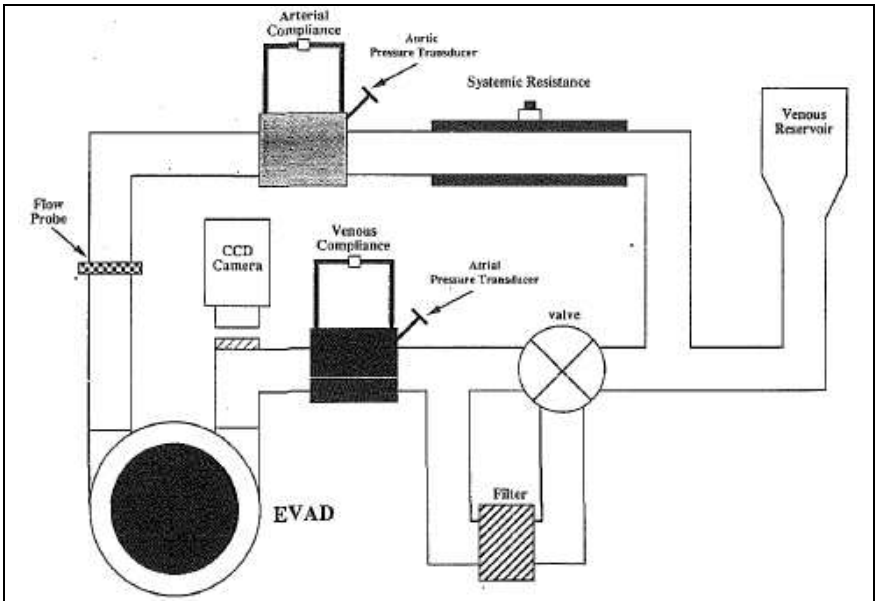

Figure 2.5. [25] Diagram of Penn State EVAD and mock circulatory loop with the location of observation equipment, filter removes air bubbles from blood analog fluid.

Further progression of AHV test arrangements included increasingly more anatomically correct structures. Milo et al [24] used a pulsed flow simulator with anatomically oriented mounts for the mitral and aortic valves that functioned to reproduce physiological conditions.

This simulator is illustrated in **Figure 2.6** and was comprised of five major components, a positive displacement pulsatile pump with a physiologic waveform generator, a left ventricular compartment, a couple of autonomous pressurized containers for systemic compliance and peripheral resistance, and an open atmosphere venous reservoir that was connected to the other components through an adjustable resistance mechanism.

Figure 2.6. [24] Photograph of left heart pulse simulator used for bubble formation detection. LV=left ventriclular sac; MV=mitral valve; MC=mitral channel; AV=aortic valve; AC=aortic channel

The discussed research provides an indication of the vast amounts of AHV mock loop experimental setups. Even as these systems progress, they consistently have the common primary objective of exposing the test AHV to a range of native physiological conditions using a bench top entity. This application is crucial to AHV design characterization. Although the described mock loops accomplish this major system objective, there continues to be room for improvement. The time demands and task intensiveness of manually controlling mock loop parameters suggest significant research progression with automated mock circulatory loop development. In reference to AHV test research, it will advance performance and comparative test methods, especially in conjunction with an AHV holding chamber that permits speedy valve interchangeability.

2.2.3 Flow Visualization

During AHV mock loop and/or test chamber performance analyses, researchers utilize several techniques to capture the observed flow field profile data. Following image capture this information is stored and properly interpreted using a number of computer software. These applications provide better understanding of flow as it correlates to theoretical assumptions and assist in AHV design modification. An early method used by Lamson et al [27] included a specialized pressure transducer to identify valve closure and trigger a strobe flash. The strobe flash contained a photodiode to activate an image capture/storage system with a high resolution CCD camera. In the case of this study, the major issue with this imaging technique was the associated time delay. Therefore, Lamson et al had to calculate and document time delays for all triggering mechanisms and the system as a whole in order to interpret the data in real time. **Figure 2.7** shows Lamson et al's flow visualization system.

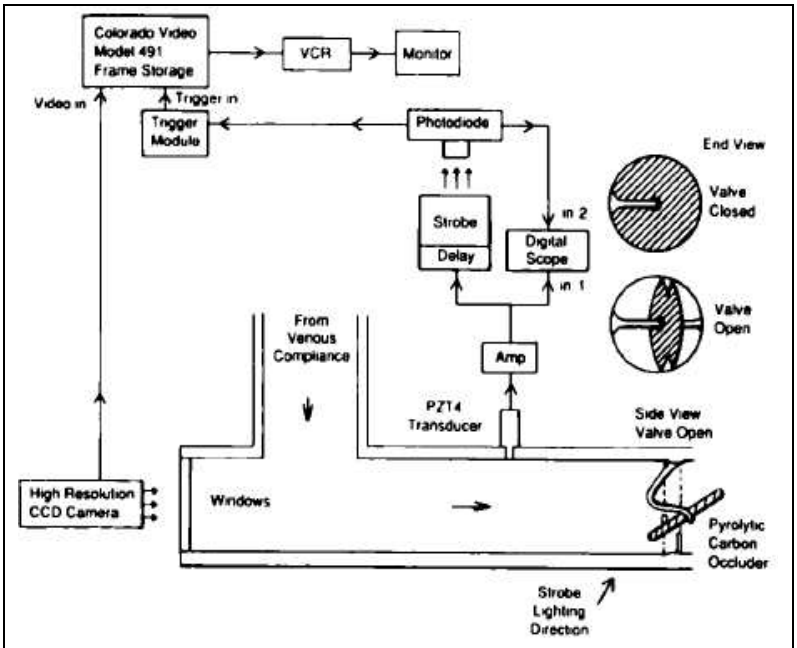

Figure 2.7. [27] Zoom in diagram of valve, viewing port in mock circulatory system, and instrumentation for cavitation observation.

Although Lamson et al were able to use the arrangement described above, there are several other techniques used in AHV fluid flow data acquisition, including hot-wire anemometry, dye tracing, laser Doppler velocimetry (LDV), and particle image velocimetry

(PIV). The latter three are based on indirect flow measurements that track an external agent within the fluid flow, particles or dye [31]. These agents flow with the researched fluid without differing in direction or magnitude from the fluid velocity, which allows for accurate recordings [31]. Hot-wire anemometry uses temperature and electrical resistance.

2.2.3.1 Hot-Wire Anemometry

Hot-wire anemometry is a relatively easy and inexpensive technique that provides extremely high frequency-response and fine spatial resolution; however, the utilized devices are exceedingly delicate. Hot-wire anemometers are devices used to measure the variables occurring in turbulent flows, such as mean and fluctuating velocity components, mean and fluctuating temperature, etc. The sensors are thin metallic elements heated by an electric current and cooled by the incident flow, which acts by virtue of its mass flux and its temperature. From the temperature (or resistance) attained by the sensor, it is then possible to deduce information on the flow. More than one sensor, or more than one value of the heating current, is often necessary to investigate thoroughly a turbulence flow [32].

2.2.3.2 Dye Tracing

Dye tracing uses dye or a chemical reaction to track fluid flow in order to analyze flow patterns. This visualization method provides qualitative data and works best with laminar flow profiles that maintain streamlines for imaging [33]. Turbulent flow profiles mix the dye lines and make characterization very difficult. Dye tracing requires using dye that follows fluid flow without incident, meaning that it has the same density as the investigated liquid [33]. The dye is also injected into the flow field at a rate that is proportional to the fluid velocity [33]. Sometimes

photo dyes are used that fluoresce when encountered by light [33]. Images are captured using a high speed camera to measure the travel distance of the dye.

2.2.3.3 LDV and PIV

The advantages and disadvantages of the LDV and PIV methods have been heavily examined. Browne et al [28] conducted a comparative study of these two techniques via an AHV steady flow investigation. The setups for each process, LDV and PIV, are shown in **Figures 2.8** and **Figures 2.9**, respectively. Three major steady flow elements, vorticity, maximum turbulent principal stress, and maximum turbulent shear stress, were computed using previously formulated equations and data from both the LDV and PIV processes. In comparing LDV data and PIV data, including but not limited to contour plots, Browne et al concluded that PIV imaging works well for purposes of gathering quantitative data in an entire flow field and LDV is better suited for obtaining more accurate, quantitative data in specific, localized areas. They supported this conclusion through their experimental results in which agreement between the two imaging techniques were found in the formation of mean velocity profiles but discrepancies were seen in areas of high turbulence, including locations of maximum normal stress and maximum turbulent shear stress. At these turbulent regions the PIV values were significantly higher than the LDV values; thus, presenting ambiguity when using PIV for turbulent flow applications.

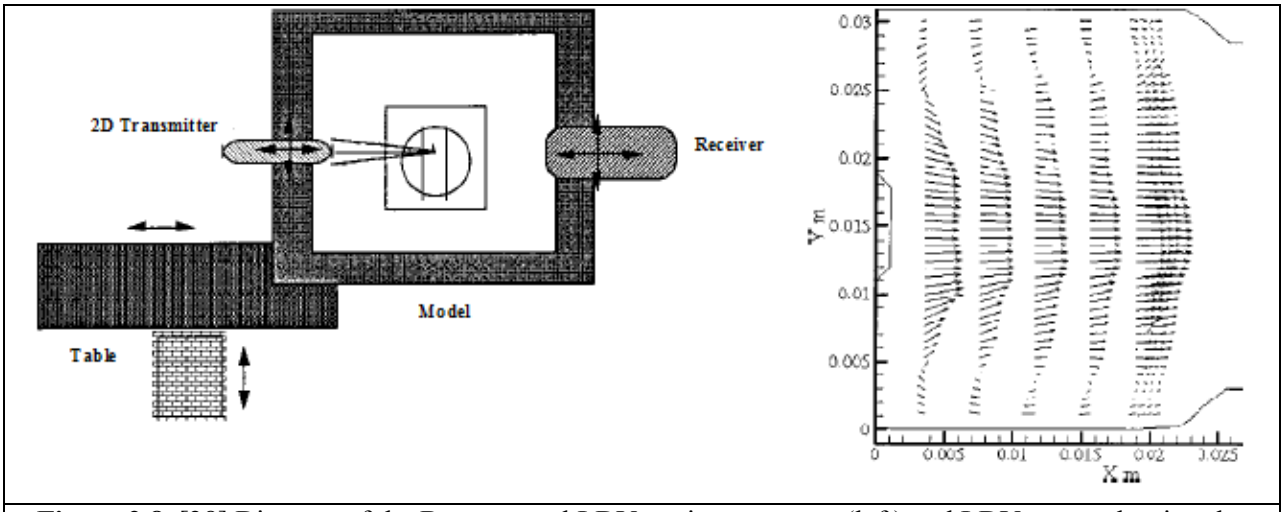

Figure 2.8. [28] Diagram of the Browne et al LDV equipment setup (left) and LDV vector density plot (right).

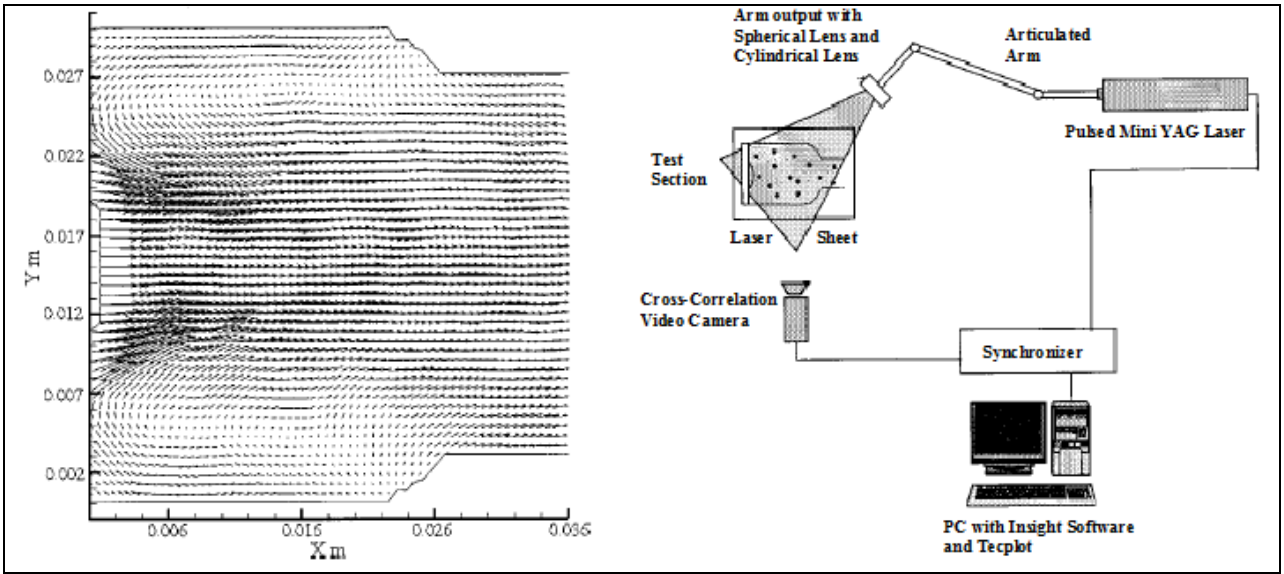

Figure 2.9. [28] Diagram of the Browne et al PIV equipment setup (right) and PIV vector density plot (left).

Based upon conclusions similar to those made by Browne et al concerning the PIV and LDV processes, Kini and company [20] deduced that the best imaging procedure would be one that eliminated the negative aspects of each by combining their positives. They decided to merge the point-based LDV and the plane-based PIV to provide an extremely advantageous flow

analysis that delivered whole-field fluid velocity information as well as high levels of accuracy and resolution. The findings of this study included a clear, spatial illustration of flow patterns associated with valve occluder motion during closure, rebound, and sustained leakage phases as well as local, temporal variations in flow. These PIV and LVD interpretations were key in determining the effects of AHV design on fluid flow, which, consequently, permits prediction of areas that may cause in vivo hemolyisis, thrombosis, cavitation, etc. Accordingly, these LDV and PIV imaging results defended Kini et al's argument that the application of both techniques enhances the ability to interpret flow information when compared to the utilization of either technique independently.

Both the LDV and the PIV procedures are tremendously valuable in AHV performance evaluation research. The combination of these imaging techniques supplies an all-inclusive interpretation of AHV flow fields with both global and localized data. On the contrary, the independent application of either LDV or PIV for flow visualization also provides very beneficial flow data, which can be sufficient depending upon the investigative objectives. For that reason, this research employs the independent PIV image capture method because it provides quantitative information of the entire flow field, which satisfies the thesis goal.

3 METHODS AND MATERIALS

3.1 Mock Circulatory Loop

As previously stated, the implementation of a mock loop to replicate the human circulatory system is essential to AHV testing. Therefore, a mock loop was developed similar to those utilized in prior cardiovascular research studies but with numerous modifications that improve loop test efficiency. **Figure 3.1** depicts the basic components of this mock loop which include a tank to serve as the venous reservoir, quick disconnect mechanisms, a pump to operate as the heart, a heart valve testing chamber, a capacitor and a resistor to represent arterial compliance and peripheral resistance, respectively. These components are connected via 1 ¼" outside diameter (OD) and ¾" inside diameter (ID) tubing that act as the native system vasculature. In addition, several monitoring devices were installed in the mock loop so as to measure a variety of circulatory system parameters. The loop is assembled in a water-resistant wood basin that isolates the loop fluid path in case of leakage. **Figure 3.1** shows the diagram and illustration of the mock circulatory loop. With the exclusion of the heart valve test chamber, design and implementation of these mock loop components were completed by Charles Taylor with help from other members of the Artificial Heart Laboratory at Virginia Commonwealth University [35].

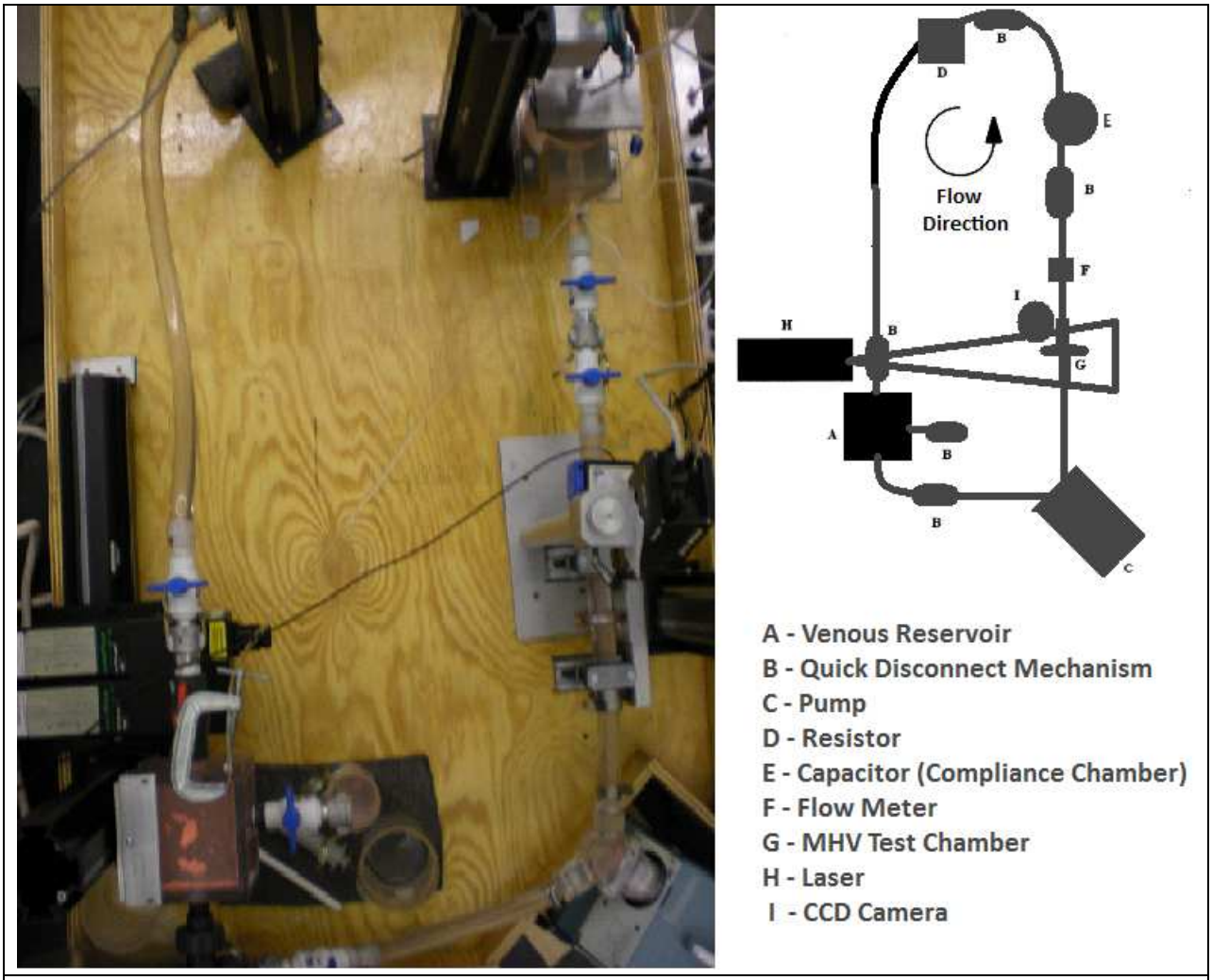

Figure 3.1. Mock circulatory loop.

3.1.1 Venous Reservoir

The container used as the venous reservoir is an acrylic box (6" x 6" x 6") with ½" wall thickness and a top open to the air. **Figure 3.2** shows the acrylic venous reservoir with one inlet and two outlet ports. The inlet port to the reservoir is centered 3" from the top edge along one of the cube faces that lies orthogonal to the open face of the acrylic box. Outlet Port 1, labeled as such in **Figure 3.2**, is located on the cube face directly across from the inlet port in the identical

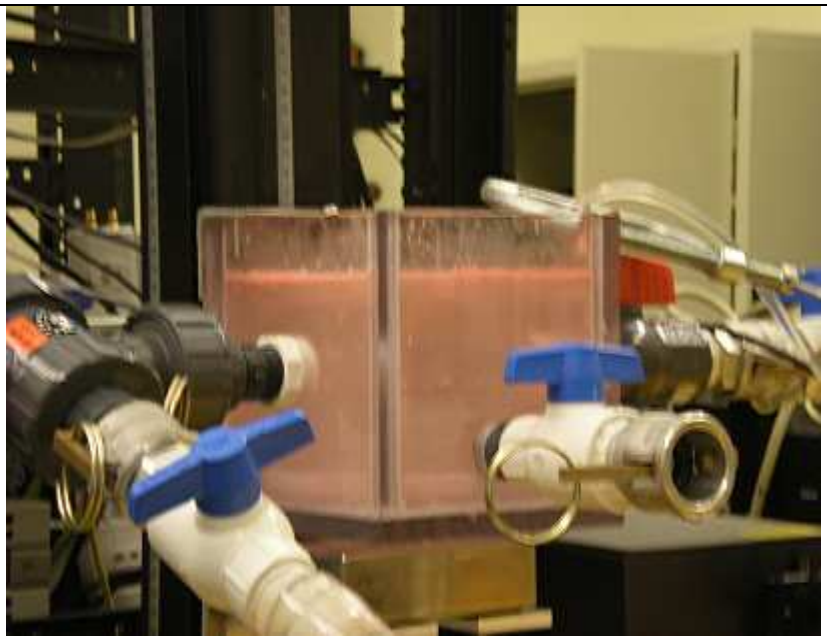

Figure 3.2. Mock loop venous reservoir.

geometric position as the inlet port on its respective cube face. Outlet Port 1 leads to the inlet of the pulsatile pump. The other outlet port, Outlet Port 2 in Figure 2.2, is stationed 1.5" from the bottom edge on an adjacent cube face relative to the inlet port side. This port leads to the inlet of the left ventricular assist device (LVAD), which, if applicable, is the steady-flow multiple disk centrifugal pump (MDCP). The backside of the container, only face without a port, attaches to a support laser rail. **Figure 3.2** depicts the mock loop venous reservoir. The venous reservoir is filled with fluid to a level just above the inlet, to ensure that the entire loop is completely filled and rid of air bubbles. Adjusting the fluid level in the container and/or the height of the container itself will vary the arterial pressure of the system. Lastly, a magnetic stirrer is stationed beneath the venous reservoir in order to maintain a homogenous mixture when required.

3.1.2 Quick Disconnect System

Figure 3.3. Mock loop quick disconnect mechanism.

In between each of the outlet ports and their respective pump is a quick disconnect mechanism, as seen in **Figure 3.3**. The quick disconnects in this mock loop serve as flow facilitators for the system. They provide independent detachment for various loop components without having to drain the entire system. Each disconnect site consists of a metal on metal cam-and-groove hose coupling in conjunction with a low-pressure PVC dual ball valve, which controls flow through the system inner diameter. These preserve the free flow path of the mock loop, while also allowing reasonably swift interchangeability of loop elements without complete system drainage. As a result, the quick disconnect application reduces spillage and diminishes manual effort commonly associated with experimental setup.

3.1.3 Pulsatile Pump

Outlet Port 1 of the system venous reservoir leads to the inlet of the pulsatile pump. The pump in this study, which mimics heart function, is a modified Harvard Apparatus Pulsatile Blood Pump 1423. This self-priming pump is a respected benchmark standard in hemodynamic research that seeks to imitate the large animal cardiovascular system. It features a mechanically

activated piston that oscillates within a clear cylinder hub. The pump design leaves minimal blood cell damage when utilized with whole blood and completely empties the cylinder hub with each stroke, despite the selected stroke volume. It has two caged ball valves located at the inlet, mitral, and outlet, aortic, positions, which facilitate laminar flow through the piston-hub, left ventricle, without incidence. The fluid flow paths of the pump can be dismantled and sterilized when applicable. Stroke volume (SV) and heart rate (HR) are dynamically adjustable during operation with a range of 15 to 100 mL and 0 to 95 beats per minute (BPM), respectively. This research modeled several stroke volume-heart rate combinations at a 50% systolic ratio, where the piston speeds during filling and emptying are identical. These varying conditions are indicative of the wide range of physiological situations. Harvard pump modifications by Charles Taylor et al in the Artificial Heart Laboratory at Virginia Commonwealth University include novel conversion of manual pump adjustments to complete automation. This transformation required preliminary computational studies in order to gain a better comprehension of the pump motor speed profile during several HR and systolic ratio stages [35]. Observation of the piston-driving shunt motor's voltage and current values throughout operation and the systolic/diastolic analog feedback presented an improved understanding of the drive motor in relation to the pumping phase [35]. These introductory investigations assisted in the selection and implementation of a replacement motor driver board that created opportunity for external control of the Harvard Pulsatile Blood Pump 1423. Furthermore, several novel parts were machined and/or purchased and then applied to advance pump automation including a linear slide potentiometer (Panasonic), Spur Gear 32 Pitch (McMaster-Carr), and Compact DC Gear Motor 12 VDC, 50 RPM (McMaster-Carr) for SV manipulation [35]. After successful pump automation development, the system stroke volume and heart rate were calibrated accordingly. Additional

pump alterations include removal of the silicon ball in the outlet pump valve so as to incorporate the tilting disk MHV into the loop farther downstream, which suggests aortic valve native orientation.

3.1.4 MHV Test Chamber

As fluid is pumped out of the Harvard pulsatile pump, it flows into the MHV test chamber. The chamber serves as the center piece for image capture in this research. It holds the test heart valve in position within the mock loop and allows fluid to pass through the device mimicking blood flow from the left ventricle to the aorta via the native mitral valve. The test chamber consists of inlet and outlet polycarbonate tube sections with a middle collar that securely pinches the annulus of the MHV so as to anchor the valve at the designated location. The collar was designed to operate with a 25 mm tilting disk valve, but will theoretically function with any 25 mm MHV type. The collar is comprised of two stainless steel halves with a 1 ½" radius and 0.170" thickness. Each half contains two 100 degree countersink, #8-32 screw through holes, which allows it to fasten to a 1/8" anchor disk that is positioned just proximal to the valve entrance. During complete assembly, the test MHV, tilting disk valve, is wedged between the collars and firmly attached to the anchor disk, which securely keeps the valve in the

correct orientation. 5/16” diameter holes were created to allocate implementation with other mock circulatory loop components and the inlet and outlet connections. The center hole of the collar was constructed to mate with the outer annulus of the valve. **Figure 3.4** shows the SolidWorks model of the collar section with the anchor disk. The MHV test chamber inlet and outlet features are made of 4” polycarbonate tubing with 1 ¼” inner diameter with 1/8” wall thickness. This tube was fixated, using Weld-On adhesive, to a 1/8” thick, 3” diameter polycarbonate disk with 5/16” diameter through holes for bonding to the collar using wide, flat-head #¼-20 bolts with nuts. **Figure 3.4** depicts the exploded SolidWorks assembly model. Computational fluid dynamics were used to simulate fluid flow through the model prior to manufacturing. **Figure 3.5** illustrates the MHV test chamber in the mock loop. Gasket material was placed between all contacting surfaces in order to discourage leaking incidence. In addition, tube holders were utilized at the inlet and outlet sections to stabilize the chamber during imaging.

Figure 3.4. SolidWorks models of 25mm valve collar (top left), inlet/outlet MHV testing chamber (bottom left), and exploded view of MHV testing chamber assembly (right).

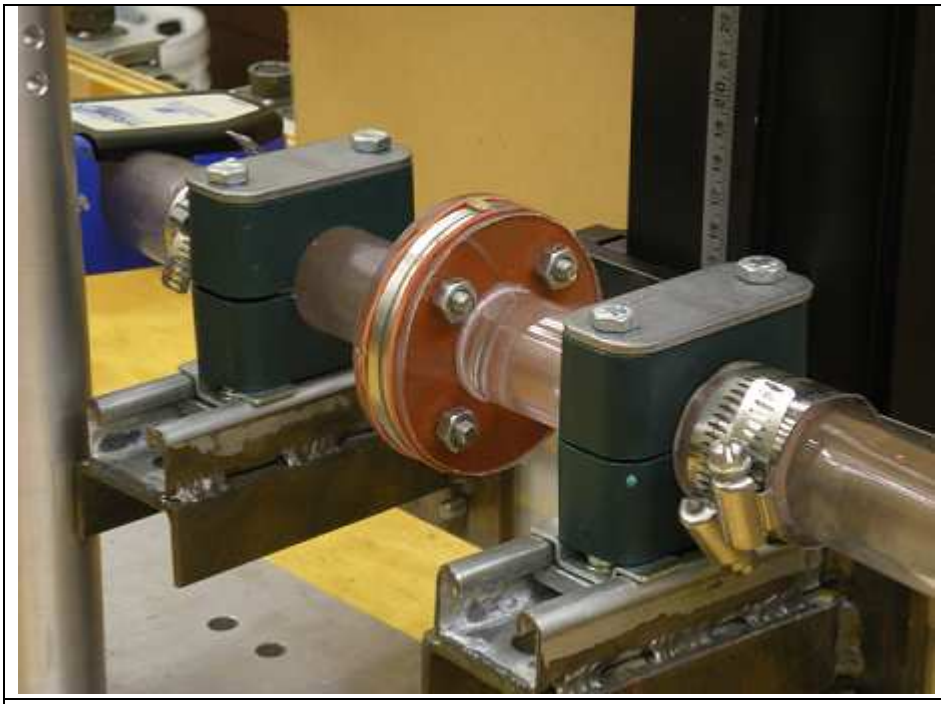

Figure 3.5. Mock loop MHV holding test chamber.

3.1.5 Compliance Chamber

Following closure of the aortic valve, tension forms in the dilated aorta because of the sudden force increase against the aortic wall due to the abrupt change in blood volume and pressure. This tension of the elastic vessel wall propels blood through the circulatory system after it is pumped from the heart. The compliance chamber used in this experimental mock loop is a lumped parameter that emulates the elasticity of all blood vessels in the native circulatory system and is shown in **Figure 3.6**. When the Harvard pulsatile pump

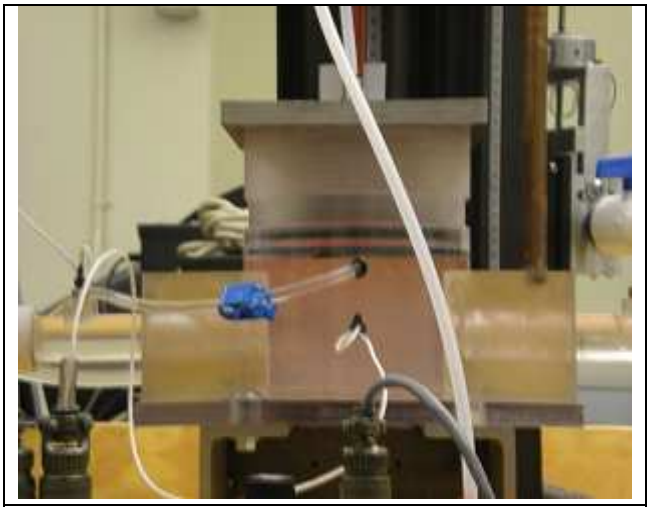

Figure 3.6. Mock loop compliance chamber.

delivers blood to the chamber, during systole, the elastic membrane inside the chamber expands and fluid is temporarily stored until the tilting disk valve closes to allow the pump to fill, during diastole. The stored energy in the membrane then pushes the fluid through the loop. The compliance chamber consists of a 5.5” hollow diameter cylinder with ¾” wall thickness and 6” height. It splits into two sections, top and bottom. The top section contains a ½” metal plate with a pressure valve that feeds and extracts air in and out of the top of the chamber when assembled using a mobile air compressor. This metal plate also has a notched center that adapts with a nonconductive composite toggle clamp that allows for a uniform compression mate of the top and bottom chamber sections. The bottom section has inlet and outlet rigid glass tubing that enables fluid flow in and out of the chamber, in addition to a platform that attaches to a laser rail. Lastly, a supplementary pressure valve in the bottom section is used to expel air pockets from the loop, if needed. During complete compliance chamber assembly, the two sections are separated by a Thera-band membrane cartridge. The Thera-band cartridge pulsates with a consistent elastic behavior as fluid flows through the bottom of the chamber and drives it through the loop, thus mimicking arterial compliance. Air pressure above the Thera-band cartridge, in top chamber section, provides resistance to Thera-band pulsation. As more air is introduced into the top chamber via the pressure valve, opposition to Thera-band movement increases and the membrane becomes more resistant to fluid flow. Furthermore, Thera-band flow resistance is variable with material thickness, which is indicative of its elastic modulus. Different Thera-band thicknesses, denoted by color, were biaxially tested for strength using a MTS machine and developed into the interchangeable cartridges [35]. The combination of digital pressure-control in the top chamber and Thera-band selection permits fast mock loop compliance manipulation.

3.1.6 Resistor

The fluid resistor of the mock loop is shown in **Figure 3.7** and represents the total peripheral resistance of the circulatory system. Increasing or decreasing the resistance of the mock loop increases or decreases the pressure in the compliance chamber, which represents arterial pressure.

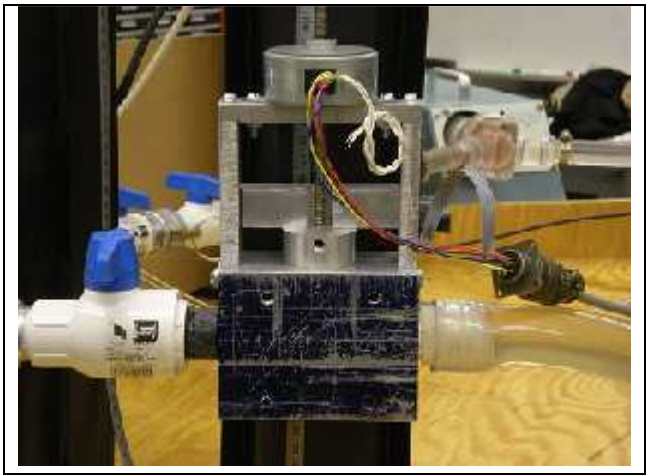

Figure 3.7. Mock loop resistor.

This change in arterial, aortic, pressure modifies the pressure gradient across the aortic valve (transvalvular gradient). A modified transvalvular gradient is a common indication of VHD. The resistor in this loop is made of an aluminum rectangle (4" x 3" x 2") with a ¾" diameter tunnel to facilitate fluid flow within the loop. This tunnel is impeded by a 1 ½" diameter solid aluminum cylinder that translates on a path oriented orthogonally to the flow path. The cylinder is secured to a linear stepper motor made by Anaheim Automation that internally converts rotary motion to linear motion. In doing so it supplies a thousandth of an inch travel per step. The digital adaptability of the motor allows for computational guidance of linearly transverse flow resistance via effective regulation of cross-sectional area [35]. This allows for highly efficient and effective dynamic control of the system resistance, which leads to the formation of physiological pressure conditions indicative of a wide range of pathologies. Fluid flow through the resistor was evaluated using computational fluid dynamics (CFD) prior to implementation [35]. Furthermore,

the range of resistor positions was 0 to 450 with a 0 setting indicating zero flow occlusion and a 450 setting indicating complete flow occlusion.

3.1.7 Instrumentation

Several monitoring devices were present throughout the mock loop. They are used to capture quantitative data during the experimental process such as flow velocity and pressure value.

3.1.7.1 Flow Meter

Flow meters acquire average fluid velocity rates at particular instances in time. The flow meter in this research was a H20XL-Sterile Tubing Flow Sensor manufactured by Transonic Systems Incorporated and is shown in **Figure 3.8**. It clamps around the mock loop tubing and employs ultrasonic transit time technology to measure the time difference of ultrasonic pulses transmitting in and against the fluid flow direction [34]. This time difference is a measure of the fluid average velocity along the ultrasonic beam path and can therefore be used to calculate the averaged fluid velocity [34]. The flow sensor was calibrated to the utilized tubing and water-glycerin blood analog via an investigative test. This test consisted of a small mock loop with reservoir and steady flow pump that drove the blood analog through a section of tubing. The outlet of the pump emptied into a graduated beaker. A fluid volume gradient was selected prior to pump activation start and end volumes. After pump initiation, the time it took for the analog to rise between the start and end volume was manually measured and a flow rate was calculated accordingly. The calculated flow rate was then compared to the calculations of the H20XL-Sterile Tubing Flow Sensor. This procedure was repeated 5 times and the results were averaged

to ensure accuracy and consistency of the method. Following linear fit to produce a calibration formula, the entire flow sensor calibration method was repeated using a higher pumping RPM to produce a variable fluid flow rate. The total calibration consisted of 2 different fluid flow rates replicated 5 times each. During mock loop experimentation, frequency responses and flow rates were acquired between the MHV holding chamber and the compliance chamber inlet in Hertz and L/min, respectively.

Figure 3.8. Mock loop H20XL Sterile Tubing Flow Sensor.

3.1.7.2 Pressure Transducers

Two types of pressure transducers were inserted at numerous locations in the mock loop to provide pressure value measurements at any given time during experimentation. These transducers are pictured in **Figure 3.9**. The Omega pressure transducer (PX203-015G5V) was utilized in a series connection between the inlet and outlet valves of the air compressor to measure pressure levels in the top section of the compliance chamber. It has internal calibration done by the manufacturer with confirmed accuracy. However, this internal calibration was used to develop a calibration formula relative to the proportional opening and closing of the inlet and

outlet pressure valves by reading displayed pressure values at correlating valve opening orifice positions. The other pressure transducers in the loop are made by Entran Sensors and Electronics. They are miniature sensors that are mounted flush against the wall of glass inlet and outlet tubings of the compliance chamber and the bottom section of the compliance chamber. The transducer in the glass inlet tube of the compliance chamber (99G99F22-X14) acquires pressure measurements of fluid prior to entry into the compliance chamber. And the sensor embedded in the bottom section of the compliance chamber gives pressure levels inside the chamber. The transducer located in the outlet glass tube of the compliance chamber was inserted but not used in this research. The Entran pressure transducers were effectively calibrated using a technique that formed calibration formulas from acquired data relating difference in fluid volume with displayed pressure and voltage values. All pressure sensors present data in mmHg.

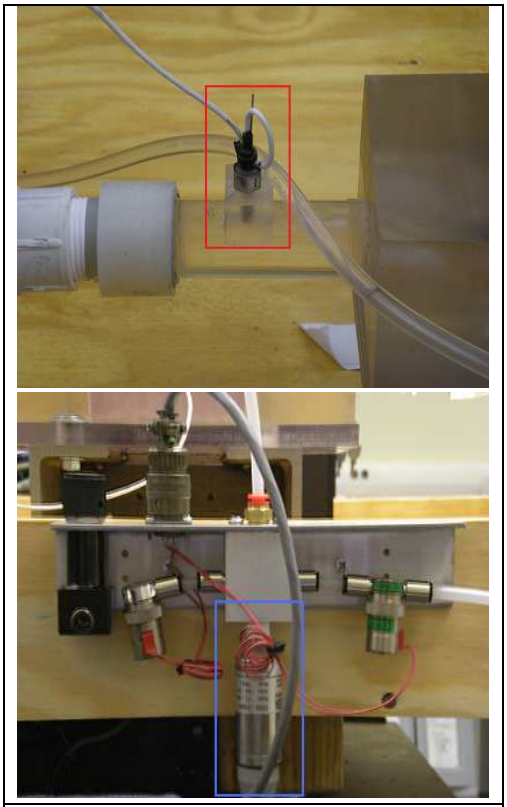

Figure 3.9. Mock loop pressure transducers, Entran (top) and Omega (bottom).

3.1.8 Computer Control and User Interface

Drivers for the loop components are controlled via a single computer workstation. This station links to an electronic control tower that houses all of the system data acquisition circuitry and power supplies. The workstation contains the Labview 8.5.1 virtual instrument developed by National Instruments that serves as the graphical user interface of the system. This software has a

“dashboard” that consists of all the control buttons and simulated waveforms during loop operation. The control tower also has the digital meters of the measurement devices installed throughout the loop. These digital meters convert analog signals to electrical pulses which are transformed to digital outputs via the data acquisition board. Labview uses a data acquisition driver called NI-DAQmx to communicate with the external data acquisition board. The Harvard pump driver utilizes a PIC microcontroller and has a serial to USB cable. The PIC microcontroller was chosen due to its low cost, wide availability, and serial programming capabilities. Lastly, the pressure regulator valves that control the compliance chamber pressure have a control loop feedback mechanism known as a proportional integral derivative, PID, controller. The PID controller calculates an "error" value as the difference between a measured process variable and a desired set point. The controller attempts to minimize the error by adjusting the process control inputs. **Figures 3.10** shows the developed Labview control dashboard.

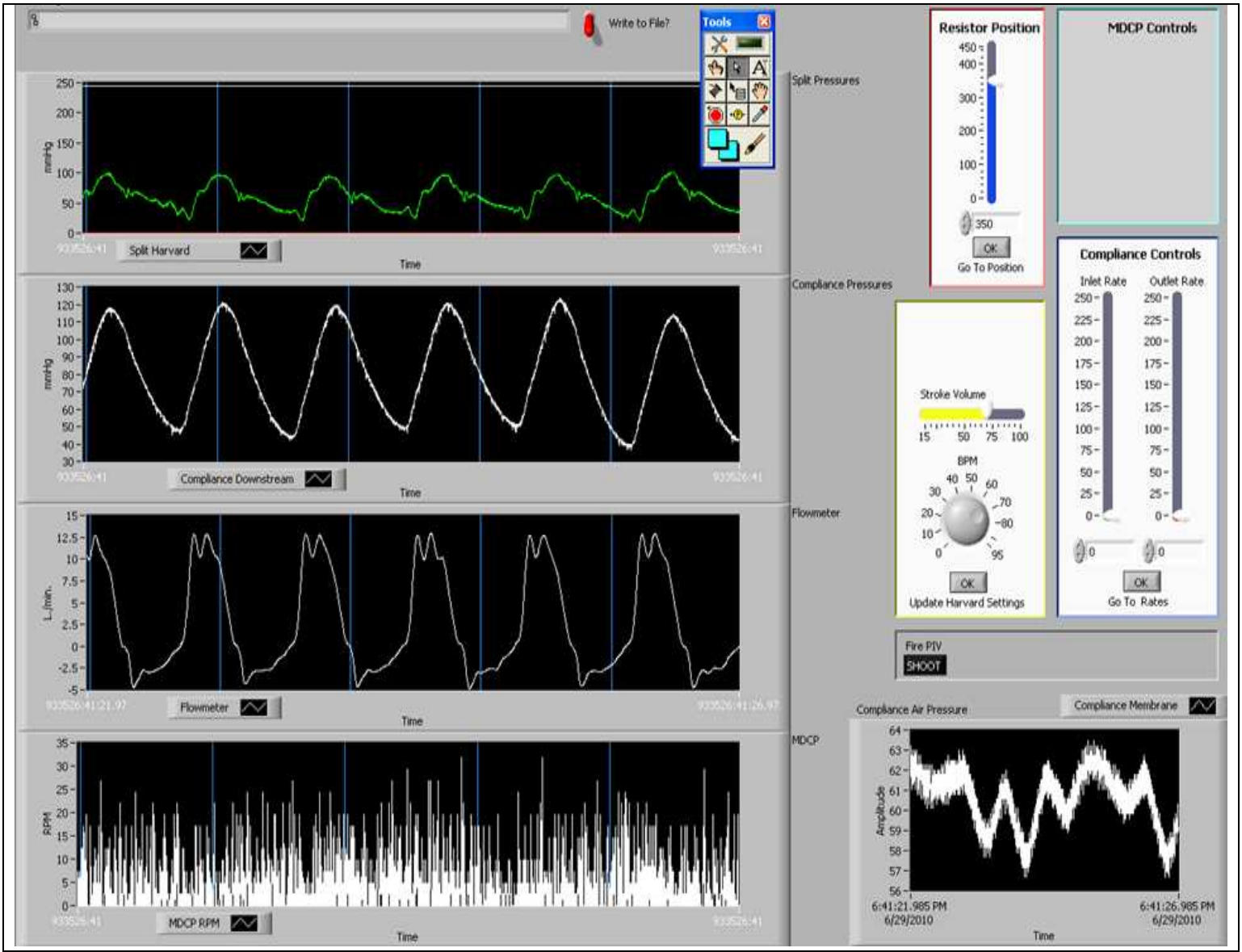

Figure 3.10. Labview control dashboard.

3.2 Blood Analog

The blood analog used in this research was a 60% water and 40% glycerin mixture. This blend is widely utilized in mock loop flow visualization applications due to its prior-validated ability to closely mimic real blood properties, especially density and viscosity. It has a density of

1.122 g/mL and a viscosity of 0.00485 N-s/m^2 (4.85 cP), whereas whole blood has density of 1.06 g/mL and viscosity of 0.0027 N-s/m^2 (2.7 cP) [33]. Unlike whole blood, this substitute fluid provides the advantage of being readily available while eliminating storage issues and blood-borne disease safety concerns. Furthermore, this mixture effectively follows a Newtonian fluid characterization, which is also indicative of whole blood in most arteries [33]. For these instances, whole blood shear stress linearly relates to deformation rate and its viscosity can be assumed to be a constant of approximately 4 cP [33]. The blood analog was mixed in a large glass graduated beaker by liter (600 mL water to 400 mL glycerin). In addition, the refractive indices of the blood analog and polycarbonate tube were matched to reduce light refraction at the test chamber-fluid interface.

3.2.1 Density

Blood analog density was effectively measured via a standard hydrometer, which is pictured in **Figure 3.11A**. This instrument utilizes the Archimedes principle to determine relative density. The Archimedes principle states that the force required to float a solid suspended in a fluid is equal to the weight of the fluid displaced. Therefore, the lower the test fluid density then the further down the hydrometer will sink. The procedure for blood analog density measurement involved of pouring a specific amount of liquid into a graduated cylinder and gently lowering the hydrometer down into the cylinder. Once the hydrometer stabilized in the blood analog fluid, the measurement was read. The hydrometer is made of glass and consists of a cylindrical stem with a mercury-weighted bulb to ensure upright buoyancy.

3.2.3 Viscosity

Following calculation of blood analog density, blood analog viscosity was determined using the density result and an Ostwald viscometer, shown in **Figure 3.11B**. The Ostwald viscometer consists of a U-shaped glass tube with two bulbs and a vertical section that has a precise narrow bore (the capillary). The smaller bulb is located above the capillary section and the larger bulb sits towards the bottom of the other arm in the U-shaped design. The test blood analog was drawn into the small bulb via suction and allowed to flow down into the larger bulb using gravitational forces. Two red marks are positioned on the glass tube, above and below the small bulb, which designates a known fluid volume. As the blood analog flows through the small bulb, from the upper red mark to the lower red mark, the decent of the fluid level is timed via a standard stop watch timing device. Inputting the measured flow time and the previously calculated blood analog density into the following equation yields the blood analog kinematic viscosity.

Viscosity (cP) = drain time (sec) * viscosity constant (cSt/sec) * density (g/mL)

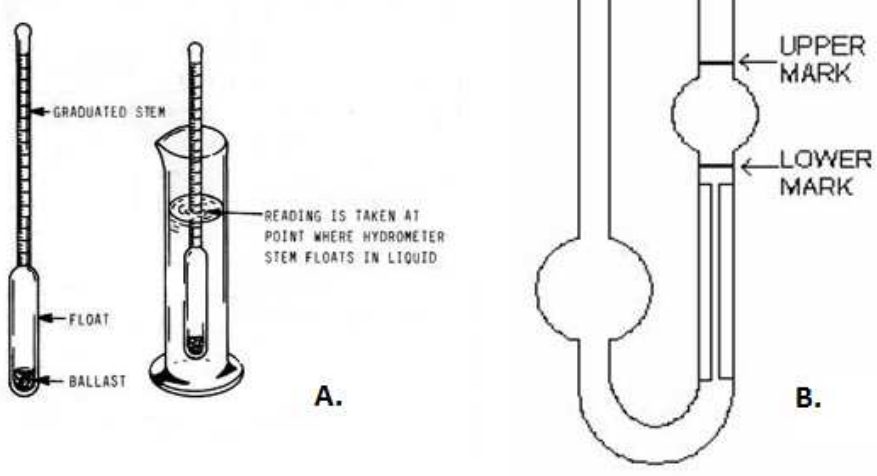

Figure 3.11. Standard hydrometer (A.) and Ostwald viscometer (B.).

3.3 PIV

3.3.1 Hardware

In this experimentation the PIV system was used for fluid flow pattern analysis. A thin and intense laser light sheet was used to illuminate neutrally buoyant particles in a 2D flow field. The particles scattered light from the laser which was imaged using a charged coupled device (CCD). The PIV system combines hardware components with a software application and a typical setup is pictured in **Figure 3.12**. The incorporated hardware includes a laser with power supply, camera, synchronizer, and computer.

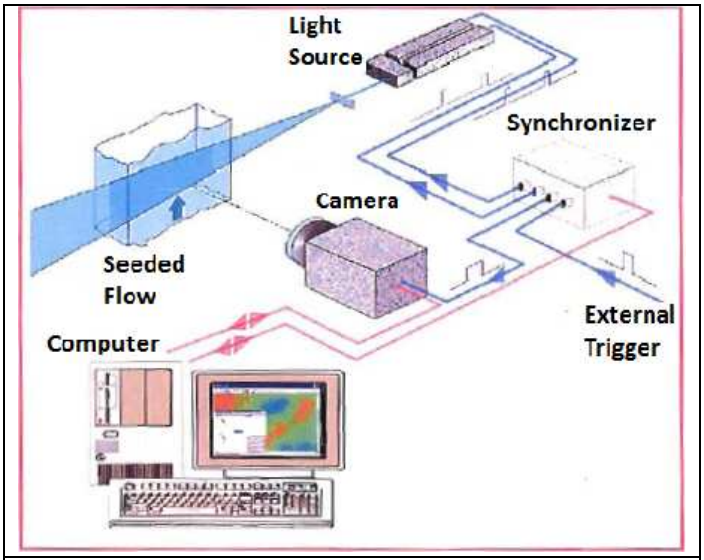

Figure 3.12. [33] PIV system setup.

3.3.1.1 Laser with Power Supply

The laser in this experiment is a dual mini Nd: YAG laser manufactured by New Wave Research. It produces a doubled Q-switched beam by generating short duration (4-20 nanoseconds), high energy (12 mJ) pulsed 532 nm light. The pulse energy is high enough to

illuminate the sub-micron particles in the water/glycerin fluid within the mock loop and the pulse duration is short enough to freeze flow motion. The laser uses a flashlamp mechanism to produce the pulse energy that transforms into the simulated laser beam [37]. The flashlamp firing frequency is 15 Hz. The dual lasers are equipped with power supply units and triggers from New Wave Research and connect to the synchronizer via color-coded connectors that denote the Q-switch and flashlamp.

The generated cylindrical laser beam is converted into a thin lightsheet using optics located in the laser head. The optics consists of a cylindrical lens to diverge the beam in the height direction and a spherical lens to control the lightsheet thickness. The cylindrical lens has a negative focal length, with smaller focal lengths producing faster lightsheet divergence, while the spherical lens focal length is usually much longer [37]. Selection of each lens is done independently of the other and has significant effects on the lightsheet formation. Lightsheet cross sectional area is inversely related to its intensity and light intensity is directly related to particle illumination. So a lightsheet with large cross sectional area will not be able to expose the particles for image capture. For optimal experimental results, the laser is positioned, relative to the imaging area, at the focal distance of the spherical lens [37]. This focal distance is the lightsheet thickness waist, where the lightsheet is thinnest. In addition, lightsheet dimensions greatly influence variation in beam intensity across the imaging area. Hence, a short focal length spherical lens produces a very thin lightsheet but a relatively large intensity gradient, which will not create uniform particle illumination across the image area. The cylindrical lens used in this experiment had a -15 mm focal length and the spherical lens had a 500 mm focal length with 25 mm diameter. Also the laser optics were oriented so as to produce a beam angled at 15.3 degrees

from the horizontal. This optic tilt complimented the tilt of the CCD camera in order to create a laser path orthogonal to the camera lens focal point, which is essential in PIV application.

3.3.1.2 Camera

The system uses a CCD camera, PIVCAM 10-30, manufactured by TSI Incorporated. It captures pictures of illuminated particles in the fluid flow path and, in conjunction with the computer, processes a digital image. The camera functions by converting light energy into electrical energy and generating an electrical signal that is then sent to a Frame Grabber in the computer, where it is digitized [37]. The digitized information is finally passed to the computer system for processing and visualization on the monitor. The PIVCAM 10-30 obtains laser light scattered by particles, with a maximum frame rate of 30 Hz, using a CCD array of 1008 x 1018 pixels. It contains a 550 nm filter attachment that improves imaging and maintains device functionality via background noise filter, glare filter, and CCD saturation avoidance. The 550 nm filter only passes wavelengths above 550 nm. Therefore, for adequate particle illumination light must be scattered at a wavelength above this threshold to be visible [37]. Nikkon AF-Nikkor 28 mm and 50 mm lenses were used during experimentation with camera aperture setting of f/11. Aperture selection is critical for PIV photography because it significantly affects the particle size recorded on the CCD sensor (diffraction limited spot size), the object focus range (depth of field), and particle illumination. Particles used in this research were manufactured by Duke Scientific Corporation. They were hollow glass spheres with 1.05 to 1.15 g/mL density range and 8 to 12 μm mean size range. The PIVCAM 10-30 was operated in triggered exposure mode with a sequenced capture and oriented orthogonal to the laser beam.

3.3.1.3 Synchronizer

The PIV synchronizer is a programmable timing mechanism that is designed to control the operation of the complete PIV system. It is the timing master of the system and manages all timing events needed to make PIV measurements [37]. The PIV measurement process requires that the different system components, camera, the laser flash lamps and laser Q-switches, are precisely time coordinated via the execution of programmed time sequences. These sequences distribute command signals to the camera, laser and other external devices (if applicable). A choice of automatic and manual configurations is available, covering a large range of experimental situations from single image acquisition to multi-sequence image bursts, phase-locked operation, internal or external triggering. In this experiment, the synchronizer was triggered by an external TTL signal that was set to coincide with specific time points in the generated PIV data. Therefore, images were instantaneously matched with correlating pressure and flow curve position. In addition, the synchronizer communicates with the other PIV hardware using TTL signals.

3.3.1.4 Computer

Research utilized a Dell Pentium 4 PC with 512 MB RAM. It contained a 40 GB hard drive and 1.2 GHz processing speed. The computer communicates with the CCD camera via the frame grabber which reads the image from the camera and displays it as a digital image on the monitor. These images are stored in the RAM and processed using the Insight 3.2 PIV software. Also, the computer is connected to the synchronizer by a RS232 serial cable connection.

3.3.2 Image Acquisition and Processing

In order to obtain accurate PIV measurements using the aforementioned hardware, TSI Inc. provided a suggested set of rules in its PIV owner manual [37].

1. The interrogation spot should be small for one vector to describe flow in a single interrogation spot. This will ensure less averaging, less noise, and good spatial resolution.

2. There must be more than ten particle image pairs in an interrogation spot. Fewer particles per interrogation area will decrease the valid detection probability.

3. Maximum in-plane displacement should be less than ¼ of the interrogation spot. This will minimize loss of particle pairs, making more particle pairs available for correlation, which increases correlation peak strength.

4. Maximum out of plane displacement should be less than ¼ of laser light sheet thickness. This will minimize out of plane particle loss.

5. Minimum in-plane displacement should be two particle-image diameters. This rule ensures that a particle pair is identified as two distinct images of the same particle as opposed to one elliptical particle image.

6. The exposure must be large enough to clearly show particles.

During the image acquisition process of this experimentation, compliance of the preceding rules was maintained. This, in addition to other specifics including the frame straddling technique and

utilization of the Insight software, ensured accurate and repeatable fluid flow representation through effective image acquisition and vector plot processing.

3.3.2.1 Frame Straddling

The frame transfer period associated with the 30 Hz CCD camera frame rate limits the minimum time separation between lasers. Hence, high velocity flow analysis is impractical [37]. However this experimentation employs frame straddling to increase the effective frame rate of the PIV hardware. The frame straddling technique uses a synchronized timing function to pulsate the laser at the end of the first camera exposure and again at the beginning of the subsequent exposure. This controlled timing permits the measurement of high velocity fluid flow by shortening the time interval between laser pulses [37]. The timing diagram for frame straddling is shown in **Figure 3.13**.

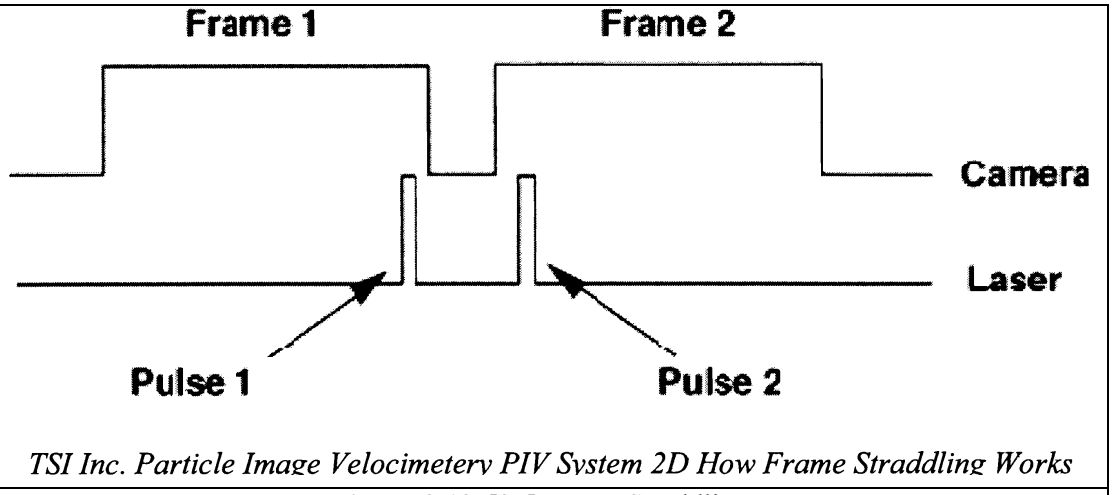

Figure 3.13. [37] Frame Straddling.

As previously stated, the utilized CCD camera has a fixed rate for frame acquisition but the time interval between any two images is adjustable, which allows for accurate representation of the flow field.

3.3.2.2 Interrogation Area Size

In addition to laser pulse time interval tuning, the size of the interrogation area is another major determining factor in image acquisition and processing. Interrogation area size was chosen to minimize noise and increase accuracy. Spatial resolution increases as the interrogation area size decreases; however, lowering the interrogation area size is more conducive to low velocity measurements because higher velocities produce more in-plane particle loss [37]. The 1008 x 1018 square pixels CCD camera provides significant precision to the detail seen in a particular region of interest. The typical size of an interrogation area, as stated by the TSI PIV owner manual, is 32 x 32 pixels [37]. The Insight software offers the user the ability to mask regions within the interrogation area so as to ignore user specified regions during post processing. Once the mask regions are selected the software continues the examination of the remaining unmasked interrogation areas of the paired frames. During processing of these unmasked areas, each particle image is identified and matched to the corresponding image of the same particle across a pair of frames. After identification, their respective locations are computed and compared to one another using an internal correlation function. The size of the pixel array of the interrogation area can be modified using the software, which will change the number of velocity vectors to be calculated.

3.3.2.3 Software

The PIV system utilizes the Insight software to analyze and display velocity vector plots. The software divides and processes digital images of designated interrogation areas within the flow field. Insight determines the number of usable particles and their corresponding locations within the paired frames. These corresponding particle images, within the designated

interrogation areas, are compared via a correlation function that identifies the most common displacement in a given time interval and displays it as a velocity vector. Velocity vectors are shown as graphic overlays across the initial image capture and consist of magnitude and direction information. The Insight software provides several cross correlation algorithm options to choose from during analysis including Fast Fourier Transforms (FFT). This experiment utilizes the HART correlation algorithm that was developed at Massachusetts Institute of Technology [33]. HART correlation presents the ability to compress data and use intensity information more efficiently [33]. It produces four times the number of vectors compared to the frequently used FFT, which enables the system to visualize more detailed fluid flow information [33].

In order to optimize the image capture process, it is critical to select the proper Δt value. The Δt is the time interval between the independently pulsed laser pulses. Δt selection can be done manually or via an internal process conducted by the Insight software that estimates an optimum Δt value. In this experiment a Δt value of 300 μs was used with 25 ms pulse separation. Additionally, post-processing by the Insight software includes the ability to remove flawed vectors using a variety of different filters such as mean, median, standard deviation, and smoothing [33]. Utilization of TecPlot, provides the ability to compute speed, vorticity, velocity gradients, and flow contours [33].

4 RESULTS

The ensuing sections present data acquired by the mock loop pressure transducers and flow meter. This information was displayed, in real-time, on the CPU Dashboard and collected and stored in an Excel file. A total of twelve different heart rate and stroke volume combinations were set with corresponding resistances to maintain a peak systolic pressure in the range of 110 to 140 mmHg. This peak systolic pressure was measured by the pressure transducer embedded within the compliance chamber. The twelve examined combinations are listed in **Table 4.1** along with their corresponding resistor positions. In addition, for each data set a sequence of 20 images was taken by the PIV system at the MHV test chamber location using a 28mm lens. Only images from one complete tilting disk valve opening cycle is displayed for each setup. The CCD camera was operated at a 30 Hz frame rate, which denotes a 33.33 ms time between image captures. Pressure and flow data are displayed for the time scale ranging from 0 to 3 seconds.

Heart Rate (BPM)	Stroke Volume (mL)	Resistor Position
60	70	330
70	70	325
80	70	325
90	70	320
70	50	330
70	60	330
70	80	320
70	90	315
90	55	325
60	60	340
80	80	315
95	80	305

Table 4.1. Experimental heart rate and stroke volume combinations with corresponding resistor position.

4.1 60 BPM at 70mL Stroke Volume

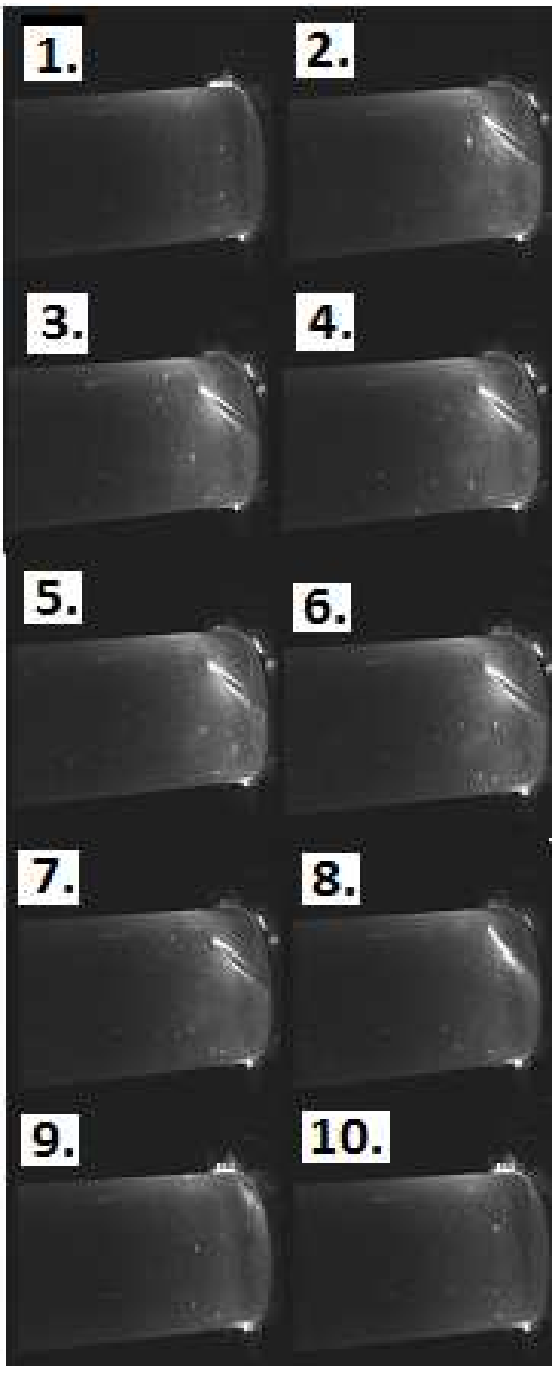

Figure 4.1a. PIV images of one complete tilting disk valve opening cycle for 60 BPM with 70mL SV.

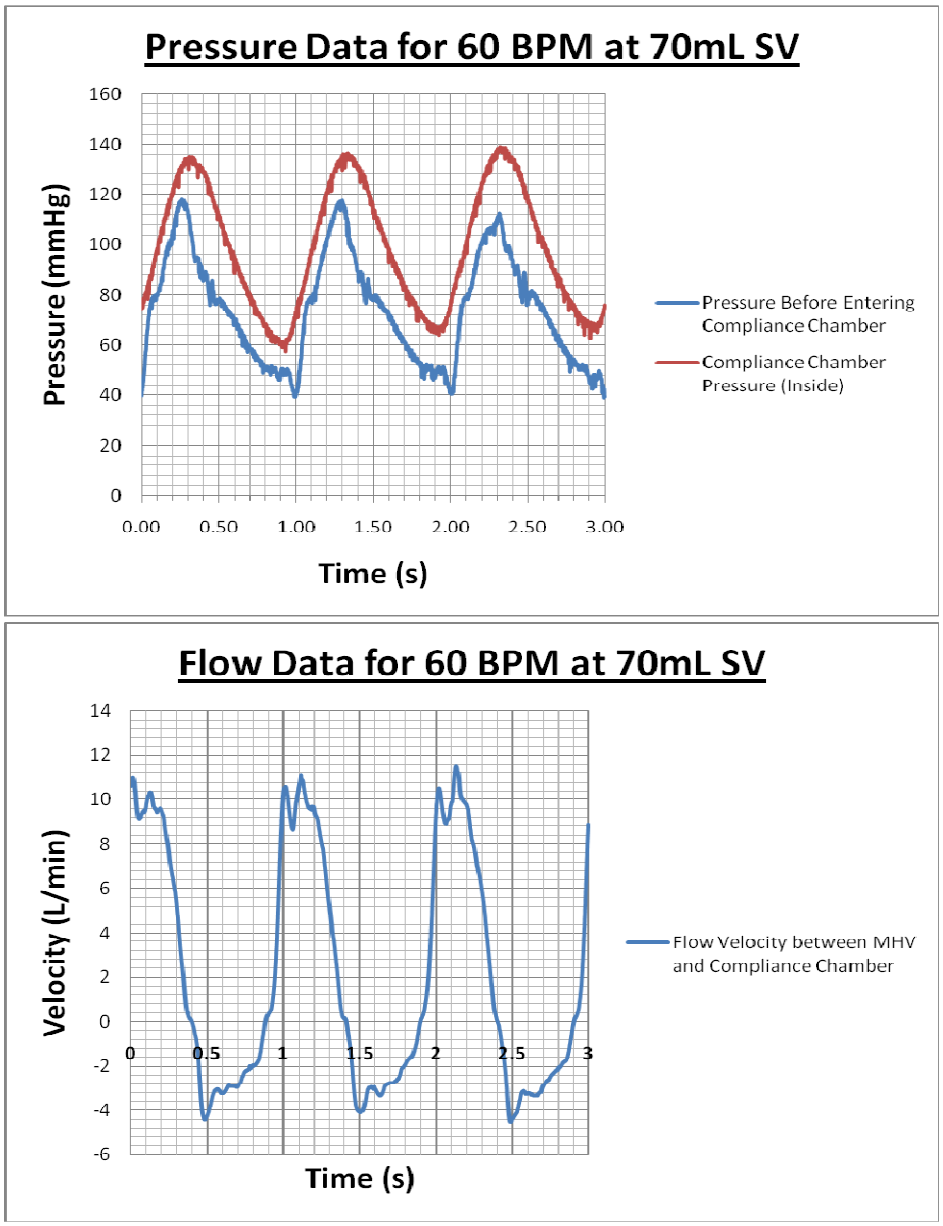

Figure 4.1b. Pressure (top) and flow (bottom) data for 60 BPM with 70mL SV.

The data in **Figure 4.1a** and **4.1b** was acquired while the Harvard pump was set to operate at 60 BPM with a 70mL SV. At this HR, the tilting disk valve successfully completes 60 opening cycles per minute. The Harvard pumping cycle is represented by one full phase in each

of the displayed waves, pressure and flow. The pumping cycle takes 1 second with an average aortic peak systolic pressure at 116.33 mmHg and average minimum diastolic pressure of 39.00 mmHg. These values were measured by the pressure transducer just before entering the compliance chamber (99G99F22-X14), which indicates the natural aortic location. Measurements inside the compliance chamber indicate a mean mock loop system pressure of 137.33/62.33 mmHg. The tilting disk valve opens 0.1 seconds after the minimum diastolic pressure occurs and closes 0.15 seconds after peak systolic pressure. The tilting disk valve is open 0.33 seconds of the pumping cycle. Valve closure is represented by the formulated "dicrotic notch" on the blue pressure wave above, which marks the end of the systolic period. The dicrotic notch is signified by the small downward deflection of the blue pressure wave that occurs at t = 0.45, 1.35, and 2.20 seconds. This small fluctuation in the downward slope of the pressure phase is created by the rebound action of the tilting disk valve, which correlates with the negative flow values seen at t = 0.45, 1.45, and 2.45 seconds on the flow wave. The flow meter measured an average high instantaneous flow rate of 11.20 L per minute during the opening of the tilting disk valve. The cardiac output of the mock loop at these conditions was 4.2 L per minute.

4.2 70 BPM at 70mL Stroke Volume

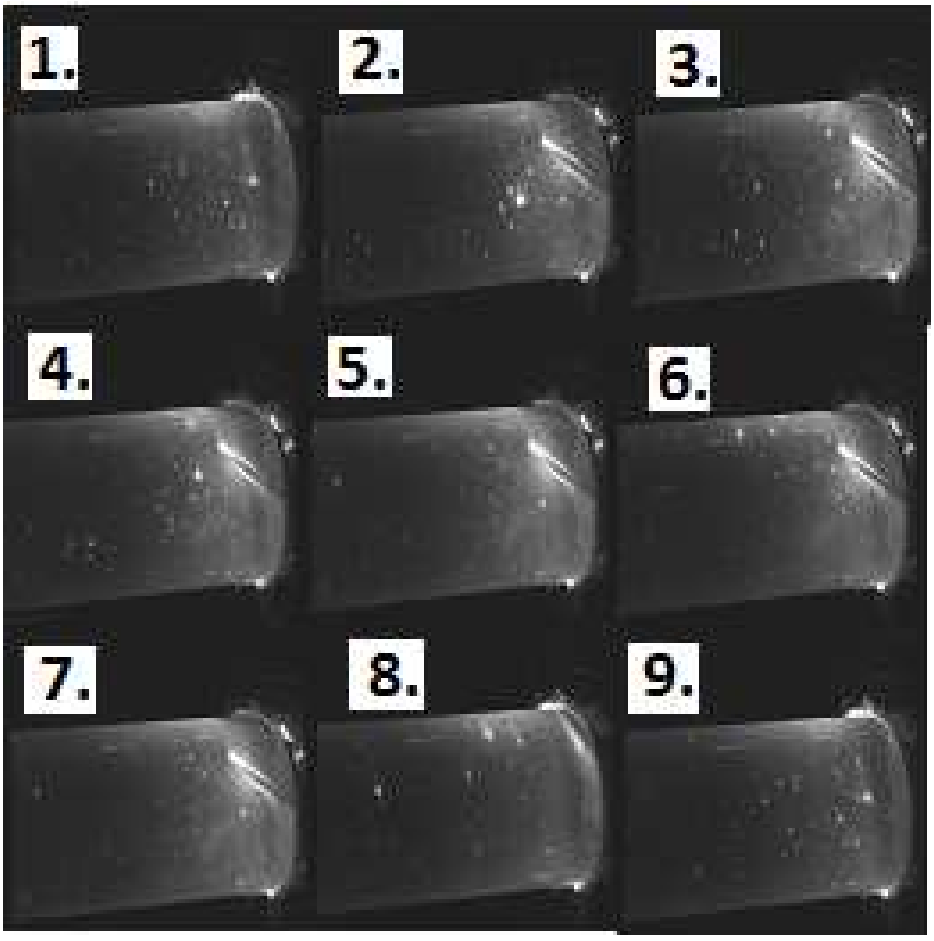

Figure 4.2a. PIV images of one complete tilting disk valve opening cycle for 70 BPM with 70mL SV.

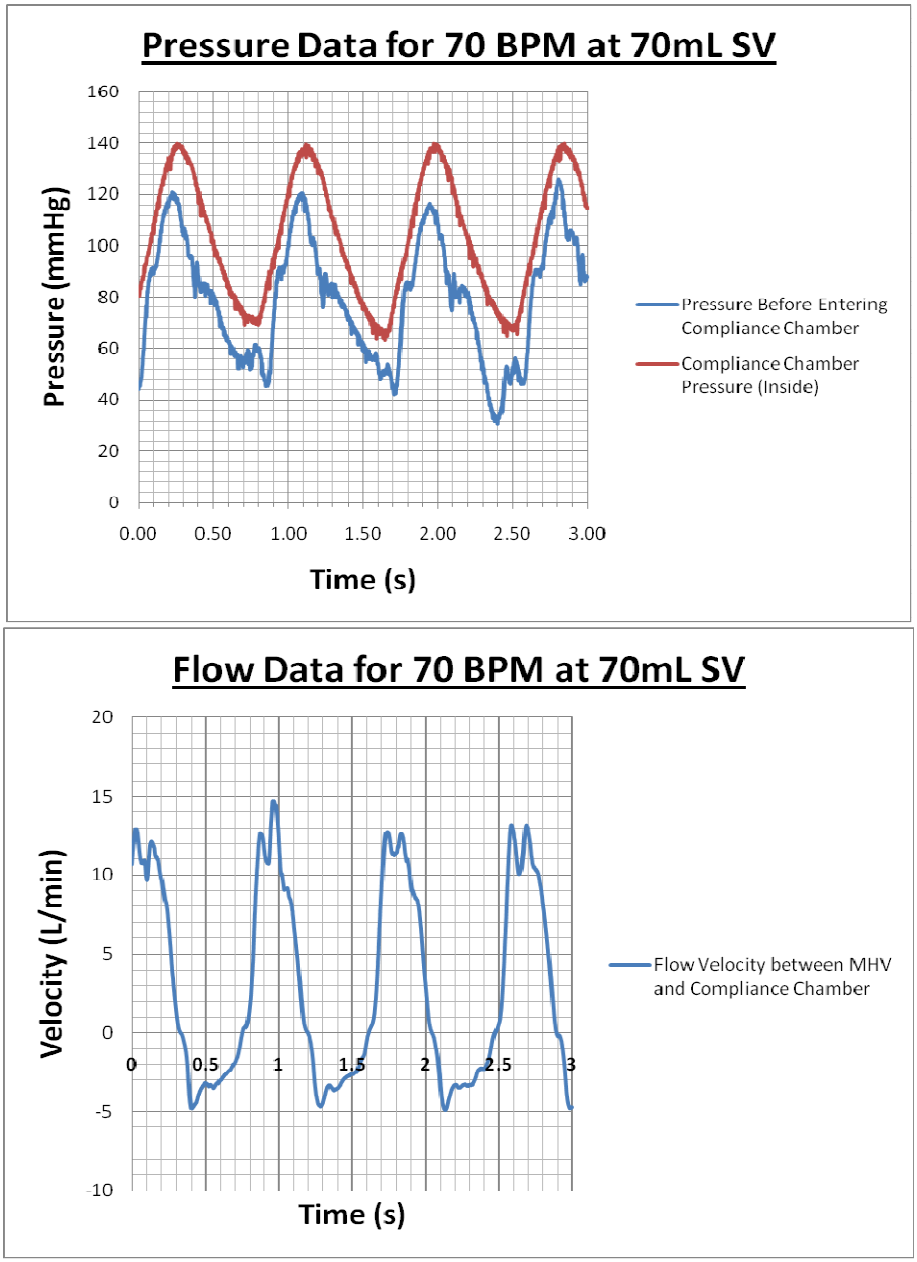

Figure 4.2b. Pressure (top) and flow (bottom) data for 70 BPM with 70mL SV.

Figure 4.2a and **4.2b** displays data when the Harvard pump operated at 70 BPM with a 70mL SV. At this HR, the tilting disk valve successfully opens 70 times per minute. The pumping cycle takes 0.86 seconds with an average aortic peak systolic pressure at 119.33 mmHg

and average minimum diastolic pressure of 44.00 mmHg measured by pressure transducer 99G99F22-X14. Measurements inside the compliance chamber indicate a mean mock loop system pressure of 140.00/66.33 mmHg. The tilting disk valve opens 0.09 seconds after the minimum diastolic pressure occurs and closes 0.13 seconds after peak systolic pressure. The tilting disk valve is open 0.30 seconds of the pumping cycle. The dicrotic notch occurs at t = 0.43, 1.29, 2.15, and 3.00 and correlates with negative flow values seen at identical times on the flow wave. The flow meter measured an average high instantaneous flow rate of 13.375 L per minute during the opening of the tilting disk valve. The cardiac output of the mock loop at these conditions was 4.9 L per minute.

4.3 80 BPM at 70mL Stroke Volume

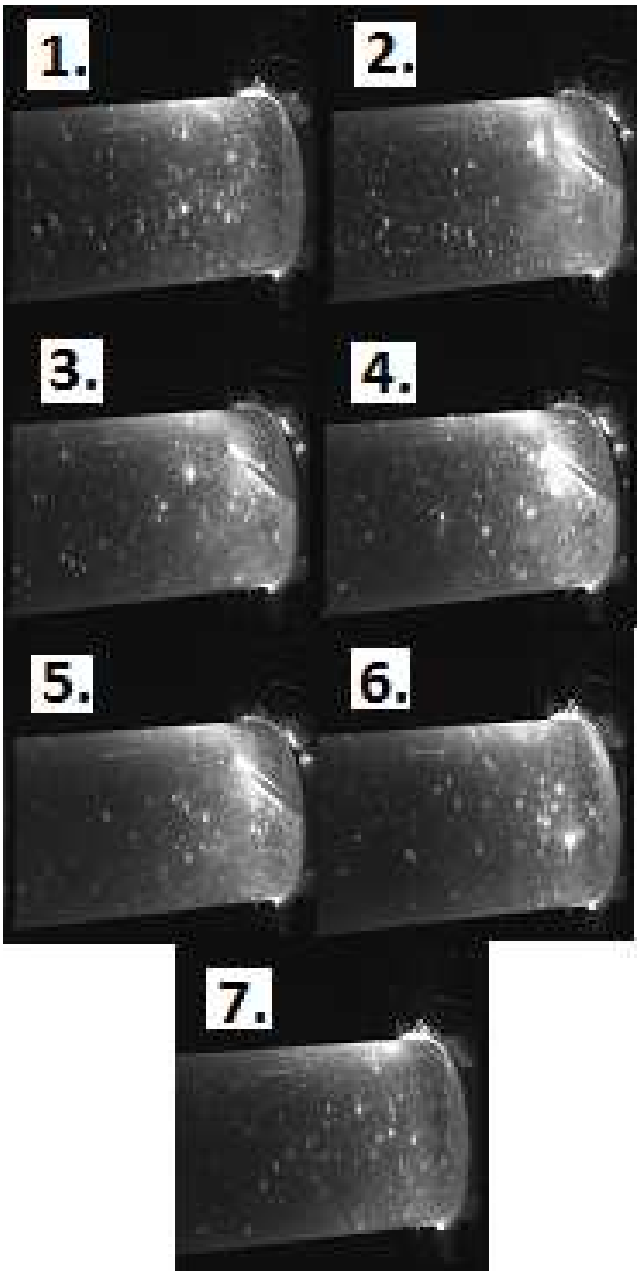

Figure 4.3a. PIV images of one complete tilting disk valve opening cycle for 80 BPM with 70mL SV.

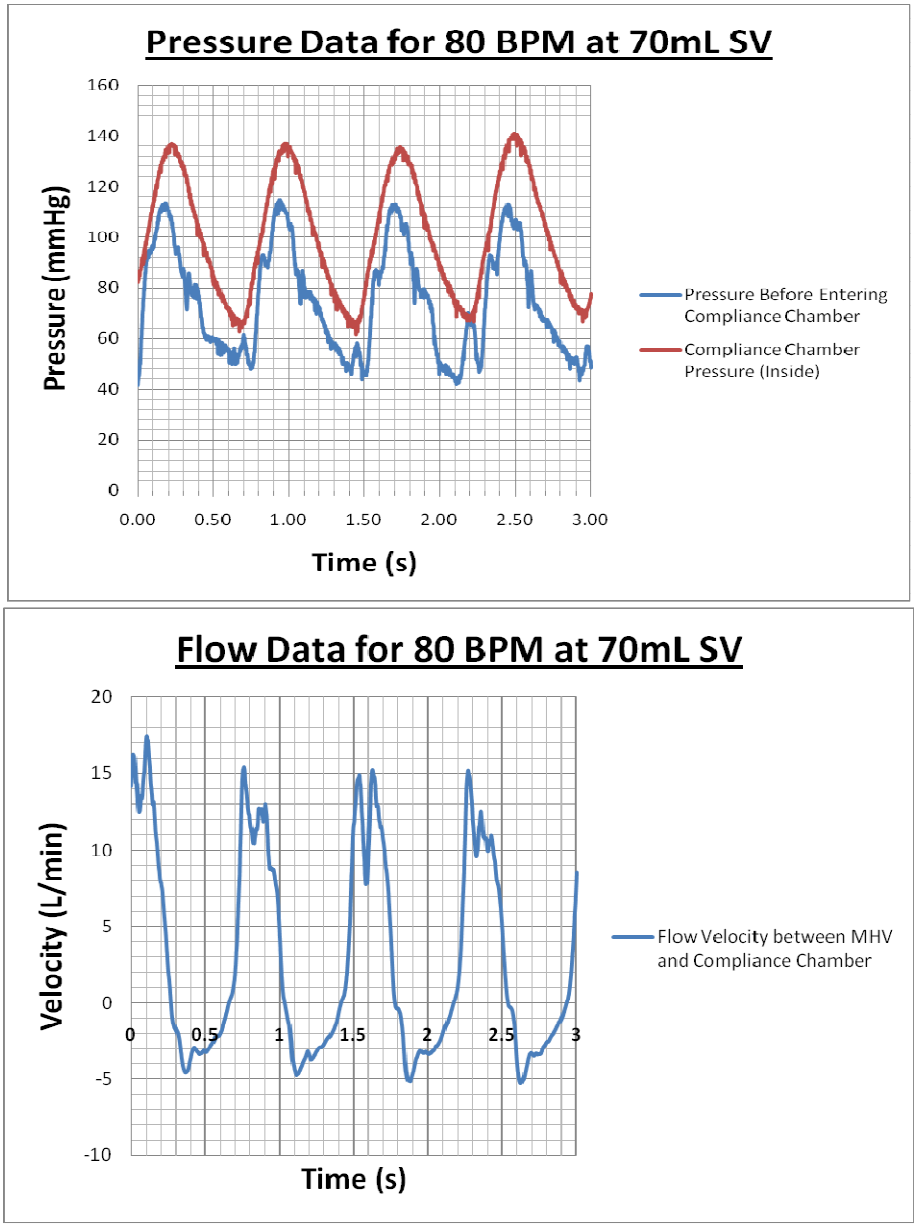

Figure 4.3b. Pressure (top) and flow (bottom) data for 80 BPM with 70mL SV.

Figure 4.3a and **4.3b** above shows information gathered from the Harvard pump operated at 80 BPM with a 70mL SV. This HR and SV combination produces a cardiac output of 5.6 L per minute in the mock loop. The pumping cycle has an average aortic peak systolic

pressure at 119.33 mmHg, average minimum diastolic pressure of 44.00 mmHg, and a total duration of 0.75 seconds with these pressure values measured by pressure transducer 99G99F22-X14. The tilting disk valve opens 80 times per minute. The pressure transducer inside the compliance chamber monitors a mean mock loop system pressure of 135.67/65.00 mmHg. The tilting disk valve opens 0.1 seconds after the minimum diastolic pressure occurs and closes 0.12 seconds after peak systolic pressure. The tilting disk valve is open 0.23 seconds of the pumping cycle. The dicrotic notch occurs at t = 0.35, 1.10, 1.85, and 2.60 seconds and correlates with negative flow values seen at identical times on the flow wave. The flow meter measured an average high instantaneous flow rate of 15.90 L per minute during the opening of the tilting disk valve.

4.4 90 BPM at 70mL Stroke Volume

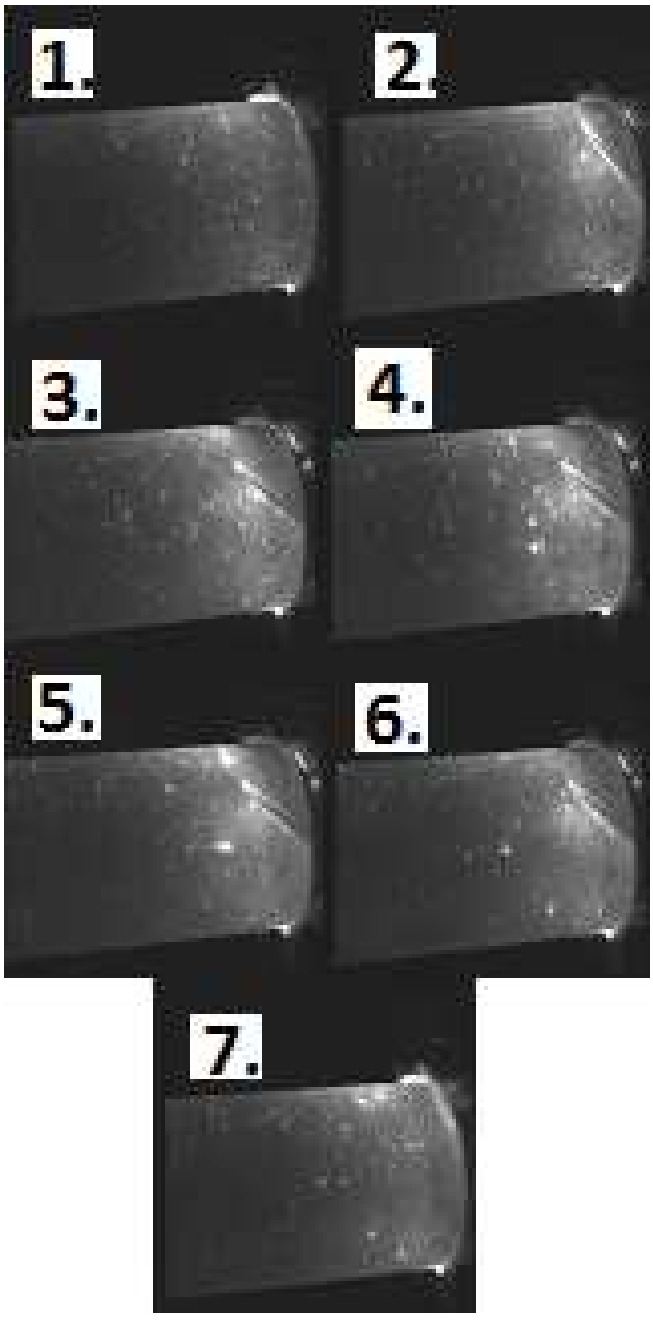

Figure 4.4a. PIV images of one complete tilting disk valve opening cycle for 90 BPM with 70mL SV.

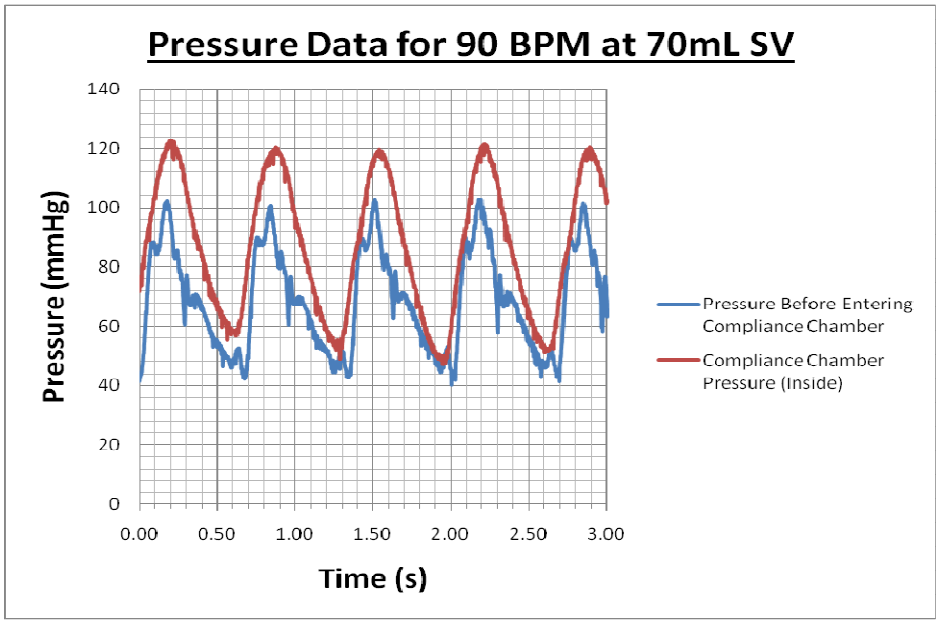

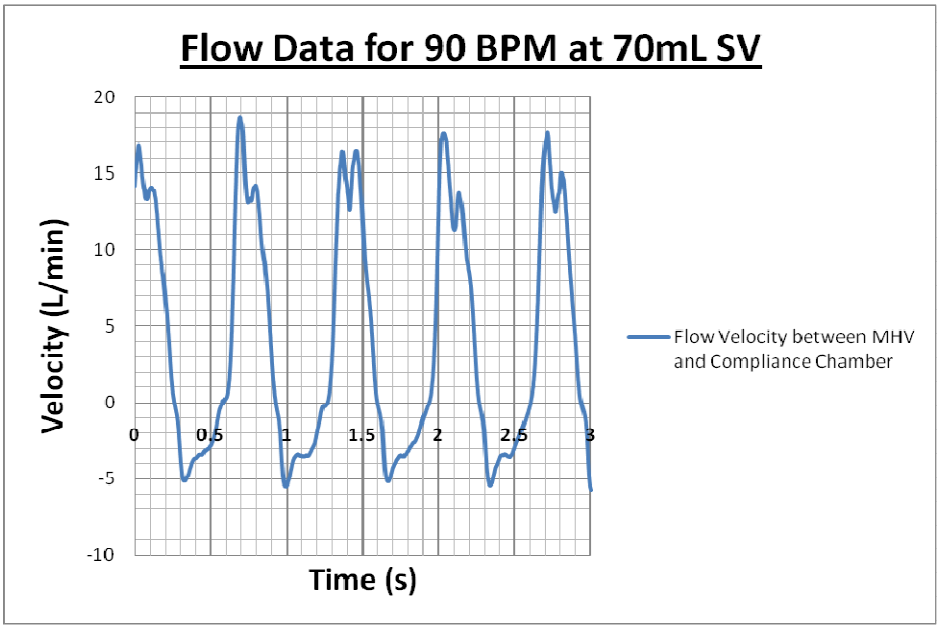

Figure 4.4a. Pressure data (top) and flow (bottom) data for 90 BPM with 70mL SV.

Data illustrated in **Figure 4.4a** and **4.4b** is representative of a 90 BPM, 70mL SV Harvard pump operation. The tilting disk valve completes 90 opening cycles per minute during a 0.67 second pumping cycle interval. The average aortic peak systolic pressure and average

minimum diastolic pressure were 102.00 mmHg and 41.50 mmHg, respectively, measured by the 99G99F22-X14 pressure transducer. Measurements inside the compliance chamber indicate a mean mock loop system pressure of 120.40/52.00 mmHg. The dicrotic notch occurs at the instance of negative flow on the flow wave at t = 0.33, 1.00, 1.67, 2.34, and 3.00. The opening of the tilting disk valve produces a mock loop average high instantaneous flow rate of 17.02 L per minute. The tilting disk valve opens 0.1 seconds after the minimum diastolic pressure occurs and closes 0.12 seconds after peak systolic pressure. One tilting disk opening sequence inhabits 0.22 seconds of the total pumping cycle time. The cardiac output of the mock loop at these conditions was 6.3 L per minute.

4.5 70 BPM at 50mL Stroke Volume

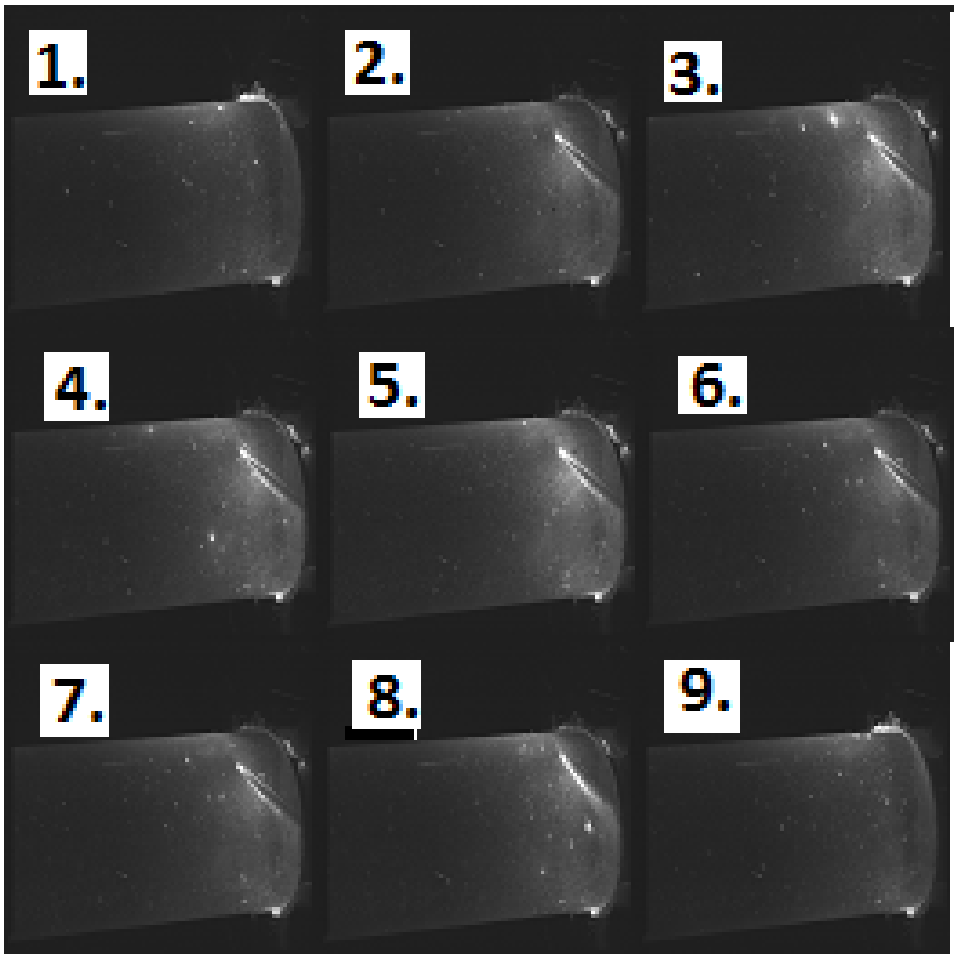

Figure 4.5a. PIV images of one complete tilting disk valve opening cycle for 70 BPM with 50mL SV.

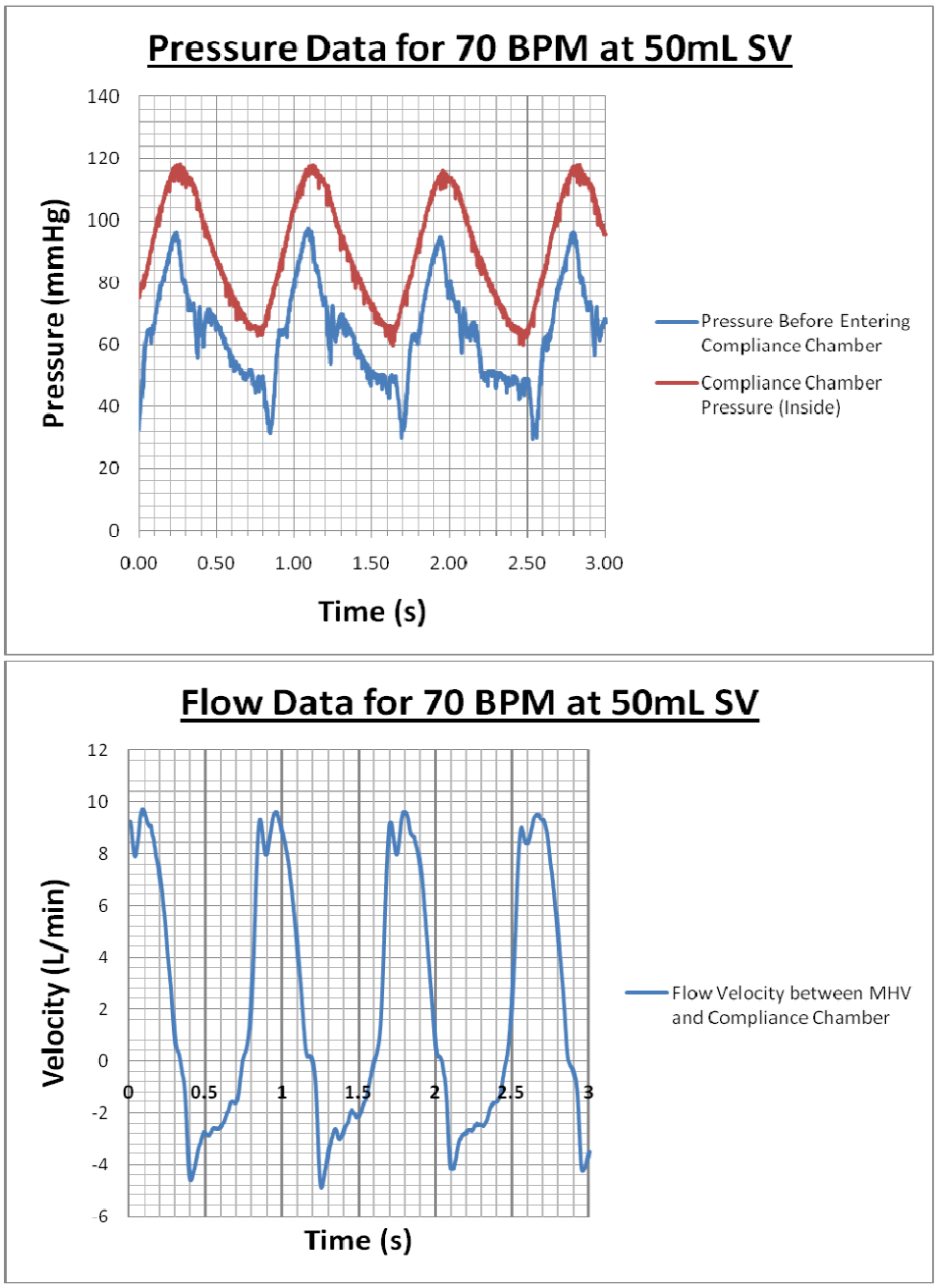

Figure 4.5b. Pressure (top) data and flow (bottom) data for 70 BPM with 50mL SV.

Figure 4.5a and **4.5b** above shows information gathered from the Harvard pump operated at 70 BPM with a 50mL SV. This HR and SV combination produces a cardiac output of

3.5 L per minute in the mock loop. The pumping cycle has an average aortic peak systolic pressure at 96.25 mmHg, average minimum diastolic pressure of 29.67 mmHg, and a total duration of 0.86 seconds with these pressure values measured by pressure transducer 99G99F22-X14. The tilting disk valve cycles 70 times per minute. The pressure transducer inside the compliance chamber monitors a mean mock loop system pressure of 117.50/61.00 mmHg. The tilting disk valve opens 0.1 seconds after the minimum diastolic pressure occurs and closes 0.13 seconds after peak systolic pressure. The tilting disk valve is open 0.30 seconds of the pumping cycle. The dicrotic notch occurs at t = 0.41, 1.27, 2.13, and 2.99 seconds and correlates with negative flow values seen at identical times on the flow wave. The flow meter measured an average high instantaneous flow rate of 9.625 L per minute during the opening of the tilting disk valve.

4.6 70 BPM at 60mL Stroke Volume

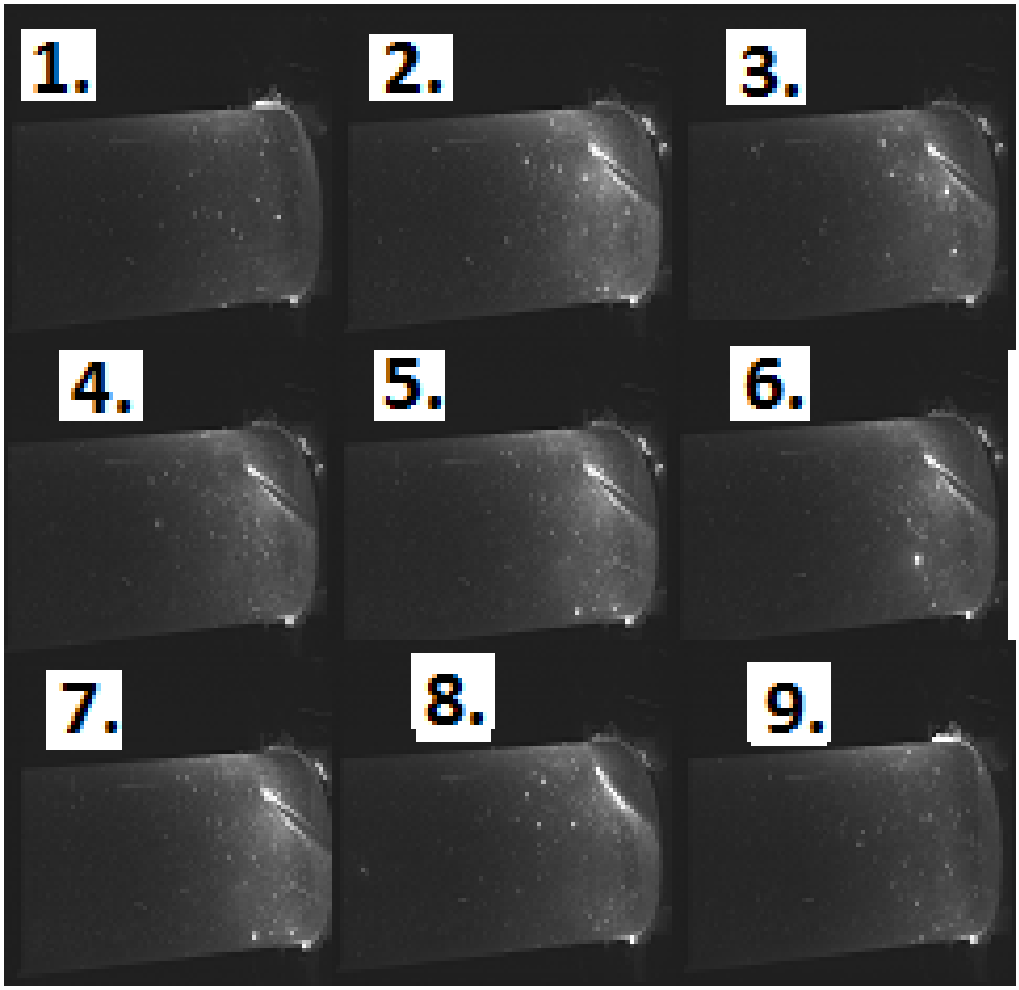

Figure 4.6a. PIV images of one complete tilting disk valve opening cycle for 70 BPM with 60mL SV.

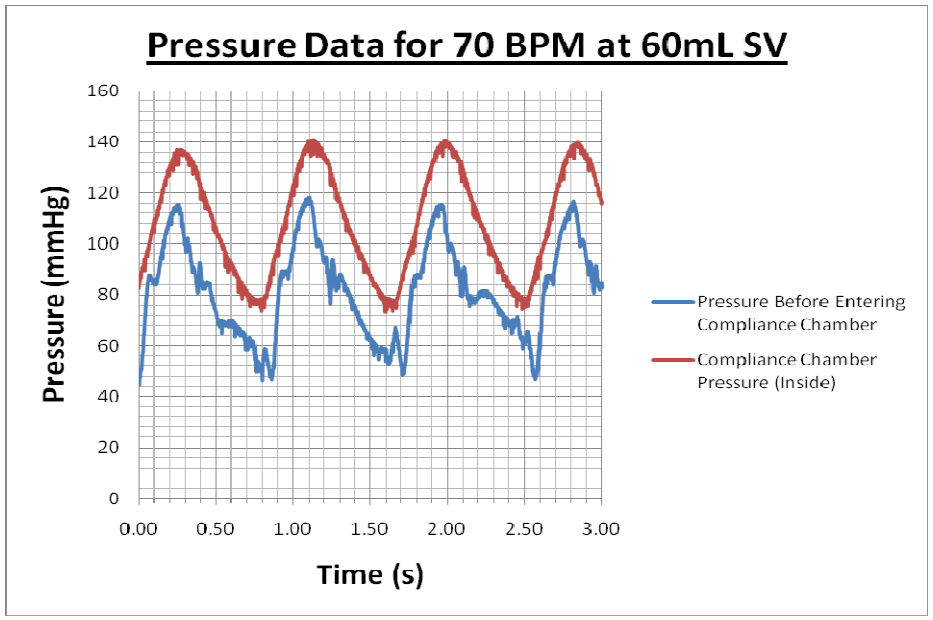

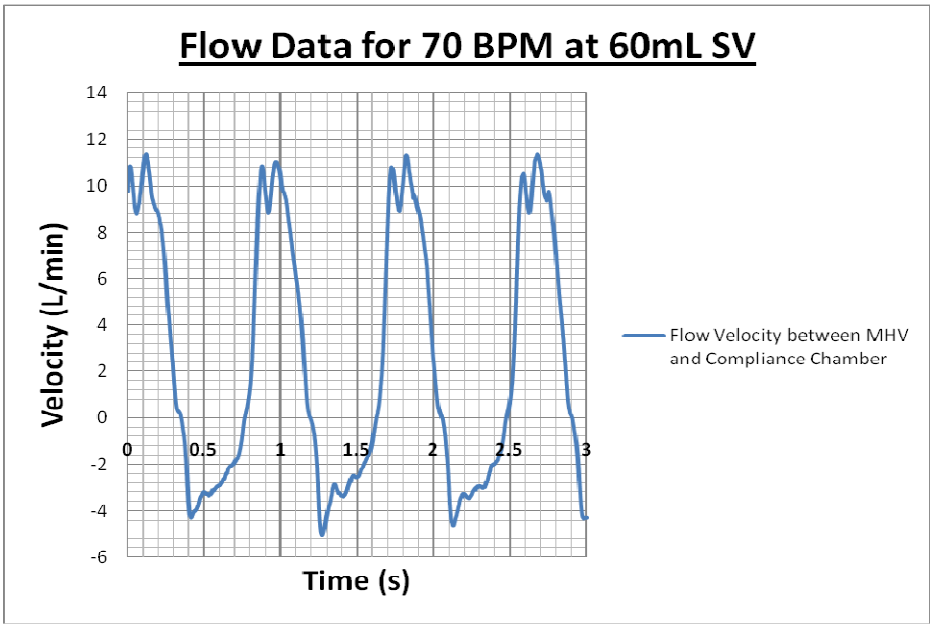

Figure 4.6b. Pressure (top) data and flow (bottom) data for 70 BPM with 60mL SV.

Figure 4.6a and **4.6b** displays data when the Harvard pump operated at 70 BPM with a 60mL SV. At this HR, the tilting disk valve successfully opens 70 times per minute. The pumping cycle takes 0.86 seconds with an average aortic peak systolic pressure at 116.50 mmHg

and average minimum diastolic pressure of 47.67 mmHg measured by pressure transducer 99G99F22-X14. Measurements inside the compliance chamber indicate a mean mock loop system pressure of 139.25/76.00 mmHg. The tilting disk valve opens 0.09 seconds after the minimum diastolic pressure occurs and closes 0.13 seconds after peak systolic pressure. The tilting disk valve is open 0.30 seconds of the pumping cycle. The dicrotic notch occurs at t = 0.43, 1.29, 2.15, and 3.00 and correlates with negative flow values seen at identical times on the flow wave. The flow meter measured an average high instantaneous flow rate of 11.275 L per minute during the opening of the tilting disk valve. The cardiac output of the mock loop at these conditions was 4.2 L per minute.

4.7 70 BPM at 80mL Stroke Volume

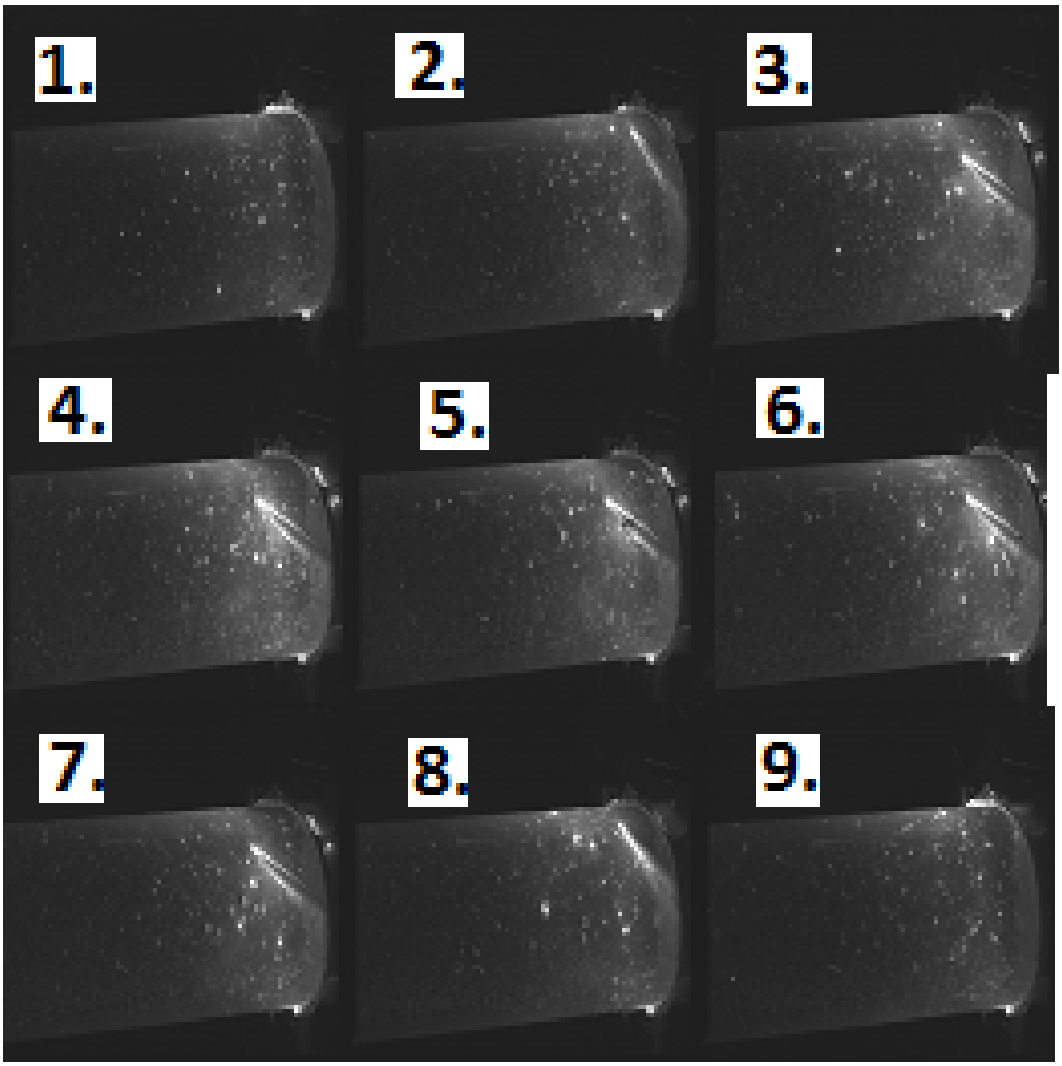

Figure 4.7a. PIV images of one complete tilting disk valve opening cycle for 70 BPM with 80mL SV.

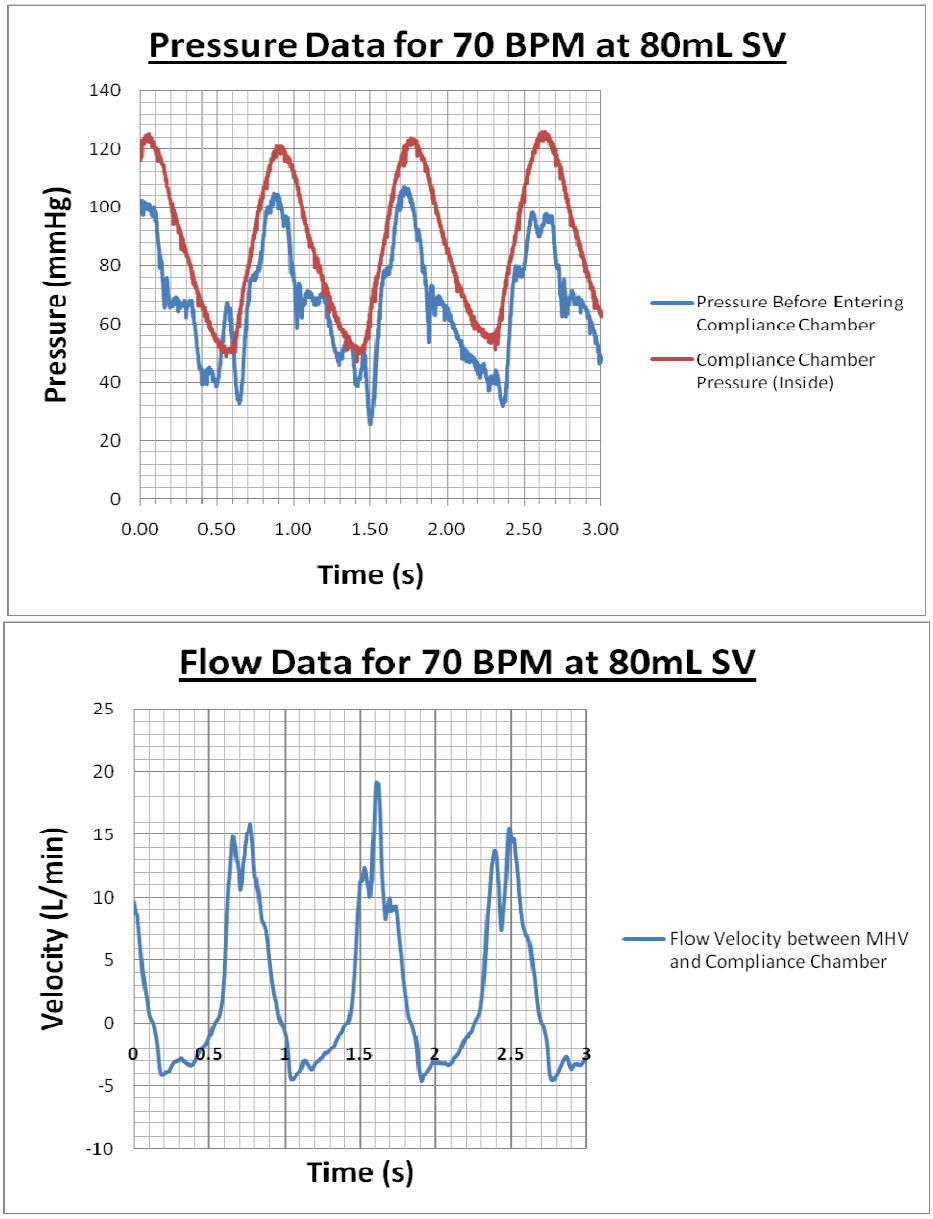

Figure 4.7b. Pressure (top) data and flow (bottom) data for 70 BPM with 80mL SV.

Graphs in **Figure 4.7a** and **4.7b** are representative of a 70 BPM, 80mL SV Harvard pump operation. The tilting disk valve completes 70 opening cycles per minute during a 0.86 second pumping cycle interval. It opens 0.1 seconds after the minimum diastolic pressure occurs and

closes 0.13 seconds after peak systolic pressure. One tilting disk opening sequence inhabits 0.30 seconds of the total pumping cycle time. The average aortic peak systolic pressure and average minimum diastolic pressure were 103.00 mmHg and 30.00 mmHg, respectively, measured by the 99G99F22-X14 pressure transducer. Measurements inside the compliance chamber indicate a mean mock loop system pressure of 124.00/49.33 mmHg. The dicrotic notch occurs at the instance of negative flow on the flow wave at t = 0.25, 1.11, 1.91, and 2.77. The opening of the tilting disk valve produces a mock loop average high instantaneous flow rate of 17.00 L per minute. The cardiac output of the mock loop at these conditions was 5.6 L per minute.

4.8 70 BPM at 90mL Stroke Volume

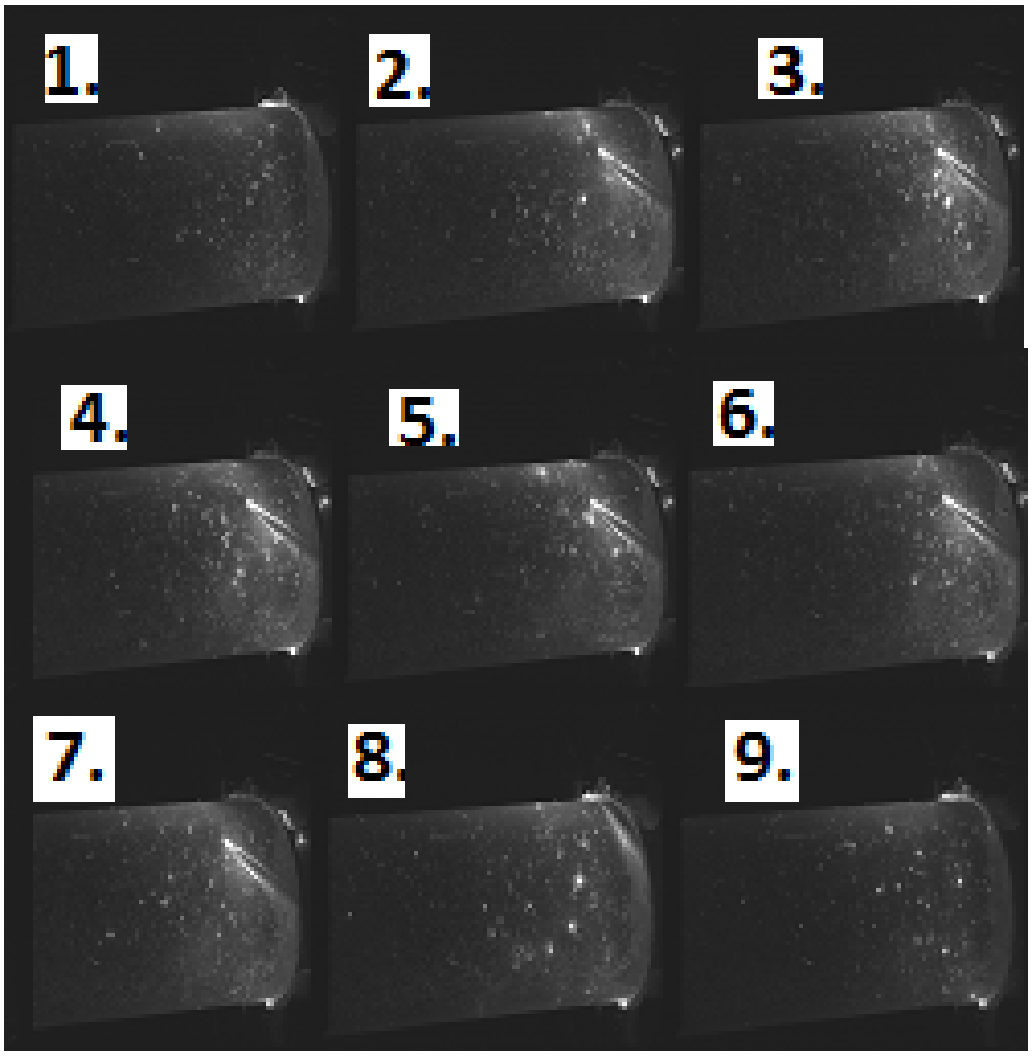

Figure 4.8a. PIV images of one complete tilting disk valve opening cycle for 70 BPM with 90mL SV.

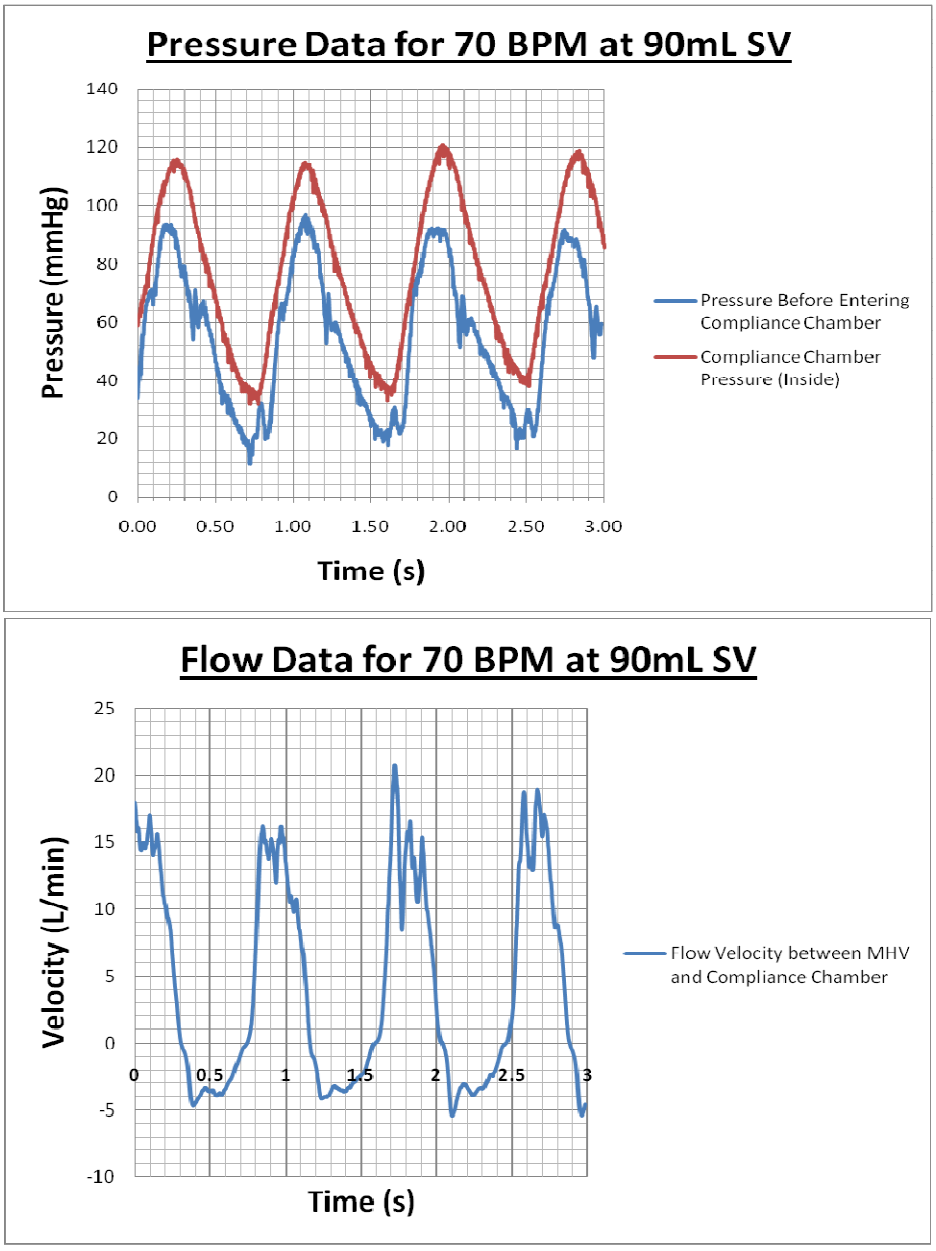

Figure 4.8b. Pressure data (top) and flow (bottom) data for 70 BPM with 90mL SV.

Figure 4.8a and **4.8b** above shows information gathered from the Harvard pump operated at 70 BPM with a 90mL SV. It creates a cardiac output of 6.3 L per minute in the mock loop. The pumping cycle has an average aortic peak systolic pressure at 93.50 mmHg, average

minimum diastolic pressure of 18.00 mmHg, and a total duration of 0.86 seconds with these pressure values measured by pressure transducer 99G99F22-X14. The pressure transducer inside the compliance chamber monitors a mean mock loop system pressure of 117.50/35.33 mmHg. The tilting disk valve opens 0.1 seconds after the minimum diastolic pressure occurs and closes 0.12 seconds after peak systolic pressure. It opens 70 times per minute during a 0.30 second pumping cycle. The dicrotic notch occurs at t = 0.40, 1.26, 2.12, and 2.98 seconds and correlates with negative flow values seen at identical times on the flow wave. The flow meter measured an average high instantaneous flow rate of 18.45 L per minute, which denotes the opening of the tilting disk valve.

4.9 90 BPM at 55mL Stroke Volume

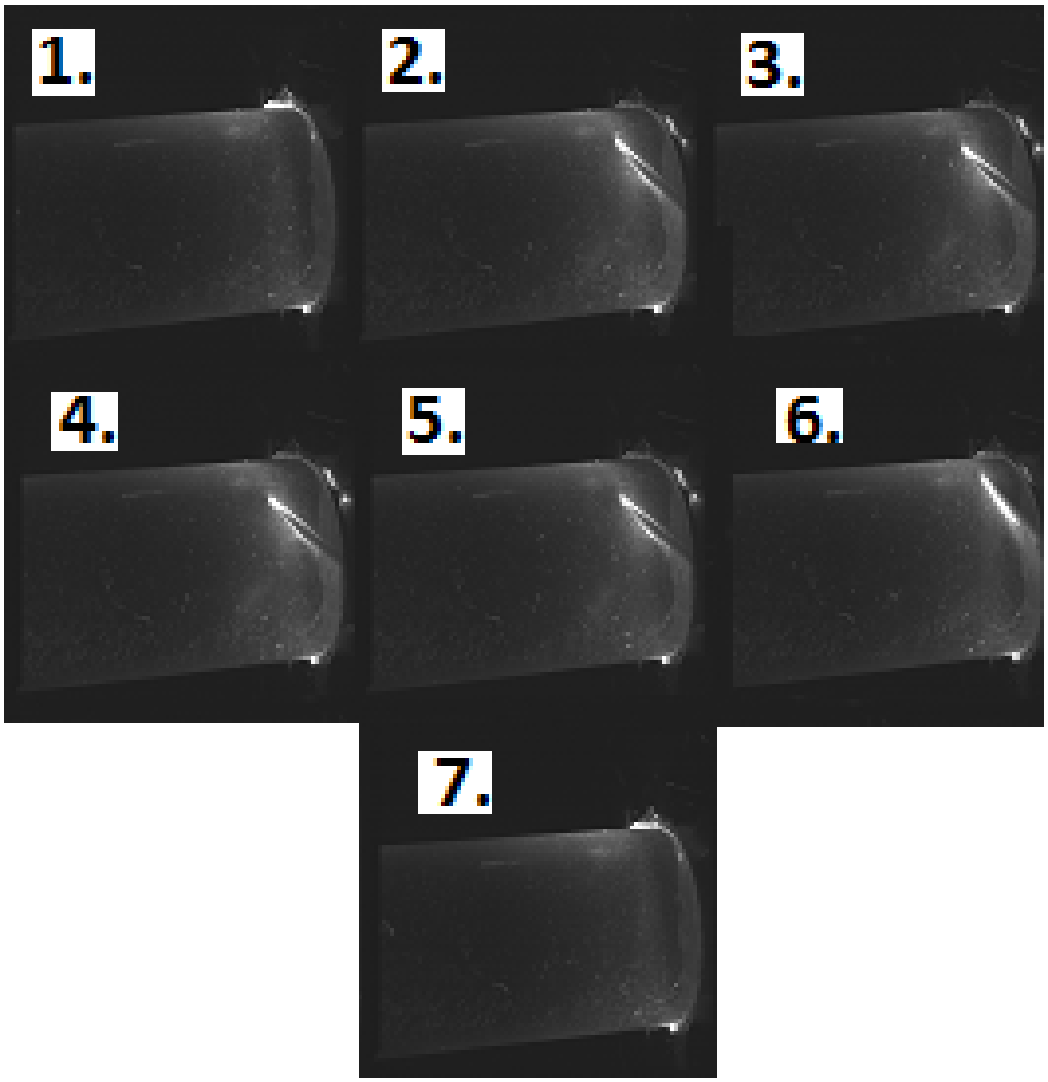

Figure 4.9a. PIV images of one complete tilting disk valve opening cycle for 90 BPM with 55mL SV.

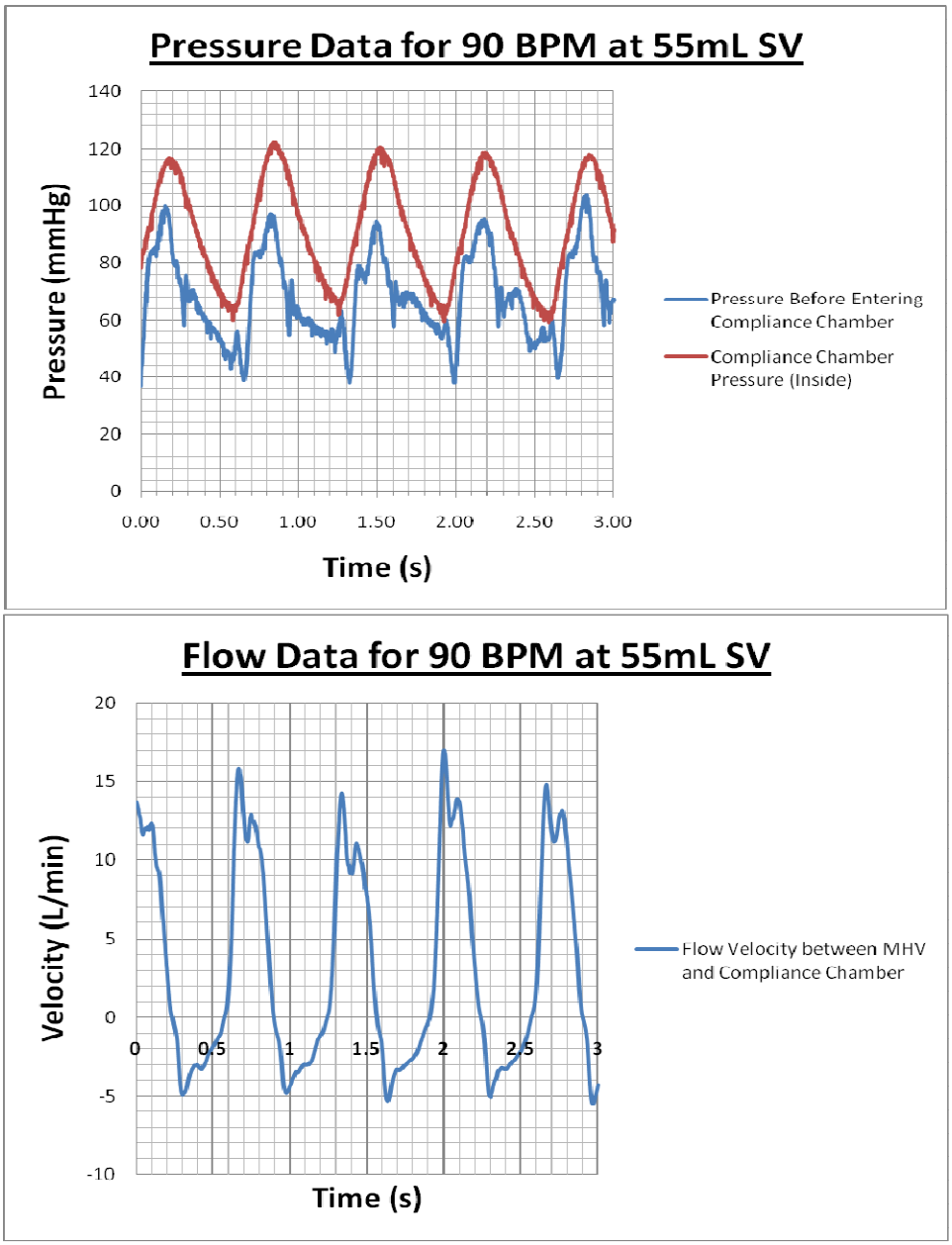

Figure 4.9b. Pressure (top) data and flow (bottom) data for 90 BPM with 55mL SV.

A cardiac output of 4.95 L per minute was created in the mock loop by running the Harvard pump at 90 BPM with a 55mL SV. **Figure 4.9a** and **4.9b** above shows the acquired data. The average aortic peak systolic pressure of the pumping cycle is 98.60 mmHg and average

minimum diastolic pressure was 38.25 mmHg measured by pressure transducer 99G99F22-X14 at the mock loop aortic location. One pumping cycle lasted 0.67 seconds and contains one valve opening phase; the tilting disk valve opens 90 times per minute under these conditions. The valve opens for 0.22 seconds during the pumping cycle where initiation occurs 0.1 seconds after the minimum diastolic pressure and closure 0.13 seconds after peak systolic pressure. The pressure transducer inside the compliance chamber registers a mean mock loop system pressure of 118.40/62.25 mmHg. The dicrotic notch and negative flow regions occur at t = 0.31, 0.98, 1.65, 2.32, and 2.99 seconds. The flow meter measured an average high instantaneous flow rate of 15.55 L per minute during the opening of the tilting disk valve.

4.10 60 BPM at 60mL Stroke Volume

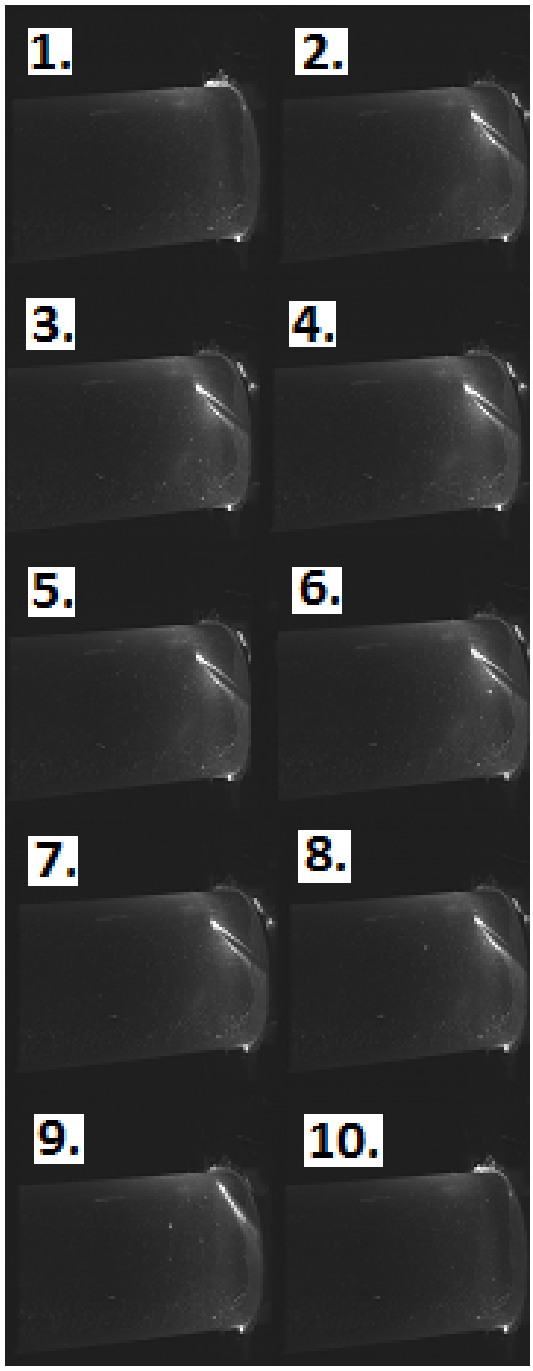

Figure 4.10a. PIV images of one complete tilting disk valve opening cycle for 60 BPM with 60mL SV.

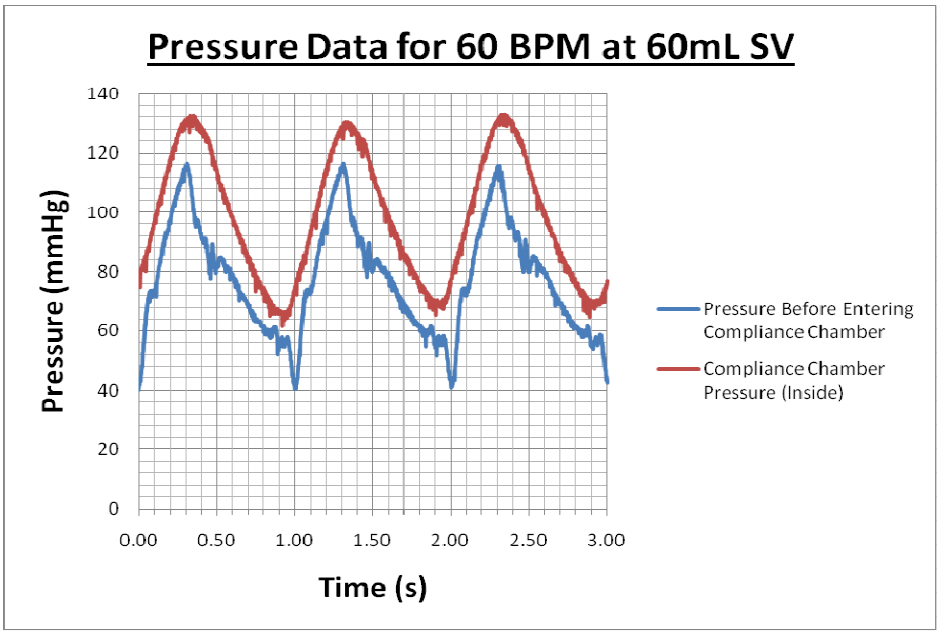

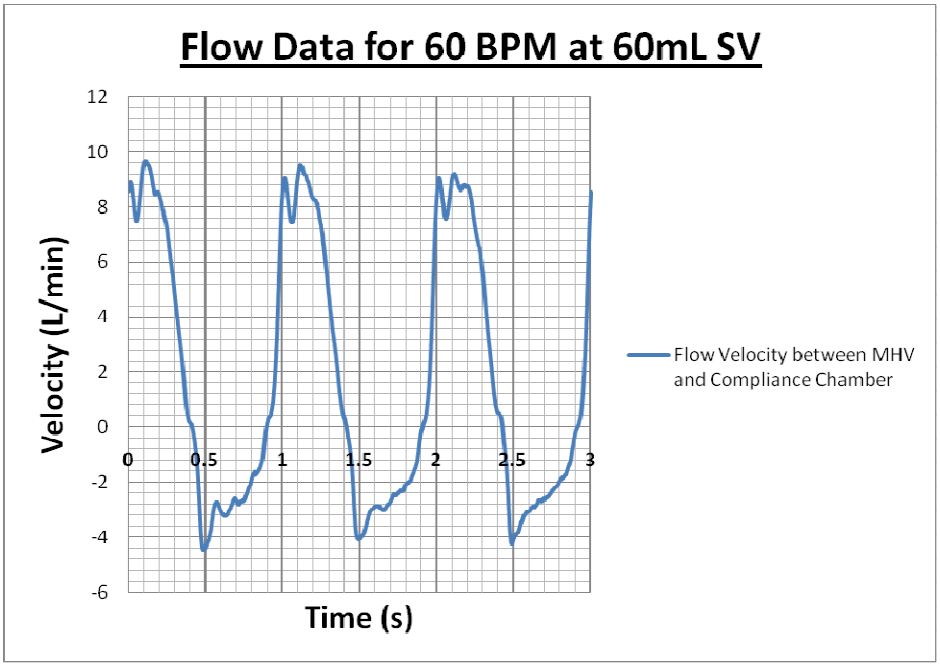

Figure 4.10b. Pressure (top) and flow (bottom) data for 60 BPM with 60mL SV.

The data in **Figure 4.10a** and **4.10b** was acquired while the Harvard pump was set to operate at 60 BPM with a 60mL SV. At this HR, the tilting disk valve completed 60 opening cycles per minute. The Harvard pumping cycle takes 1 second with an average aortic peak systolic pressure at 116.00 mmHg and average minimum diastolic pressure of 40.00 mmHg measured by the pressure transducer just before entering the compliance chamber (99G99F22-X14). Measurements inside the compliance chamber indicate a mean mock loop system pressure of 132.00/66.67 mmHg. The tilting disk valve opens 0.1 seconds after the minimum diastolic pressure occurs and closes 0.14 seconds after peak systolic pressure. The tilting disk valve is open 0.33 seconds of the pumping cycle. Small downward deflection of the blue pressure wave (dicrotic notch) at t = 0.45, 1.45, and 2.45 correlate with the negative flow values on the flow wave. The flow meter measured an average high instantaneous flow rate of 9.47 L per minute during the opening of the tilting disk valve. The cardiac output of the mock loop at these conditions was 3.6 L per minute.

4.11 80 BPM at 80mL Stroke Volume

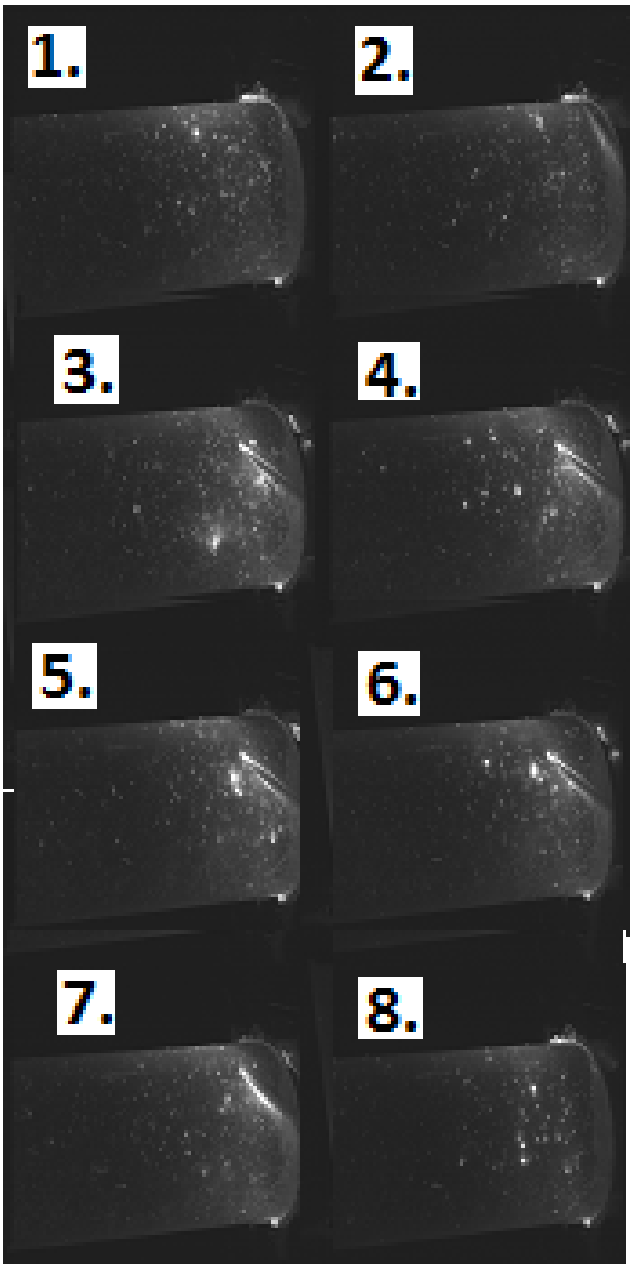

Figure 4.11a. PIV images of one complete tilting disk valve opening cycle for 80 BPM with 80mL SV.

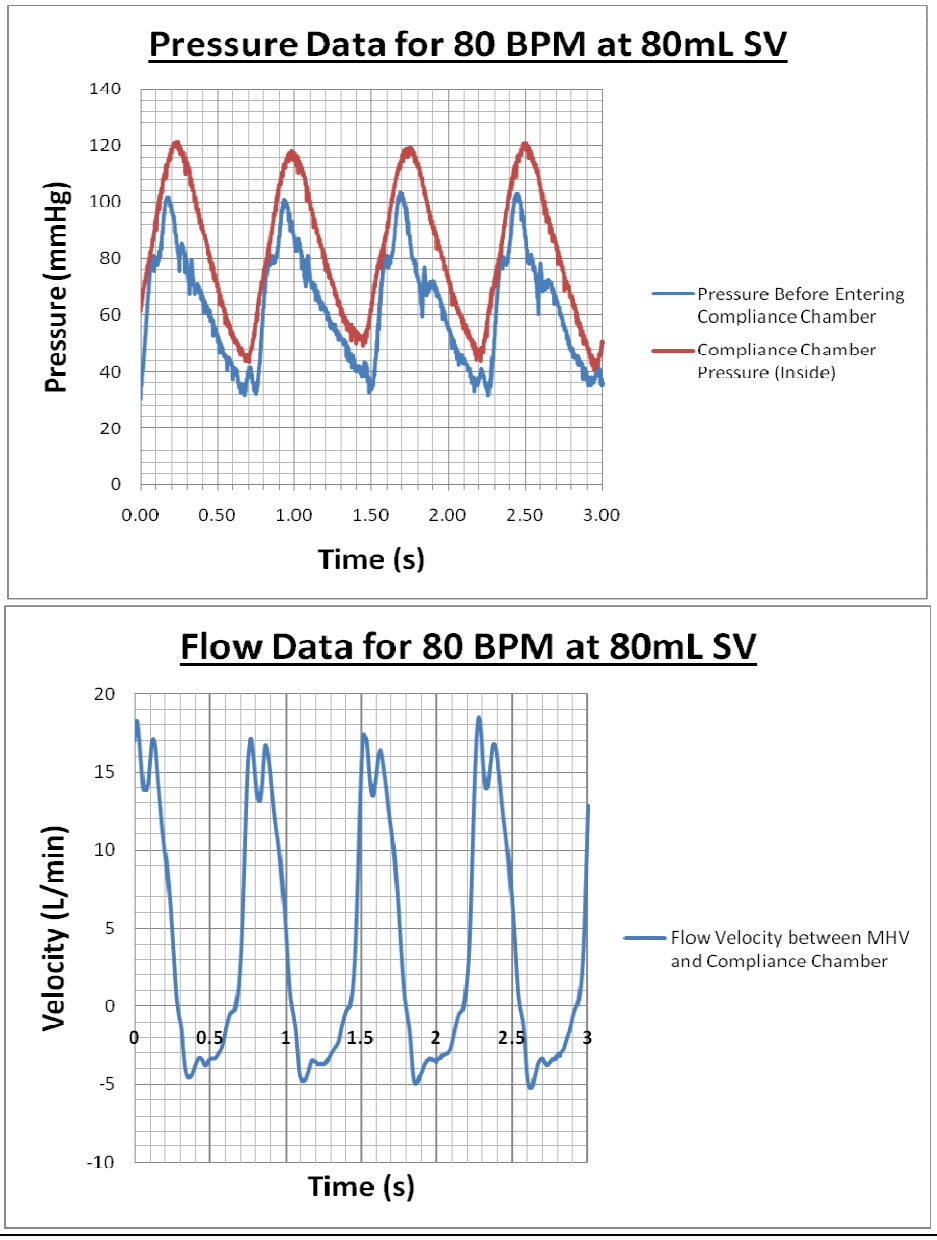

Figure 4.11b. Pressure (top) and flow (bottom) data for 80 BPM with 80mL SV.

Figure 4.11a and **4.11b** above shows information gathered from the Harvard pump operated at 80 BPM with a 80mL SV. This HR and SV combination produces a cardiac output of 6.4 L per minute in the mock loop. The pumping cycle has an average aortic peak systolic pressure at 101.50 mmHg, average minimum diastolic pressure of 33.25 mmHg, and a total

duration of 0.75 seconds with these pressure values measured by pressure transducer 99G99F22-X14. The tilting disk valve opens 80 times per minute. The pressure transducer inside the compliance chamber monitors a mean mock loop system pressure of 120.00/44.25 mmHg. The tilting disk valve opens 0.1 seconds after the minimum diastolic pressure occurs and closes 0.12 seconds after peak systolic pressure. The tilting disk valve is open 0.23 seconds of the pumping cycle. The dicrotic notch occurs at t = 0.30, 1.05, 1.82, and 2.60 seconds and correlates with negative flow values seen at identical times on the flow wave. The flow meter measured an average high instantaneous flow rate of 17.675 L per minute during the opening of the tilting disk valve.

4.12 95 BPM at 80mL Stroke Volume

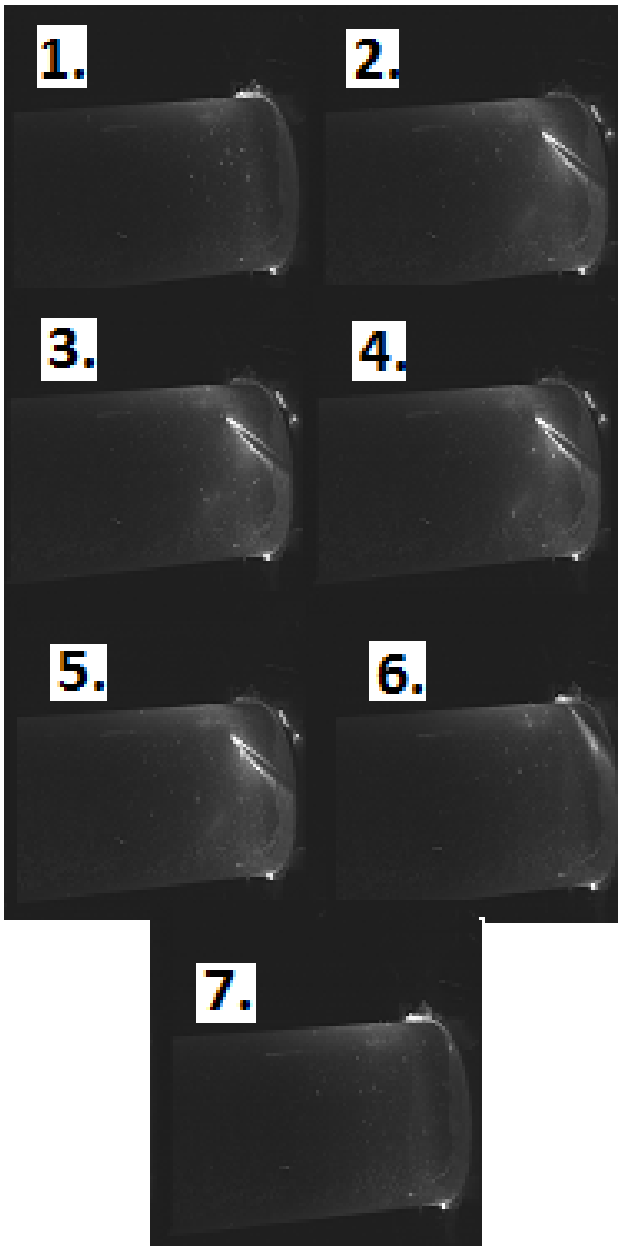

Figure 4.12a. PIV images of one complete tilting disk valve opening cycle for 95 BPM with 80mL SV.

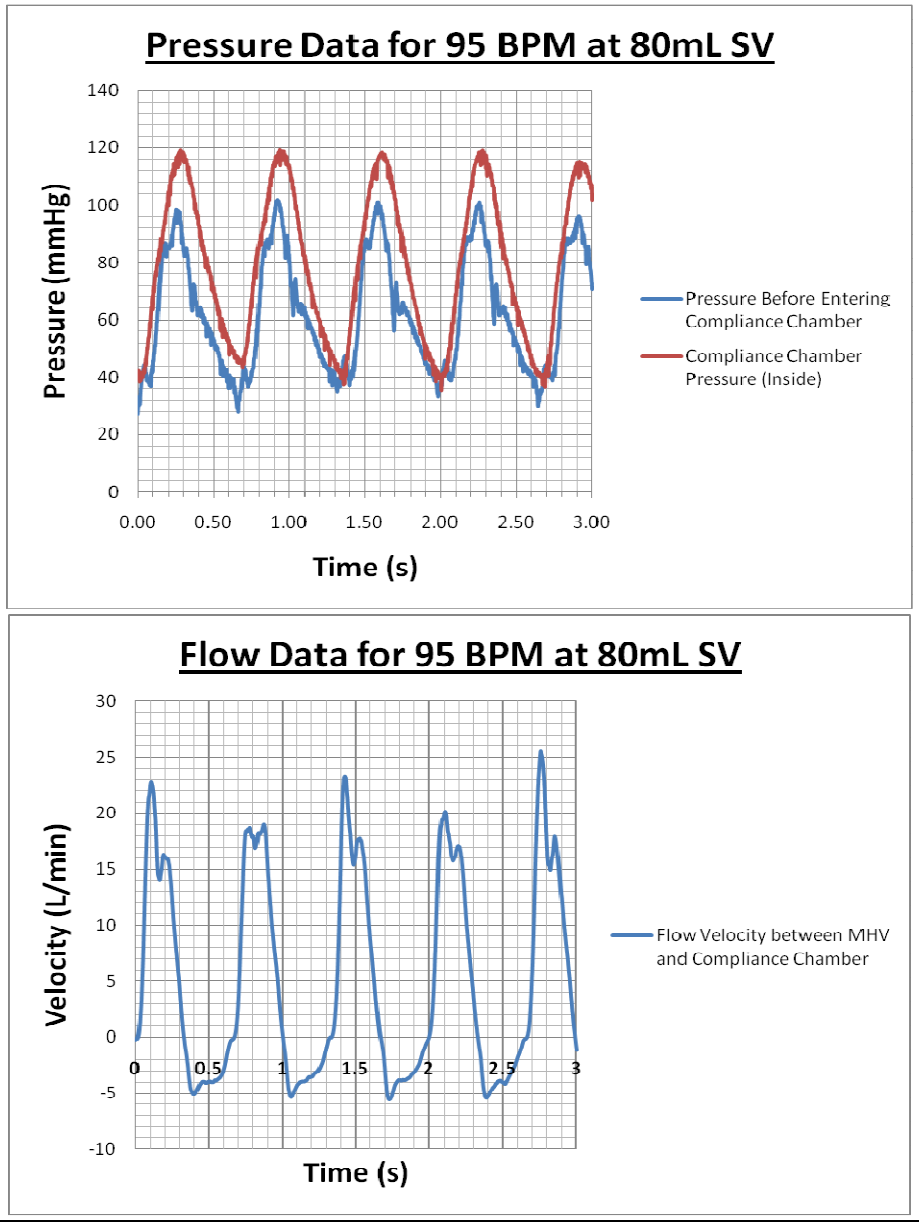

Figure 4.12b. Pressure (top) and flow (bottom) data for 95 BPM with 80mL SV.

Illustrations in **Figure 4.12a** and **4.12b** present data for a 95 BPM, 80mL SV Harvard pump operation. The tilting disk valve completes 95 opening cycles per minute during a 0.63 second pumping cycle interval. The average aortic peak systolic pressure and average minimum diastolic pressure were 99.80 mmHg and 32.25 mmHg, respectively, measured by the

99G99F22-X14 pressure transducer. Measurements inside the compliance chamber indicate a mean mock loop system pressure of 118.20/38.00 mmHg. The dicrotic notch occurs at the instance of negative flow on the flow wave at t = 0.38, 1.01, 1.72, and 2.35. The opening of the tilting disk valve produces a mock loop average high instantaneous flow rate of 22.14 L per minute. The tilting disk valve opens 0.12 seconds after the minimum diastolic pressure occurs and closes 0.15 seconds after peak systolic pressure. One tilting disk opening sequence inhabits 0.21 seconds of the total pumping cycle time. The cardiac output of the mock loop at these conditions was 7.6 L per minute.

4.13 Vector Plots

In order to provide evidence of the ability to obtain vector plot data using this system, one set of PIV images were post-processed. **Figure 4.13a** through **4.13i** show vector information downstream of the experimental tilting disk valve at 60 BPM with 60mL SV. Unlike the previous results, these images were captured orthogonal to the fluid flow region using a 50 mm lens, which provides a more localized imaging area. In these vector plots, positive fluid flow is indicated by right pointing arrows and the tilting disk valve is located to the left of the vector plot.

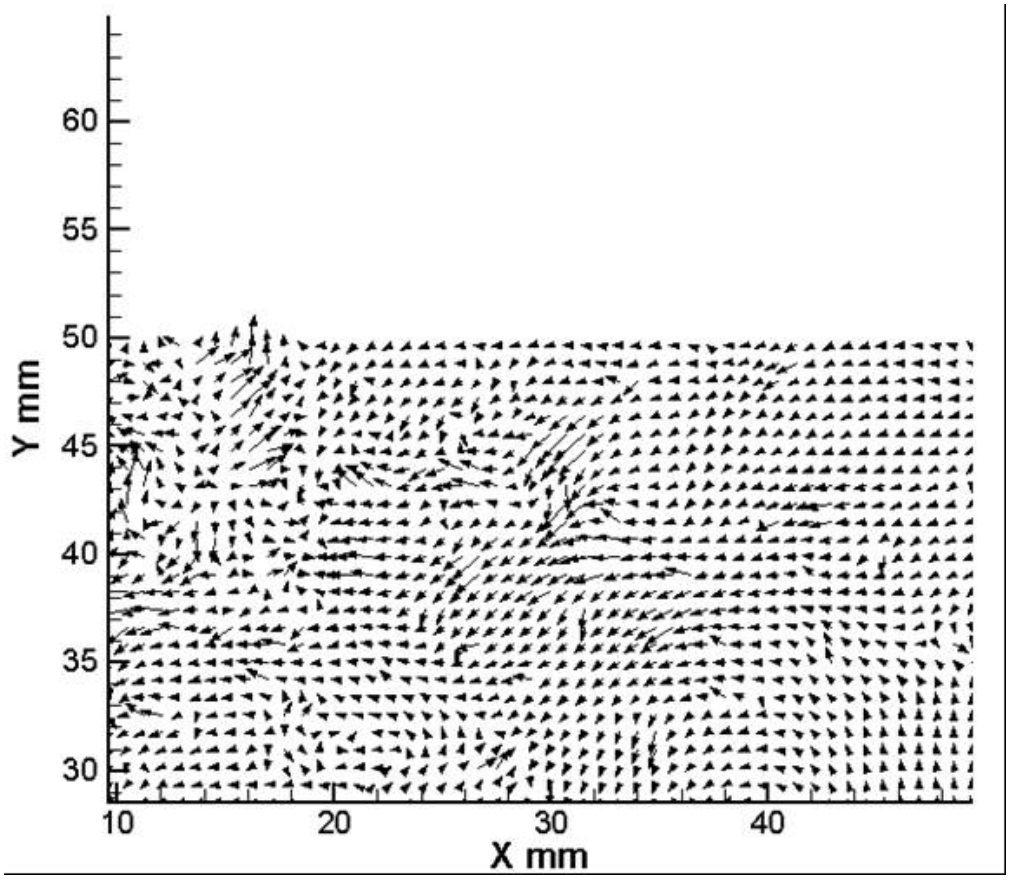

Figure 4.13a. Vector plot for 60 BPM with 60mL SV. End of systolic phase, just before valve closure. Entering pump drawback.

Figure 4.13a represents flow at the end of the pump systolic phase and just before the valve closes. The majority of the shown vectors are oriented in the reverse direction. This indicates that the pump is entering drawback and there is negative fluid flow. Several regions present a swirling, turbulent flow area within the flow as the fluid flow transfers from predominantly positive, forward movement to negative, backflow.

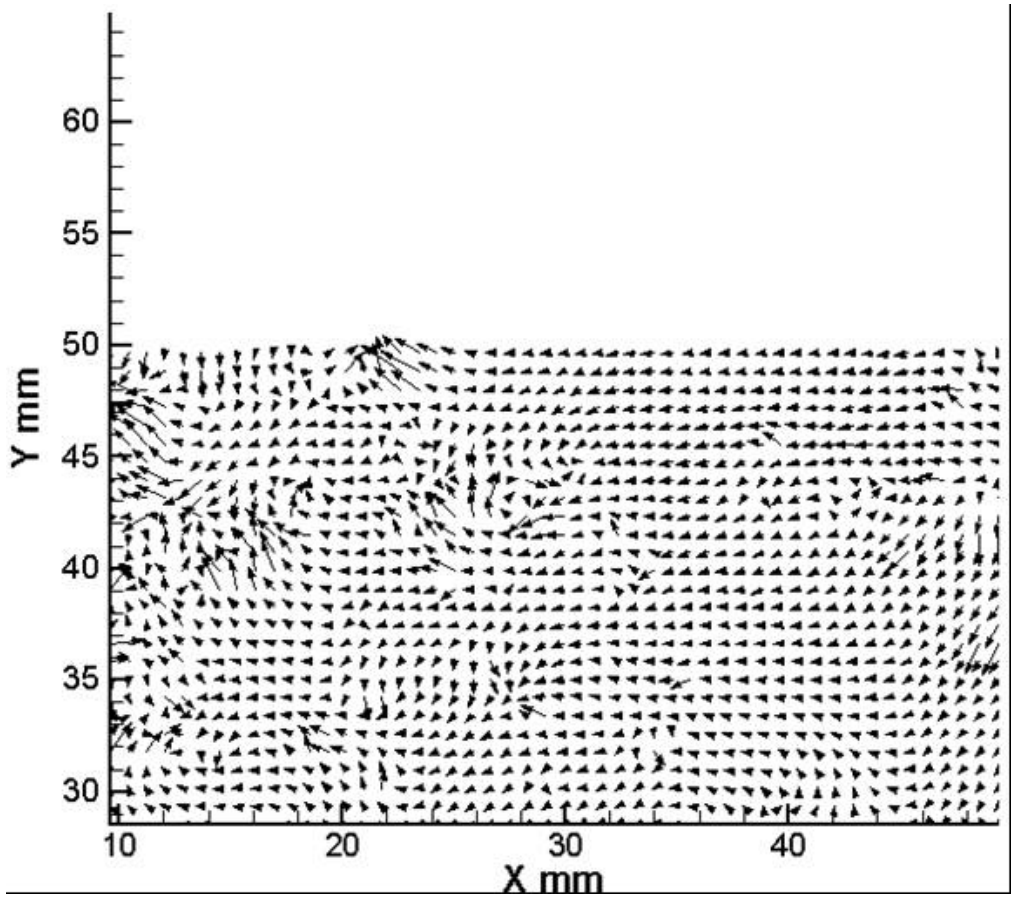

Figure 4.13b. Vector plot for 60 BPM with 60mL SV. Beginning of diastolic phase, just after valve closure, start of pump drawback.

Figure 4.13b represents flow at the beginning of the pump diastolic phase and just after the valve closure. Most vectors are oriented in the reverse direction except those involved in areas of

turbulence. Pump drawback continues to induce negative fluid flow. Once again, several regions present a swirling, turbulent flow area within the flow; however, those regions are limited when compared to Figure 4.13a.

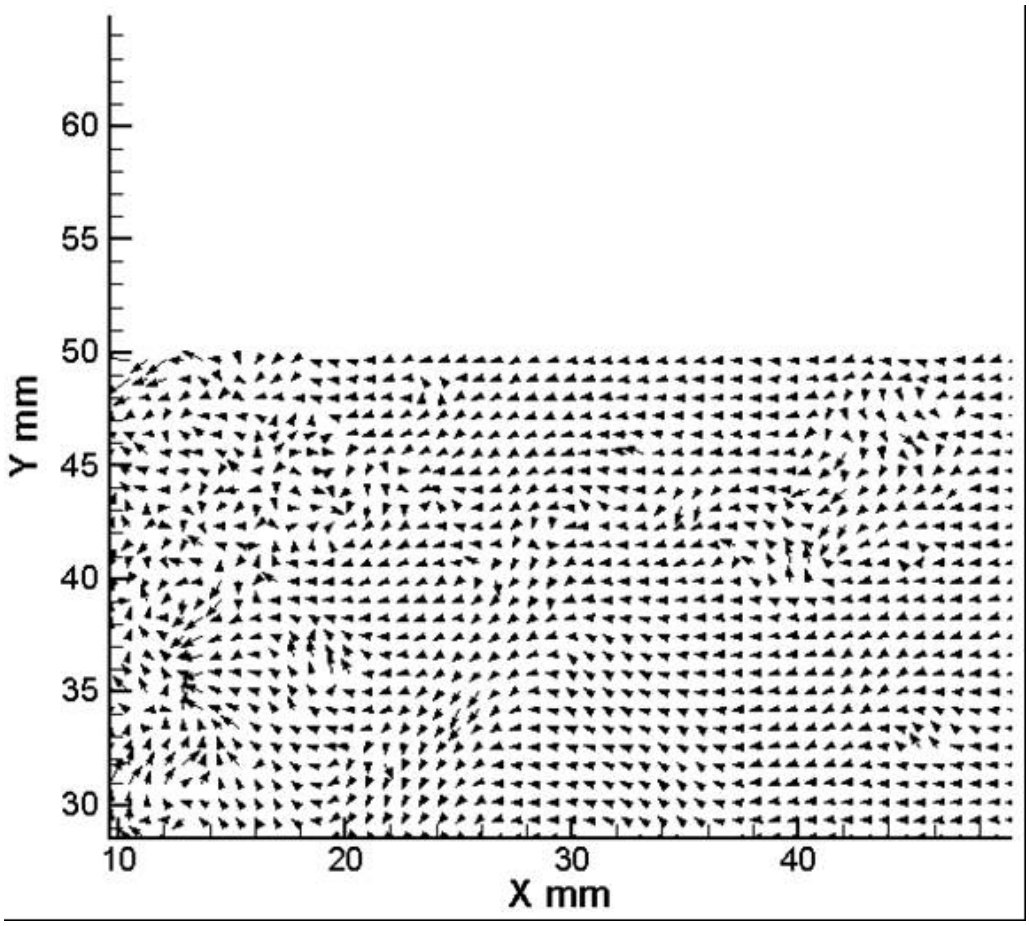

Figure 4.13c. Vector plot for 60 BPM with 60mL SV. Diastolic phase, valve closed, middle of pump drawback.

Figure 4.13c displays fluid flow during the pump diastolic phase. The test tilting disk valve has completely closed at this point. Pump drawback continues to induce negative fluid flow, which gives the vector an overall reverse current orientation. It shows a large stagnant region just downstream of the MHV location.

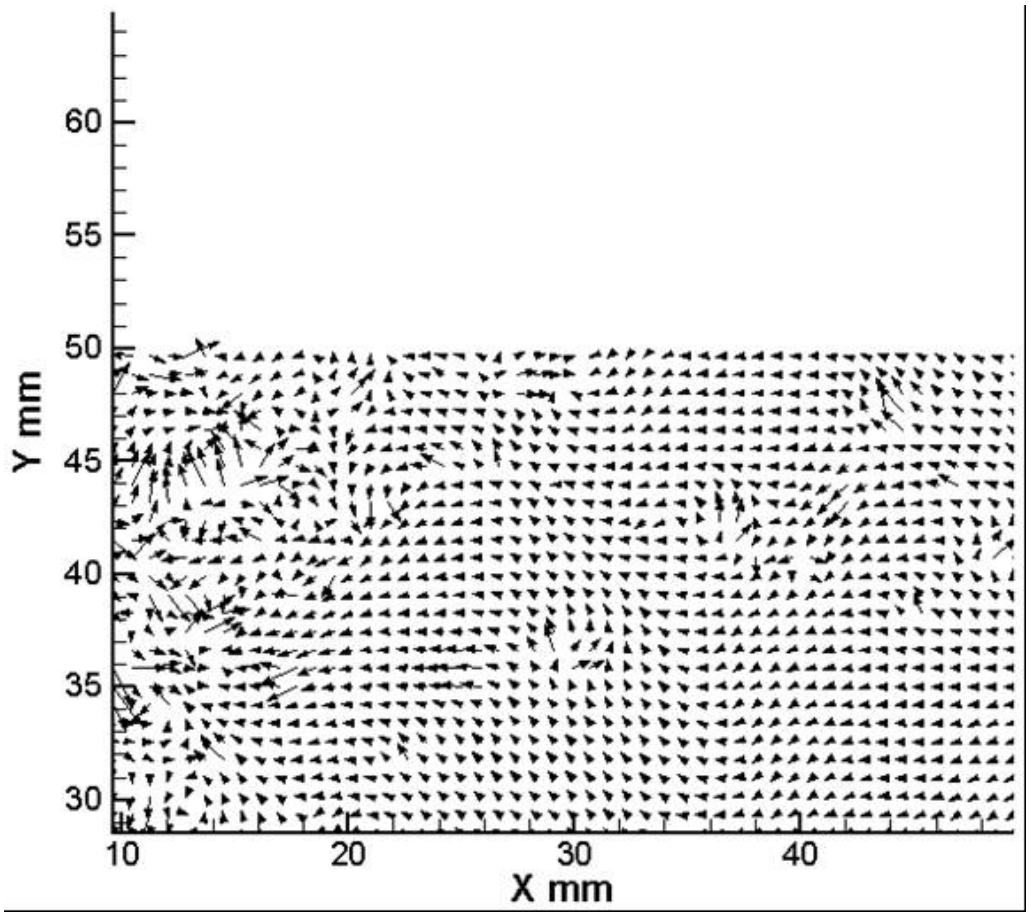

Figure 4.13d. Vector plot for 60 BPM with 60mL SV. Diastolic phase, valve closed, pump still in drawback.

Figure 4.13d looks very similar to Figure 4.13c. In this figure fluid flow is presented during the pump diastolic phase. The test tilting disk valve is still completely closed and pump drawback causes negative fluid flow, as evidenced by the negative vector plot directions. The large stagnant region remains just downstream of the MHV location.

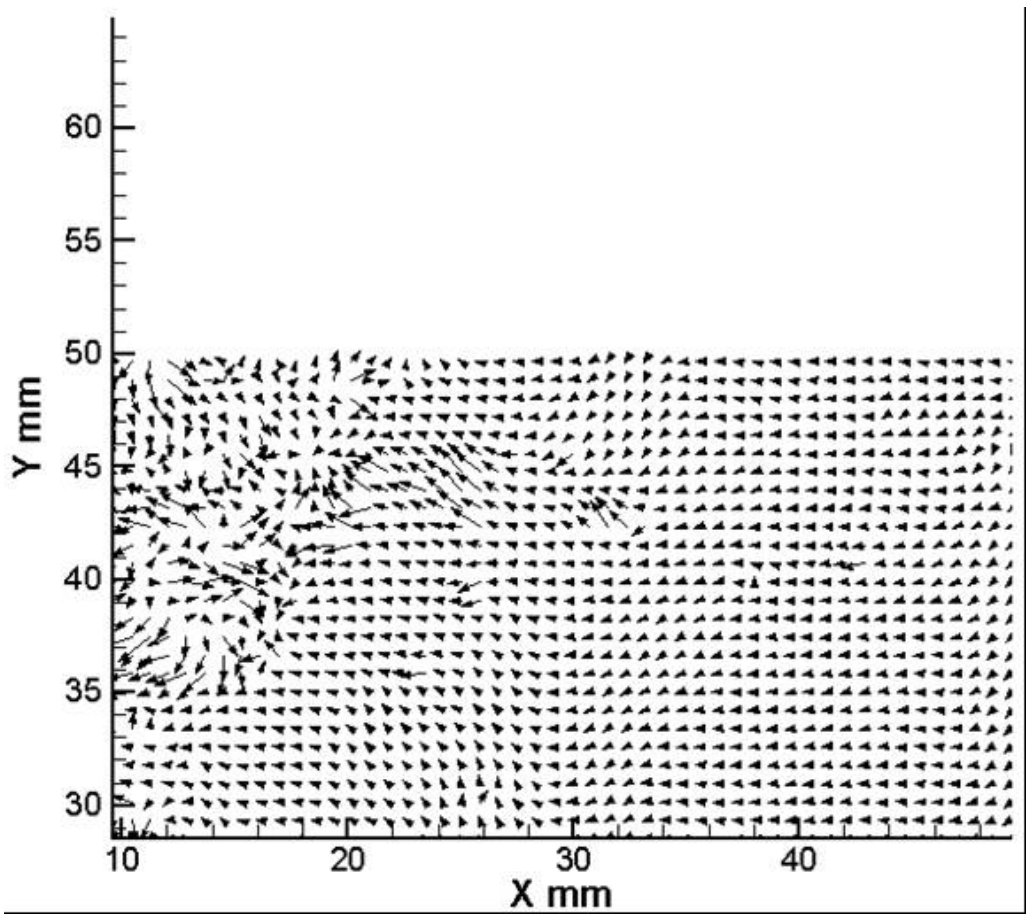

Figure 4.13e. Vector plot for 60 BPM with 60mL SV. Diastolic phase, valve closed, end pump drawback.

Figure 4.13e displays fluid flow during the pump diastolic phase and at the end of pump drawback. The test tilting disk valve is completely closed and reverse fluid current is still evident. A stagnant flow region to the far left of the vector plot area is present.

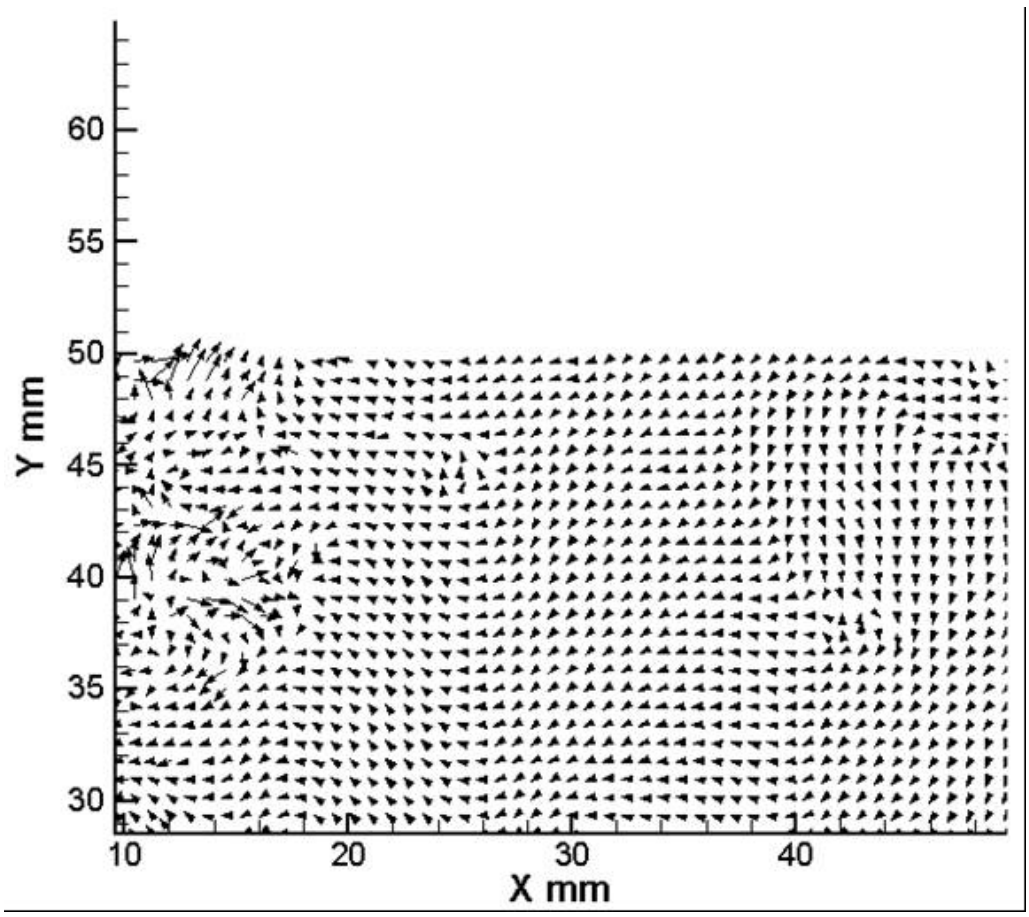

Figure 4.13f. Vector plot for 60 BPM with 60mL SV. End of diastolic phase, just prior to valve opening.

Figure 4.13f displays fluid flow at the end of the pump diastolic phase, just prior to opening of the tilting disk valve. The pump piston has begun its forward progression as it forces fluid out of the pump chamber; however, the effects have yet to show up in the vector plot. It still displays predominantly negative flow orientation but the stagnant flow region just downstream of the MHV location has reduced when compared to the previous figures.

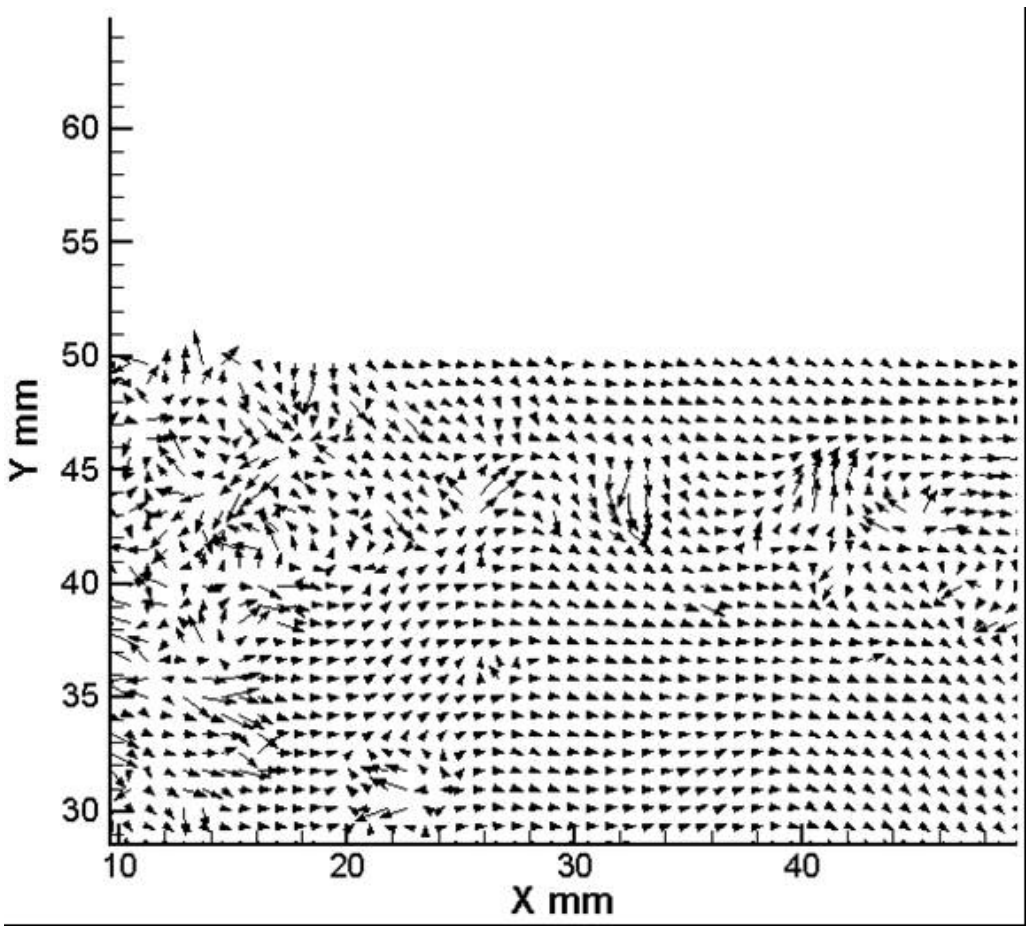

Figure 4.13g. Vector plot for 60 BPM with 60mL SV. Start of systolic phase, just after valve opening.

Figure 4.13g displays fluid flow at the start of the pump systolic phase. The test tilting disk valve has just opened and the vector plot reflects the positive fluid flow caused by the rush of fluid through the valve. It shows a large stagnant region just downstream of the MHV location. Several regions present a swirling, turbulent flow area as the fluid flow transfers from predominantly negative, backflow to positive, forward movement.

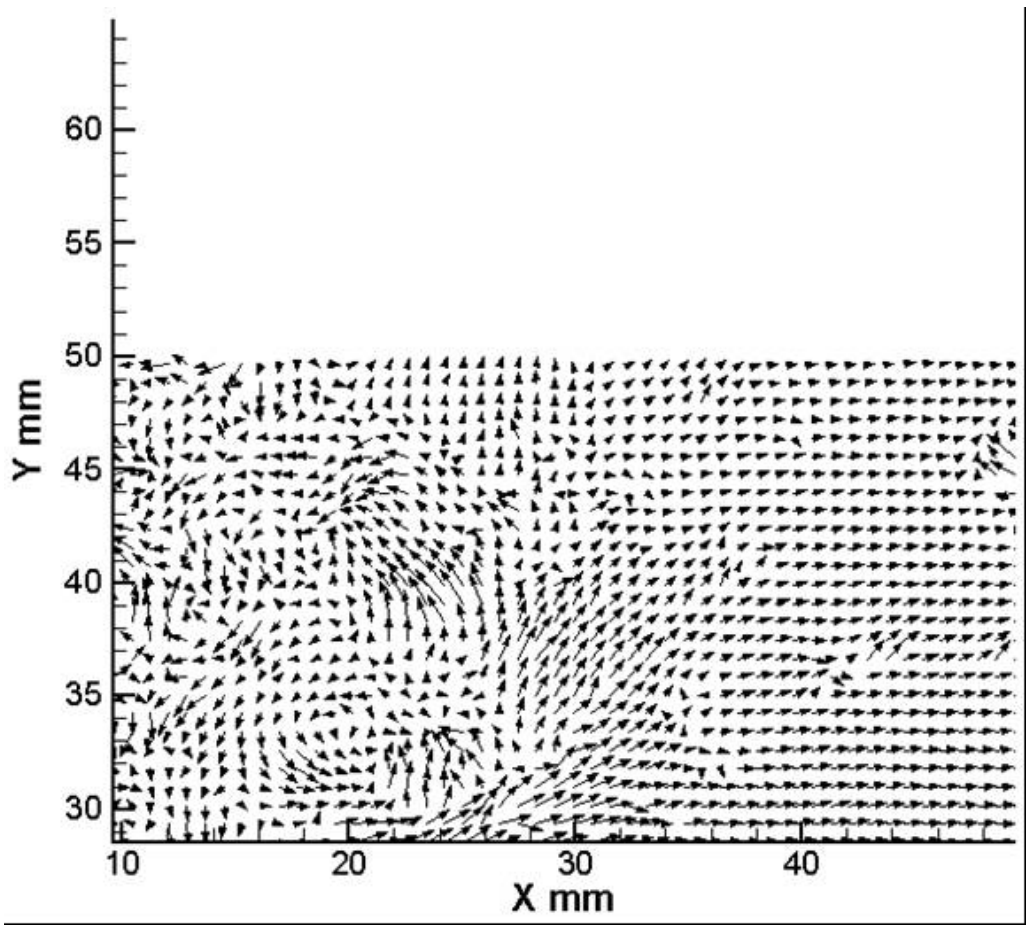

Figure 4.13h. Vector plot for 60 BPM with 60mL SV. Systolic phase, valve open.

Figure 4.13h displays fluid flow during the pump systolic phase. The test tilting disk valve is open. The vector plot shows several swirling, turbulent flow regions as fluid velocity increases through the MHV. The longer vectors indicate larger absolute velocity measurements.

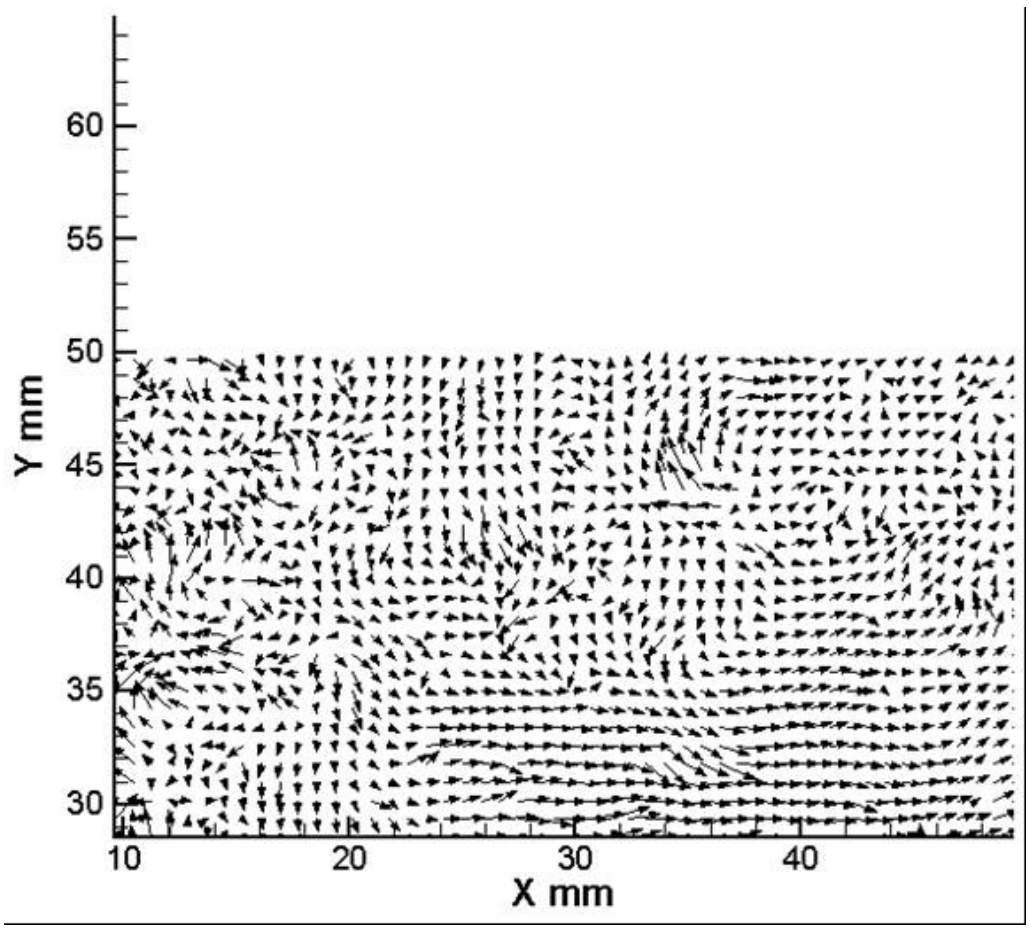

Figure 4.13i. Vector plot for 60 BPM with 60mL SV. Peak systolic phase, valve completely open.

Figure 4.13i presents fluid flow at peak pump systole when the test tilting disk valve is completely open. The vector plot continues to display several swirling, turbulent flow regions as fluid velocity is at its maximum.

5 DISCUSSION, CONCLUSION, AND LIMITATIONS

5.1 Discussion

This experiment included 12 different conditional setups with 20 images captured for each at the MHV test chamber location in the automated mock circulatory loop in the Artificial Heart Laboratory at Virginia Commonwealth University. The images are captured in sequence, 33.33 ms apart, and depicted the operation of an experimental tilting disk valve for the following combinations of HR-SV parameters: 1. 60BPM-70mL, 2. 70BPM-70mL, 3. 80BPM-70mL, 4. 90BPM-70mL, 5. 70BPM-50mL, 6. 70BPM-60mL, 7. 70BPM-80mL, 8. 70BPM-90mL, 9. 90BPM-55mL, 10. 60BPM-60mL, 11. 80BPM-80mL, and 12. 95BPM-80mL. One tilting disk valve opening cycle was presented for each experimental condition set. The systolic to diastolic phase ratio was 50% for all setups and the mock loop peripheral resistor was altered for each in order to maintain a peak systolic pressure in the mock loop compliance chamber within the range of 110 to 140 mmHg. This experiment helps to determine the effectiveness of a completely automated mock circulatory loop and a novel test chamber in the evaluation of MHVs. It primarily focuses on the ability to gather relative fluid dynamic data, at the MHV location, while providing the capability to quickly interchange MHV types and set various physiological conditions. Thus, the objective was to improve upon the efficiency of current MHV in vitro test methods by developing a system that requires less time to manipulate loop parameters and components while maintaining current MHV testing loop and chamber standards.

5.1.1 Mock Circulatory Loop Performance

Evaluation of the experimental mock circulatory loop system for MHV performance testing consisted of satisfaction of two primary criterion: 1. the system's capacity to produce pressure waves similar to those shown in a typical Wiggers diagram, and 2. the system's ability to expose the test MHV at a wide range of mimicked physiological conditions.

5.1.1.1 Wiggers Diagram Comparison

The observed shapes of the collected mock loop pressure waveforms effectively compare to the theoretical cardiac Wiggers diagram. As shown in **Figure 5.1**, the three major regions of the aortic pressure response, denoted by the theoretical Wiggers diagram, were successfully exhibited by the experimental mock loop system. The labeled regions designate the following occurrences within the native heart cycle.

- **a.** represents the opening of the aortic valve and the beginning of left ventricular systole
- **b.** represents the peak systolic pressure
- **c.** represents the closing of the aortic valve and the end of left ventricular systole

Furthermore, **Figure 5.2** shows the left ventricular pressure response, which also indicates a high correlation between the Wiggers diagram and the experimental mock loop pressure waveform. Presence of the labeled regions in **Figure 5.2** indicates the following.

- **d.** represents closure of the mitral valve and the end of left ventricular diastole
- **e.** represents the opening of the mitral valve and the beginning of left ventricular diastole

The generation of the aforementioned regions by the experimental mock loop confirms its ability to adequately duplicate the events of the native left ventricle heart cycle.

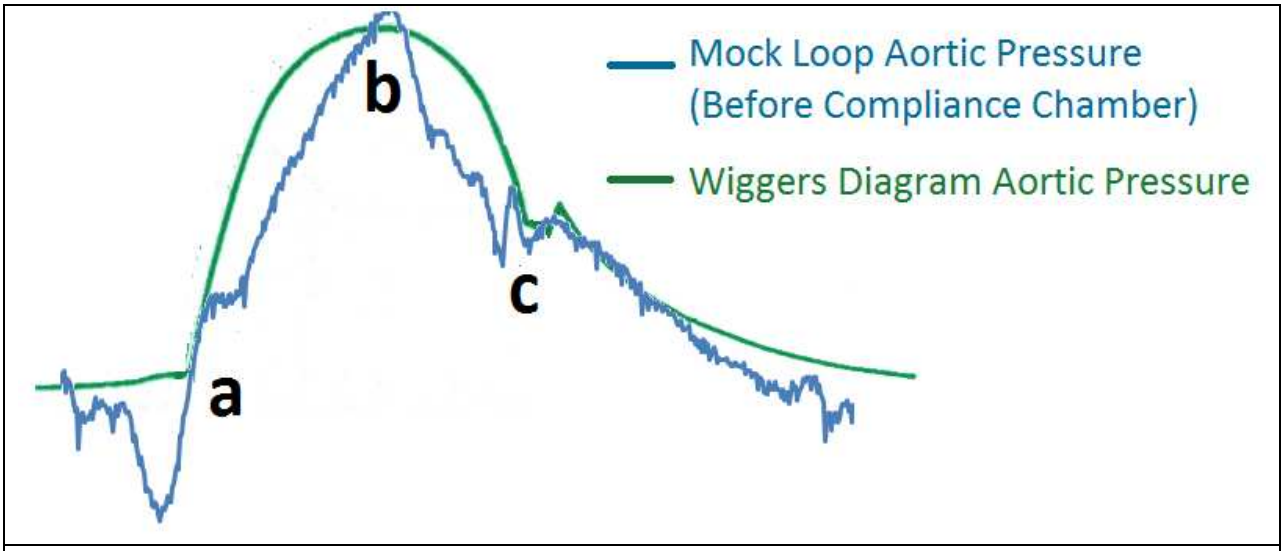

Figure 5.1. Aortic pressure waveform shape comparison to theoretical Wiggers diagram.

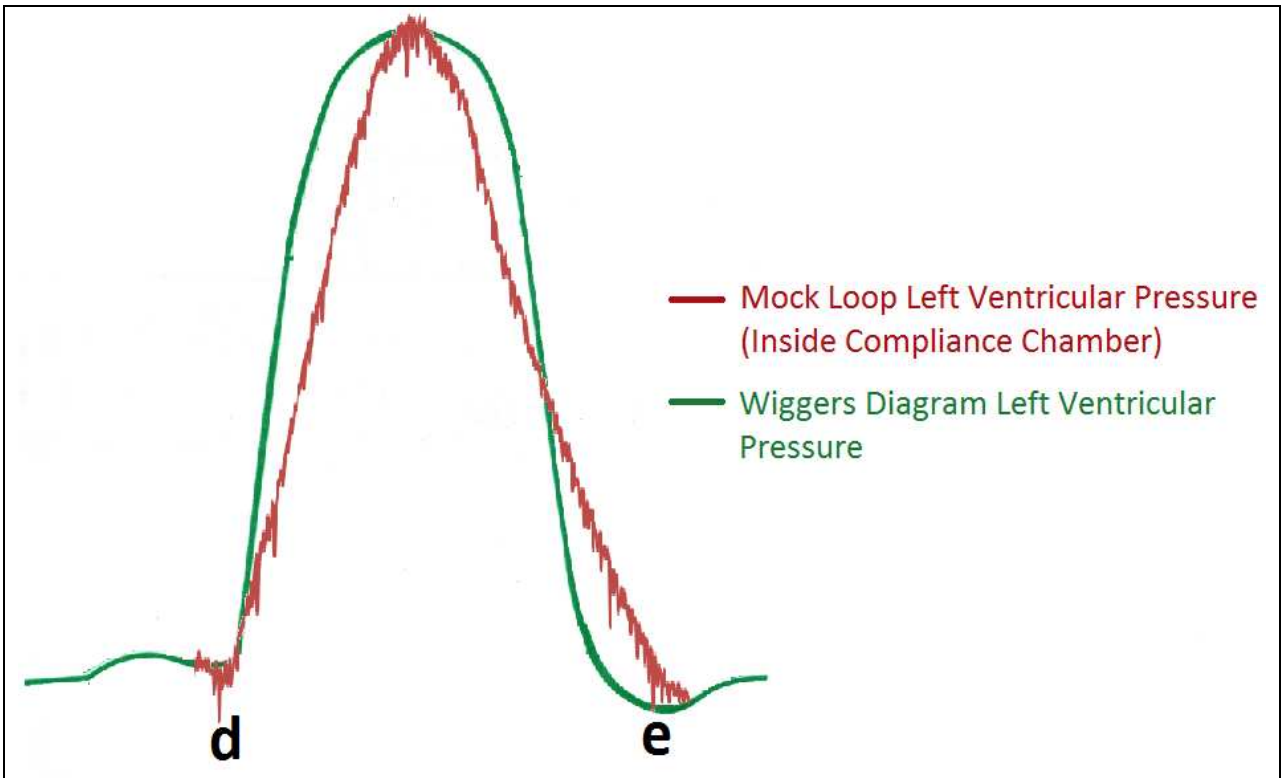

Figure 5.2. Left ventricular pressure waveform shape comparison to theoretical Wiggers diagram.

Figure 5.3 illustrates the typical pressure range (mmHg) presented by the Wiggers diagram as compared to the pressure range (mmHg) created by the experimental mock loop at 60 BPM and 60 mL SV. The Wiggers diagram has an effective left ventricular pressure range of 120 mmHg and an effective aortic pressure range of 40 mmHg. In addition, both Wiggers diagram pressure waveforms peak at approximately 120 mmHg. For the experimental mock loop, the effective left ventricular pressure range is approximately 65 mmHg and the effective aortic pressure range is approximately 50 mmHg. In addition, the difference between the peak systolic pressure of the aortic pressure replication and the left ventricular pressure representation is approximately 15 mmHg. This loss of energy can be attributed to the drawback nature of the pump which lowers the pressure values considerably. Since the test MHV is located closer to the pump than the compliance chamber, the pumps negative pressure has a much greater effect on the aortic pressure replication data than on the left ventricular pressure representation data. In sense, the MHV shields the compliance chamber pressure from being dragged down as the pulsatile pump enters diastole. This pump drawback is explained in more detail in the "Experimental Errors and Limitations" section.

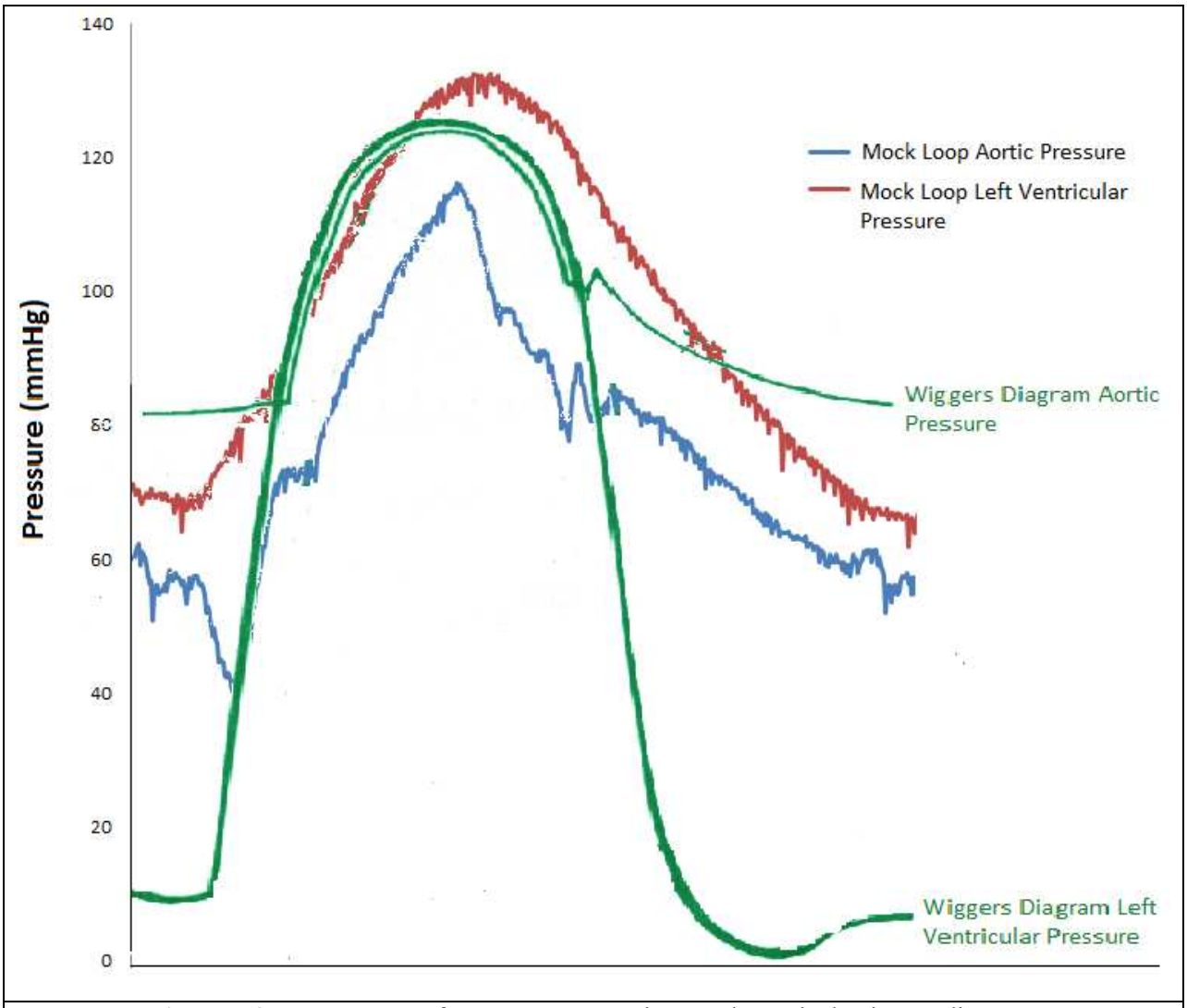

Figure 5.3. Pressure waveform range comparison to theoretical Wiggers diagram.

5.1.1.2 Physiological Simulation Range

The experimental mock loop was able to effectively mimic a wide range of physiological pathologies via manipulation of fluid dynamics. The Harvard pulsatile pump was able to produce a number of HR-SV combinations with HR ranging from 0 to 95 BPM and SV ranging from 15 to 100 mL. Increasing or decreasing one or both HR or SV alters the system cardiac output which simulates conditions including rest, normal, exercise, and failing heart scenarios. This

allows for the observation of MHV performance through the measurement of fluid dynamic information such as pressure and flow rate. Validation of HR and SV settings was completed via analysis of pressure and flow data waveforms. HR was checked for accuracy by pressure and flow wave frequency calculation and SV was confirmed by integration under the flow wave. The scope of the Harvard pump in conjunction with capacitance and resistance manipulation presented the ability to effectively imitate the native's heart capacity to operate in various pathologies. Furthermore, the transformation from manual control to digital control of these components, with feedback assessment, allowed for relatively instantaneous interchangeability between the mimicked physiological conditions.

5.1.2 Pressure and Flow Data

Pressure measurements throughout experimentation provided feedback for the monitoring of aortic pressure just after the tilting disk valve in the mock loop. Each of the acquired pressure waveforms effectively mimic the aortic pressure waveforms created by the native heart. These waveforms include a rapid increase in pressure up to the peak systolic pressure and a slower decline to minimum diastolic pressure. Observation of the aortic pressure waveform also shows the opening of the tilting disk valve during the rapid increase phase and closure during the slow decline phase. Both the opening and closure are denoted by sudden pressure value fluctuations in the relatively smooth wave. At the onset of valve opening, aortic pressure drops suddenly due to the increase in volume area because the valve no longer provides resistance to the fluid. This pressure drop is fairly small in time because the abrupt rush of fluid into the aorta causes the aortic pressure to once again rise until it reaches the peak systolic pressure. Similarly, a sudden rise in pressure occurs during the slow fall of aortic pressure as the valve closes. This pressure

fluctuation is more commonly known as the dicrotic notch. The dicrotic notch occurs when the valve closes and restricts fluid flow, thus, momentarily trapping a high volume of fluid in the aorta. Almost instantaneously the aorta constricts and forces the fluid through the circulatory system, which once again causes the aortic pressure to fall. These changes form a small "sawtooth" indentation in the pressure waveform. Location of the dicrotic notch is a major notification in the diagnosis of several pathologies such as hypovolemia. Therefore, the dicrotic notch is a good indication of valve functionality and its consequent effects on fluid flow. Valve closure is also indicative of flow stagnation, which is linked to thrombotic activity. Furthermore, manipulation of the peak systolic pressure by capacitance and resistance variability presents the ability to expose test MHVs to different mechanical conditions, which is important during durability and mechanical failure testing. The system also created a fairly low diastolic pressure for all condition experiments, which will be further discussed in the errors and limitations section.

In addition to pressure data, flow data is extremely important in MHV performance evaluation. The instantaneous detection of fluid flow just after the valve provides information for the effects of valve design on fluid dynamics. Negative flow regions on the flow waveform suggests periods of backflow during circulation, especially at the test MHV location. Backflow plays a role in valve closure and is a means of washing thrombus deposition from the valve. It is created when filling of the pump during the diastolic phase presents a low pressure in the pump while the pressure in the aortic section remains high. This pressure gradient forces flow to move from the region of high pressure towards the region of low pressure in order to stabilize the system. Low aortic pressures present little to no backflow; however, high aortic pressures cause the magnitude of fluid backflow to rise. Thus, in the instance of a faulty valve and high aortic

pressure, backflow will negatively affect cardiac output. Additionally, backflow also leads to flow recirculation or swirling. So if MHV design creates a high shear stress region and the blood flows back through that region during backflow it raises the exposure time of the red blood cells to high shear stress which raises the potential for hemolytic activity. MHVs that present high potentials for thrombosis and/or hemolysis are not ideal for implantation, which enhances the significance of in vitro testing and measurement of fluid flow. Therefore, the instantaneous flow measurement and ability to quickly change physiological conditions become increasingly more important.

5.1.3 PIV Imaging

For the purpose of this research, images acquired by the PIV system were used to validate proper valve mechanical functionality and particle illumination for post-processing. Particle illumination is a key element in computing fluid flow profiles. These profiles, usually vector and/or contour plots, provide local velocity information for a designated flow field. Therefore, they relay qualitative and quantitative visualization data relevant to stagnant and swirling backflow regions that may promote thrombotic and/or hemolytic activity. In this experimentation, imaging at the test valve site in the mock loop showed adequate particle illumination and thus, with further processing, will provide local velocity data of fluid flow exiting the valve. This will allow in vitro prediction of native fluid dynamics for a particular valve design. In order to establish proof of concept for this imaging data, vector plot post-processing was completed for only one parameter set, 60 BPM at 60mL SV.

Furthermore, synchronization of the image acquisition process with the mock loop measuring instruments enabled flow field interpretations to be developed from the computed

pressure and flow waveforms. This was completed via the implementation of a time-stamp, generated TTL signal that initiated the PIV imaging process. As previously noted, negative measurements on the flow waveform indicate reversal of fluid flow, backflow. These negative flow time periods begin just before the valve closes, as the last couple of images in each set of tilting disk valve opening cycle illustrations. Furthermore, negative flow recordings coincide with the Harvard pump's diastolic phase in which its function is dominated by the motor drawback mechanics. Pump diastole ensues throughout valve closure. The combination of these phenomena implies regurgitant or swirling flow at the tilting disk valve location during its closing phase. Integration of the negative flow region provided quantitative data with respect to the amount of backflow observed during each set of operating conditions. From this data, it was observed that regurgitant volume increased with SV increase and decreased with HR escalation. These regurgitant volume responses can be attributed to direct relationships to total volume discharged by the pump, SV, and total time spent in diastolic phase, HR. Total backflow volume is proportional to SV, so a change in one represents a similar change in the other, when all other loop parameters are held constant. In contrast, total backflow volume is indirectly related to the amount of time that the valve is exposed to the diastolic phase of the pump. Therefore, as HR increases, the pump diastolic phase duration is lowered and less backflow occurs. The highest amount of backflow was seen at 60 BPM and 70mL SV, while the least was at 90 BPM and 55mL SV. Indicating that HR had a greater effect on regurgitant volume than SV in the investigated mock loop system. Lastly, all acquired images showed the tilting disk valve opening to a 60 degree tilt that produced a major and minor flow region.

5.2 Experimental Errors and Limitations

A consistent, uniform experimental setup is always ideal in research. However, procedural errors and/or limitations will continually present the opportunity for deviation away from the ideal scenario. During this experimentation, most faults were attributed to the Harvard pulsatile pump with the biggest setback occurring in the diastolic phase of the pumping cycle. Unlike the natural positive pressure filling ventricle, the Harvard pulsatile pump in this research creates a negative pressure head, up to -90 mmHg, during its filling phase. This large negative pressure creates a larger transvalvular pressure gradient across the test valve, when compared to observed native behavior, because it pulls down the pressure in the section of the mock just before the valve. The enhanced pressure differential on each side of the valve causes an increased backflow response as the fluid rapidly attempts to move from the high pressure aortic region back through the valve, in the reverse direction, towards the lower pressure area on the other side. So as the valve prepares to close, a larger than normal amount of fluid regurgitates back through the valve prior to shutting. The pump's negative pressure phenomenon drags the diastolic pressure in the system down to a lower than expected value and also slightly raises the systolic pressure. It also lowers the anticipated cardiac output value. For example, running the pump at 60 BPM with a 60mL SV produces a regurgitant value of approximately 25mL per stroke, which creates a cardiac output of 2.1 L/min. This is a 1.5 L/min reduction from the expected 3.6 L/min cardiac output, which is about a 40% deviation. This creates major errors when attempting to evaluate valve performance during the diastolic phase and in relation to the amount of reverse flow generated by a particular valve design.

In addition to the error created by the problem above, another limitation is seen in the Harvard pump's systolic to diastolic phase ratio. At the time of this experimentation, the pump was only able to operate in a 50% systolic to diastolic phase ratio setting because digital control had yet to be resolved for this aspect of pump functionality. The manual version of the Harvard pump was able to pulse with systolic/diastolic phase ratios ranging from 35 to 50%. Therefore, upon resolution of pump phase automation the pump will have similar limits. Native normal systolic/diastolic phase ratio is around 35 to 40%, which produces a slower pressure decent during the diastolic phase on a native normal ventricular pressure waveform, duplicated by the mock loop compliance chamber. In this experimentation, analysis of the pressure waveform within the compliance chamber shows a symmetrical wave phase. This is attributed to the equal amount of time spent in the systolic and diastolic phases during one pumping cycle. Therefore, the Harvard pulsatile pump will be able to provide a broader range of physiological pathologies when the initial manual systolic/diastolic phase ratio range is reestablished.

5.3 Possible Future Progression

The research location, Artificial Heart Laboratory at Virginia Commonwealth University, is in the process of making numerous other advancements in mock loop in vitro evaluation including improvements in aortic anatomical relevancy and adaptation of a second loop capacitor to simulate ventricular compliance. These improvements will further push the envelope of MHV in vitro independent and comparative testing by providing an advanced duplication of the native cardiovascular system. This assumption is based upon the notion that the ideal in vitro mock loop setup will perfectly simulate native physiology and provide the most reliable data.

5.4 Conclusion

With CHD being the leading cause of death in the United States and the number of global surgical heart valve procedures expected to exceed 850,000 annually by the year 2050 [4], heart valve treatment continues to major effects on the world's population. In particular, patients who suffer from severe heart valve disorder and require replacement are in need of the development of an ideal valve replacement that provides longevity and minimal complications after implantation. MHVs are known to excel in durability concerns; however, questions of biocompatibility continue to warrant investigation into design improvements. The research presented here details the formulation of an in vitro process used to evaluate MHV functionality prior to patient implantation based upon fluid flow dynamics. The experimentation involves the design and manufacturing of a novel MHV test chamber in conjunction with an automated mock circulatory loop to improve upon the efficiency of other previous test setups. Emphasis was placed on the ability to reproduce a wide range of physiological pathologies as well as effectively image fluid flow and valve operation at the MHV test chamber location. Results presented positive feedback in reference to the mock loop's ability to mimic the native cardiovascular system and the PIV system's capacity to illuminate particles at the exit region of the test tilting disk heart valve, placed in the aortic valve position. A total of 12 HR-SV combinations were examined with all producing acceptable pressure and flow waveforms and image capture. Transformation from one set of parameters to another was relatively instantaneous and required minimal movement from the control computer site. Furthermore, proof of vector plot computation was presented. For these reasons, the researched novel MHV

test chamber, in conjunction with an automated mock loop, effectively functions as a test apparatus for MHV evaluation while improving upon the time and accuracy associated with alternate methods and systems. To increase accuracy in diastolic phase studies, the effects of the Harvard pump's production of negative pressure during the diastolic phase should be further investigated and improved upon.

REFERENCES

1. Spoor, Martinus, & Bolling, Stephen F. (2007). Valve pathology in heart failure: which valves can be fixed?. *Heart Failure Clinic*, 2007, Vol 3, pp 289-98.

2. *Mitral Valve Repair*. Wikipedia Encyclopedia. http://en.wikipedia.org/wiki/Mitral_valve_repair. (27 Oct. 2008).

3. Maganti, Kameswari, Rigolin, Vera H., Sarano, Maurice E., & Bonow, Robert O. (2010). Valvular heart disease: diagnosis and management. *Mayo Clinic Proceeedings*, 2010, Vol 85, Issue 5, pp 483-500.

4. Dasi, Lakshmi P., Simon, Helene A., Sucosky, Phillippe, & Yoganathan, Ajit P. (2009). Fluid mechanics of artificial heart valves. *Clinical and Experimental Pharmacology and Physiology: Frontiers in Research Review,* 2009, Vol 36, pp 225-237.

5. Sun, Jack CJ, Davidson, Michael J, Lamy, Andre, & Eikelboom, John W. (2009). Antithrombotic management of patients with prosthetic heart valves: current evidence and future trends. *Lancet*, Aug 2009, Vol 374, pp 565-76.

6. Brigham and Womens. *Heart Blood Flow*. http://www.brighamandwomens.org/cvcenter/advancedheart/Images/HeartBloodFlow.bmp. (10 June 2010).

7. Bark Bytes. *Heart 2*. http://www.barkbytes.com/medical/Heart2.jpg (10 June 2010).

8. *Mitral Valve Repair*. St. Jude Medical Center. (Oct. 2008).

9. Carabello, BA (2005). Modern management of mitral stenosis. *Circulation*, 2005, Vol 112, Issue 3, pp 432–7.

10. Di Sandro, D (2009). *Mitral Regurgitation*. *eMedicine*. Medscape. http://emedicine.medscape.com/article/758816-overview. (8 December 2009).

11. Texas Heart Institute (updated August 2009). *Valve Repair or Replacement*. Heart Information Center. http://www.texasheartinstitute.org/hic/topics/proced/vsurg.cfm. (10 November 2009).

12. Nair, Kalyani, Muraleedharan, C.V., & Bhuvaneshwar, G.S. (2003). Developments in mechanical heart valve prothesis. *Sādhanā,* June/August 2003, Vol 28, Issue 3 & 4, pp 575–587.

13. Dickson, Craig Brendan (2004). Venous Thrombosis: On the History of Virchow's Triad. University of Toronto Medical Journal. May 2004, Vol 3, Issue 81, pp 166-71. Historical Review.

14. Soren Schenk et al. (2003). *In Vivo* performance and biocompatibility of the MagScrew Ventricular Assist device. *American Society of Artificial Internal Organs Journal*, 2003, pp 594-98.

15. Martin, A.J., & Christy, J.R. (2004). An in-vitro technique for assessment of thrombogenicity in mechanical prosthetic cardiac valves: evaluation with a range of valve types. *Journal of Heart Valve Di*s., May 2004, Vol 3, Issue 13, pp 509-20.

16. Van Nooten, G.J., Taeymans, Y., Van Belleghem, Y., François, K., Van Overbeke, H., Poelaert, J., Caes, F., & De Pauw, M. (2003). Lower anticoagulation for mechanical heart valves: experience with the ATS bileaflet valve. *Heart Lung Circ*., 2003, Vol 3, Issue 12, pp 164-71.

17. Keggen, L.A., Black, M.M., Lawford, P.V., Hose, D.R., & Strachan, J.R. (1996). The use of enzyme activated milk for in vitro simulation of prosthetic valve thrombosis. *Journal of Heart Valve Dis.,* Jan 1996, Vol 1, Issue 5, pp 74-83.

18. *Mitral Valve Replacement*. University of Maryland Medical Center: 1-2. http://www.umm.edu/heart/mitral.htm. (26 Apr. 2007).

19. Meyer, Richard S., Deutsch, Steven, Bachmann, Christopher B., & Tarbell, John M. (2001). Laser Doppler velocimetry and flow visualization studies in the regurgitant leakage flow region of three mechanical mitral valves. *International Society of Artificial Organs,* 2001, Vol 25, Issue 4, pp 292-9.

20. Kini, V., Bachmann, C., Fontaine, A., Deutsch, S., & Tarbell, J.M. (2001). Integrating particle image velocimetry and laser Doppler velocimetry measurements of the regurgitant flow field past mechanical heart valves. *International Society of Artificial Organs,* 2001, Vol 25, Issue 2, pp 136-145.

21. Sabbath, H.N., & Stein, P.D. (1984). Comparative study of the amount of backflow produced by four types of aortic valve prostheses. *Journal of Biomechanical Engineering,* February 1984, Vol 106, pp 66-71.

22. Wu, Z.J., Gao, B.Z., Slonin, J.H., & Hwang, Ned H.C. (1996). Bileaflet mechanical heart valves at low cardiac output. *Journal of American Society of Artificial Internal Organs,* September-October 1996, Vol 42, Issue 5, pp M747-9.

23. Gross, Jeffrey M., Shermer, Charles D., & Hwang, Ned H.C. (1988). Vortex shedding in bileaflet heart valve prostheses. *Transactions of American Society of Artificial Internal Organs,* 1988, Vol 34, pp 845-50.

24. Milo, Simcha, Rambod, Edmond, Gutfinger, Chaim, & Gharib, Morteza (2003). Mitral mechanical heart valves: in vitro studies of their closure, vortex, and microbubble formation with possible medical implications. *European Journal of Cardio-thoracic Surgery,* 2003, Vol 24, pp 364-70.

25. Johansen, Peter, Manning, Keefe B., Tarbell, John M., Fontaine, Arnold A., Deutsch, Steven, & Nygaard, Hans (2003). A new method for evaluation of cavitation near mechanical heart valves. *Journal of Biomechanical Engineering,* October 2003, Vol 125, pp 663-70.

26. Manning, Keefe B., Przybysz, T. Michael, Fontaine, Arnold A., Tarbell, John M., & Deutsch, Steven (2005). Near field flow characteristics of Bjork-Shiley monostrut valve in a modified single shot valve chamber. *American Society of Artificial Organs,* 2005, pp 133-38.

27. Lamson, Theodore C., Stineberg, David R., Deutsch, Steven, Rosenberg, Gerson, & Tarbell, John M. (1991). Real-time in vitro observation of cavitation in a prosthetic heart valve. *Transactions of American Society of Artificial Internal Organs,* 1991, Vol 37, Issue 3, pp M351-3.

28. Browne, Paul, Ramuzat, Agnes, Saxena, Rahul, & Yoganathan, Ajit P. (2000). Experimental investigation of the steady flow downstream of the St. Jude bileaflet heart valve: a comparison between laser Doppler velocimetry and particle image velocimetry techniques. *Annals of Biomedical Engineering,* 2000, Vol 28, pp 39-47.

29. Bjork, V.O., Intonti, F., & Meissl, A. (1962). A mechanical pulse duplicator for testing prosthetic mitral and aortic valves. *Thorax,* 1962, Vol 17, pp 280-83.

30. Lim, W.L., Chew, Y.T., Chew, T.C., & Low, H.T. (2001). Pulsatile flow studies of a porcine bioprosthetic aortic valve in vitro: PIV measurements and shear-induced blood damage. *Journal of Biomechanics,* 2001, Vol 34, pp 1417-27.

31. Adrian, RJ. (1991). Particle-imaging techniques for experimental fluid mechanics. *Annu Rev Fluid Mech*, 1991, Vol 23, Issue 1, pp 261-304.

32. Comte-Bellot, G. (1976). Hot-wire anemometry. *Annual Review of Fluid Mechanics*, Jan 1976, Vol 8, pp 209-31.

33. Thatte, Suhas M. (2006). In vitro flow visualization study of the interface between outflow graft of ventricular assist device and aorta. Thesis. Virginia Commonwealth University, 2006.

34. *Flow Measurement*. Wikipedia Encyclopedia. http://en.wikipedia.org/wiki/Flow_measurement#Ultrasonic_.28Doppler.2C_transit_time.29_flow_meters. (22 May 2010).

35. Taylor, C. (2009). Automated mock loop designed for left ventricular assist device testing. Poster presented at SEBCC 2009.

36. Viscosity.

37. TSI Particle Image Velocimetry Hardware Operations Manual and INSIGHT Software Version 3.2 Quick Start Guide.

38. Verdonck, Pascal R., Dumont, Kris, Segers, Patrick, Vandenberghe, Stijn, & Van Nooten, Guido (2002). Mock loop testing of On-X prosthetic mitral valve with Doppler echocardiography. *International Society of Artificial Internal Organs,* 2002, Vol 26, Issue 10, pp 872-8.

39. Castellini, Paolo, Pinotti, Marcos, & Scalise, Lorenzo (2004). Particle image velocimetry for flow analysis in longitundinal planes across a mechanical artificial heart valve. *International Society of Artificial Organs,* 2004, Vol 28, Issue 5, pp 507-13.

40. Yubing Shi, Tony Joon Hock Yeo, Yong Zhao, & Hwang, Ned H.C. (2006). Particle image velocimetry study of pulsatile flow in bi-leaflet mechanical heart valves with image compensation method. *Journal of Biological Physics,* April 2006, Vol 32, pp 531-51.

41. Zapanta, Conrad M., Liszka Jr., Edward G., Lamson, Theodore C., Stineberg, David R., Deutsch, Steven, Geselowitz, David B., & Tarbell, John M. (1994). A method for real-time in vitro observation of cavitation on prosthetic heart valves. *Journal of Biomechanical Engineering,* November 1994, Vol 116, pp 460-8.

42. Walker, J.D., Tiederman, W.G., & Phillips, W.M. (1989). Effect of tilting disk, heart valve orientation on flow through a curved aortic model. *Journal of Biomechanical Engineering,* October 1989, Vol 111, pp 228-32.

43. Sato, Manabu, Harasaki, Hiroaki, Wika, Kent E., Soloviev, Maxim V., & Lee, Andrew S. (2003). Blood compatibility of a newly developed trileaflet mechanical heart valve. *American Society of Artificial Internal Organs Journal*, 2003, pp 117-22.

44. Rosenberg, G. (1972). A mock circulatory system for in vitro studies of artificial hearts. MS Thesis, Pennsylvania State University, State College, Pennsylvania, 1972.

VITA

Antonio Walker was born January 29, 1984 in Nashville, NC. He graduated from North Carolina State University with a Bachelors of Science degree in Biomedical Engineering and a minor in Applied Mathematics in May of 2006. Upon graduation he accepted a job opportunity at Siemens Power Transmission and Distribution in Wendell, NC as an Electrical and Mechanical Assembling Technician. After rediscovering his desires to work in the biotechnology and medical device industry, he entered the Masters of Science program in Biomedical Engineering at Virginia Commonwealth University in August of 2007 and began research in the Artificial Heart Laboratory under the tutelage of Dr. Gerald Miller. Currently he is working at Novan Incorporated in Raleigh, NC as a Biomedical Engineer.